Electrochemical Energy Reviews (2022) (Suppl 1) 5:31
https://doi.org/10.1007/s41918-022-00146-6

REVIEW ARTICLE

Atomic Layer Deposition for Electrochemical Energy: from Design to Industrialization

Zhe Zhao[1,2] · Gaoshan Huang[1] · Ye Kong[1] · Jizhai Cui[1] · Alexander A. Solovev[1] · Xifei Li[3] · Yongfeng Mei[1,2,4,5]

Received: 18 May 2021 / Revised: 1 January 2022 / Accepted: 17 February 2022 / Published online: 24 November 2022

Abstract

The demand for high-performance devices that are used in electrochemical energy conversion and storage has increased rapidly. Tremendous efforts, such as adopting new materials, modifying existing materials, and producing new structures, have been made in the field in recent years. Atomic layer deposition (ALD), as an effective technique for the deposition of conformal and thickness-controllable thin films, has been widely utilized in producing electrode materials for electrochemical energy devices. Recent strategies have emerged and been developed for ALD to construct nanostructured architectures and three-dimensional (3D) micro/nanostructures. These strategies emphasize the preparation of active materials for devices such as batteries and supercapacitors or as catalysts for hydrogen evolution. Additionally, ALD is considered to have great potential in practical industrial production. In this review, we focus on the recent breakthroughs of ALD for the design of advanced materials and structures in electrochemical energy devices. The function and merits of ALD will be discussed in detail from traditional thin film depositions for the coating and engineering/modification layers to complex 3D micro/nanostructures that are designed for active materials. Furthermore, recent works regarding metal–organic framework films and transition metal dichalcogenide films, which were prepared with the assistance of ALD oxide, will be highlighted, and typical examples will be demonstrated and analysed. Because it is within a rapidly developing field, we believe that ALD will become an industrial deposition method that is important, commercially available, and widely used in electrochemical energy devices.

Keywords Atomic layer deposition · Electrochemical property · Energy storage · Electrocatalysis · Industrialization

1 Introduction

1.1 Emerging Demand of Electrochemical Energy

Energy is an essential subject in the history of mankind. In modern society, energy that supports all aspects of human life has become increasingly significant in everyday life and industrial manufacturing [1–7]. Historically, every revolution that involved energy introduced significant innovations into society [8–10]. The energy that humanity relies on the most today is fossil energy, such as coal, oil, and natural gas. However, reserves of fossil energy are quite limited [11–16]. Due to overexploitation, fossil energy will be exhausted in the near future. In addition, the combustion process of fossil energy releases large amounts of harmful gases, such as CO, CO_2, NO_x, and SO_2, which affect human health and the Earth's environment [17–21]. These problems have exacerbated the energy crisis [22]. Exploring new energy sources to replace traditional fossil energy and developing highly

Zhe Zhao and Gaoshan Huang contributed equally to this work.

✉ Yongfeng Mei
yfm@fudan.edu.cn

1 Department of Materials Science & State Key Laboratory of Molecular Engineering of Polymers, Fudan University, Shanghai 200438, China

2 Shanghai Frontiers Science Research Base of Intelligent Optoelectronics and Perception, Fudan University, Shanghai 200438, China

3 Institute of Advanced Electrochemical Energy & School of Materials Science and Engineering, Xi'an University of Technology, Shaanxi Xi'an 710048, China

4 International Institute of Intelligent Nanorobots and Nanosystems, Fudan University, Shanghai 200438, China

5 Yiwu Research Institute of Fudan University, Yiwu 322000, Zhejiang, China

efficient energy conversion and storage technologies have become a top priority [23–25].

Studies have shown that green energy such as solar energy, wind energy, biomass energy, and tidal energy, which is currently underutilized, may have great potential in solving the energy crisis [26–29]. If the energy can be converted into a more convenient and effective form (usually electrical energy) and stored stably, they should meet the long-term energy demands of mankind while remaining environmentally sustainable [23, 30–33]. At the present time, technologies, including solar cells [8, 34, 35], wind power generation [36, 37], friction nanogenerators [38, 39], and biofuel cells [40, 41], which can convert a variety of sustainable energy into electrical energy have been developed. However, these novel energy sources are highly dependent on the environment and exhibit irregular fluctuations; therefore, they cannot provide a very continuous power supply [35, 42–45]. A meaningful way to solve this is electrochemical energy storage, which converts the electrical energy generated by these renewable energy sources into chemical energy and stores it effectively [16, 46–48]. Conventional forms of electrochemical energy storage are mainly batteries (e.g. lithium-ion batteries, lithium-sulphur batteries, lead-acid batteries, etc.) and supercapacitors, which operate through electrochemical processes by charging and discharging electrons and ions [46, 49, 50]. These devices can meet the needs of stationery products, electronic products, aerospace fields, and other fields and have shown a very large application potential in large-scale power grids and transportation; the devises are especially important for electric vehicles, which are being rapidly developed [2, 28, 51, 52].

There are other alternative energy sources. For instance, hydrogen energy is believed to be a promising alternative to fossil energy and has received extensive attention in recent years [53, 54]. Hydrogen is the most abundant element in the universe, and therefore, it is considered to be inexhaustible. The combustion value of hydrogen is 142.5 kJ g^{-1}, which is much higher than that of gasoline [55], while the only product after combustion is water. Therefore, hydrogen energy is non-toxic and can produce zero carbon emissions. Most importantly, hydrogen energy can be efficiently and controllably converted into other forms of energy [56–58]. Thus, the production of hydrogen energy, which is basically an energy conversion method, can also be viewed as an electrochemical energy storage approach if hydrogen is produced by electrocatalytic water splitting, which uses electrical energy to split water into hydrogen and oxygen at the electrodes [59–62]. Therefore, we combined these fields as electrochemical energy and paid special attention to the materials/structures for applications in electrocatalysts, batteries, and supercapacitors.

With the increasing demand for electrochemical energy, continuous efforts have been made for developing devices from the perspective of energy density, stability, lifetime, and so on [63–66]. In all these electrochemical processes, electrochemical reactions occur in cells consisting of electrodes (anodes and cathode) and electrolytes [67–70]. Researchers in this field have optimized the devices and components by adopting new materials, modifying existing materials, and producing new structures [71–73]. To date, various physical and chemical methods have been employed to produce materials and structures for energy devices, and emerging approaches are continuously being explored [74–80]. Since the electrochemical properties of devices strongly depend on surface reactions at the electrolyte/electrode interface, approaches that can tune the surface of the electrode are tremendously important [81–85]. Based on this consideration, atomic layer deposition (ALD), which can deposit conformal coatings and produce nanostructures with different materials, is considered a powerful tool [86–91].

1.2 ALD: Mechanism and Materials

ALD is an essential gas-phase thin film deposition technique that was discovered in the recent decades [92–97], and it possesses atomic level control of the film thickness and a high conformality on 3D surfaces [98–100]. A typical ALD process consists of four steps: a pulse of precursor/purge/pulse of co-reactant/purge. This four-step process can be repeated to grow the desired material while precisely controlling the thickness. Ultrathin deposition with a precisely controlled thickness made it possible to grow films as thin as one monolayer, which is highly desirable for surface

Table 1 Comparison of the characteristics of major deposition techniques

Method	Substrate	Material versatility	Controllability	Uniformity	Conformality	Throughput	Cost
Solution-based wet chemistry	Limited	Low	Low	Low	Varies	Low	Low
Sol–gel	Flat	Low	Low	Low	Low	Low	Low
CVD	Less limited	High	High	Medium to high	Varies	High	Medium to high
PVD	Flat	High	High	Medium to high	Low	High	Medium to high
ALD	Less limited	Medium to high	Very high	Very high	Very high	Low	High

modifications [99, 101–104]. The self-limiting nature of the half-reaction allows conformal deposition on a high-aspect-ratio substrate, and the film obtained could be dense and pinhole-free with desirable mechanical and chemical properties for surface modification [105–110]. In addition, by adopting metal precursors with various counter-reactants, such as H_2O, O_2, O_3, NH_3, H_2S, and H_2, an enormous variety of materials, including oxides, nitrides, sulphides, carbides, and elementary metals, have been successfully produced [111–113]. In addition, the atomically controlled growth and the separated pulse for the reactant make it possible to apply multiple binary ALD processes into a supercycle for the deposition of multicomponent films [114–116]. This versatility allows the deposition of a wealth of materials with potential for various applications [117–119]. Table 1 summarizes the characteristics of the major deposition techniques. Compared with other liquid phase or gaseous phase deposition approaches, ALD demonstrated obvious advantages in the structural control of films deposited on substrates with different geometries. It is worth noting that the devices and components in the electrochemical energy field always involve low-dimensional structures and powders/particles, and thus, the ALD technique can handle this situation well with accurate thickness and stoichiometric control. In addition to interface engineering, previous investigations have demonstrated that ALD can be conveniently utilized in preparing active materials with optimal size, morphology, crystallinity, and composition for electrochemical energy devices [98, 120–122]. Specifically, versatile nanostructures such as films, particles, and tubes have recently been intensively investigated for their advantageous electrochemical applications. However, the low throughput of ALD compared with chemical vapour deposition (CVD) and physical vapour deposition (PVD) approaches might adversely affect future industrial manufacturing. Fortunately, researchers from both academia and industry are now working together to improve the throughput and productivity of the ALD process, and some achievements have been accomplished.

Very recently, a strategy based on post-treating the ALD films has been developed to synthesize transition metal dichalcogenides (TMDs) [123–125] and metal–organic frameworks (MOFs) [59, 86, 126–131]. In this so-called ALD-induced growth process, the induced layers (e.g. oxide films) grown by ALD were used as reactants (or seed layers) in the following step. This pretreatment step was followed by a subsequent synthesis of a specific material through the corresponding post-treatment, and consequently, TMDs/MOFs in the film forms can be attached firmly on substrates with complex geometries. This ALD-induced growth greatly expands the ALD material family and provides more creativity. Since TMDs/MOFs are widely involved in energy-related electrochemical applications, devices with enhanced performance are expected to be developed.

1.3 Framework of the Review

Here, in this review, we summarized the recent progress in the applications of ALD in electrochemical energy. As schematically shown in Fig. 1, ALD has been widely used in both energy conversion (e.g. in electrocatalysis for hydrogen evolution) and energy storage (e.g. in batteries and supercapacitors) in three different manners. In the first manner, as mentioned above, ALD is engaged in modifying the surface (as a surface coating layer) of the electrode, separator, etc., and the performance of the device can be enhanced. In the second manner, active materials in the form of nanostructures were also reported to be fabricated by ALD. Recent studies concerning the induced growth of TMDs and MOFs by using ALD layers as reactants are considered the third method. Among these applications, the design of materials and structures and their corresponding performance enhancements will be emphasized in this review. We have specifically considered the possibility of industrializing the ALD approach with potential applications in electrochemical energy devices, and several other possible developing directions have also been discussed. With further optimization, we believe that with its precise control over thickness and excellent material diversity, ALD will become a powerful tool in the electrochemical energy field and has great potential for mass production.

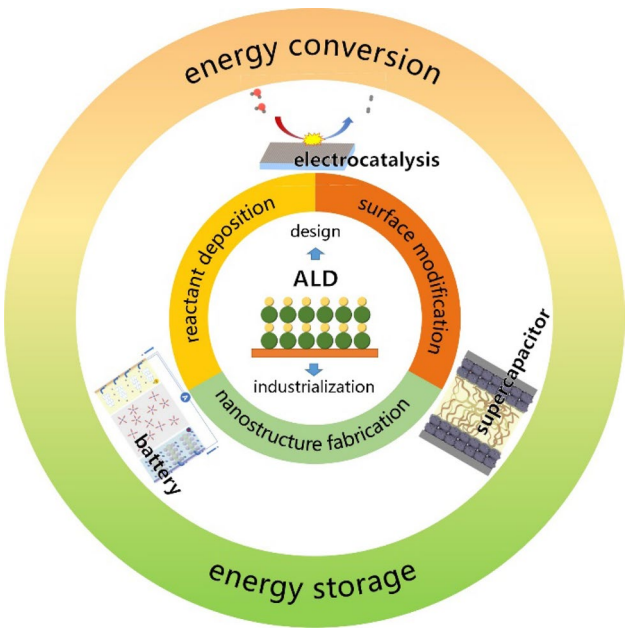

Fig. 1 Schematic diagram showing the outlines of the review. Generally, ALD can be used to modify the surface, fabricate nanostructured active materials, and deposit reactants for subsequent treatment; therefore, it has been widely adopted in electrochemical devices for energy conversion and storage

2 ALD for Efficient Electrochemical Catalysts

Hydrogen evolution in acidic or alkaline media has drawn considerable attention in the field of electrochemical catalysts. The electrochemical processes that produces hydrogen in water consume large amounts of electrical energy due to hydrogen overpotential [60, 61]. Hence, reducing overpotential is very important in the attempts to reduce energy consumption. In addition, preventing the destruction of catalysts in electrodes should be seriously examined, as this would maintain stable catalytic performance [132]. To date, much effort has been devoted to enhancing electrocatalytic performance by designing and fabricating electrodes with new materials and structures. ALD is a valuable technique that is commonly applied in electrochemical catalysts and two routes: depositing a protective layer on the electrode to prevent catalyst decomposition and direct deposition of functional materials such as transition metals, TMDs, and single-atom catalysts. Recently, a new strategy has also been developed utilizing ALD-oxide nanomembranes as a reactant/seed layer to induce the assembly of MOFs for hydrogen evolution. The application of the ALD technique in producing protective layers and functional materials is summarized in this section.

2.1 Prevention of Catalyst Decomposition

Current electrochemical catalyst designs suffer from severe degradation of electrode active materials through electrochemical reactions and experience a loss in efficiency [133]. Hence, a coating layer wrapped on the surface of the electrode could be used to protect the active materials and maintain charge transfer between the electrolyte and electrode. ALD has become an ideal strategy for this purpose.

For example, in a typical photoelectrochemical hydrogen evolution process, p-type Si and diimine–dioxime cobalt complexes (CoC11Ps) are used as catalysts, while the corrosion of active materials from electrolytes leads to unstable performances. To solve this problem, Chandrasekaran et al. [132] reported a strategy for preparing a modified electrode. In the approach, a p-type silicon surface was protected by a 15 nm ALD TiO_2 layer. CoC11P was covalently grafted onto TiO_2, and an additional 0.2 nm ALD TiO_2 layer was applied for stabilization. Here, ALD TiO_2 can not only protect active materials but can also provide loaded active materials. Fig. 2a demonstrates the cross-sectional SEM image of the ALD TiO_2-modified electrode, in which the top ALD TiO_2 layer covers the surface of the electrode. Due to the protection of the two ALD TiO_2 layers on both the top and bottom surfaces of the electrode, the modified electrode (the red trace) displays staggered variations due to the intermittent release of H_2 bubbles from the electrode surface (Fig. 2b). The highly improved property of the ALD-modified electrode can be attributed to the fact that a dense ultra-thin TiO_2 coating layer produced by ALD stabilizes the anchoring of the molecular catalyst.

Moreover, halide perovskite photocathodes are viewed as another ideal active material for hydrogen evolution electrodes, although the rapid decomposition of electrodes in

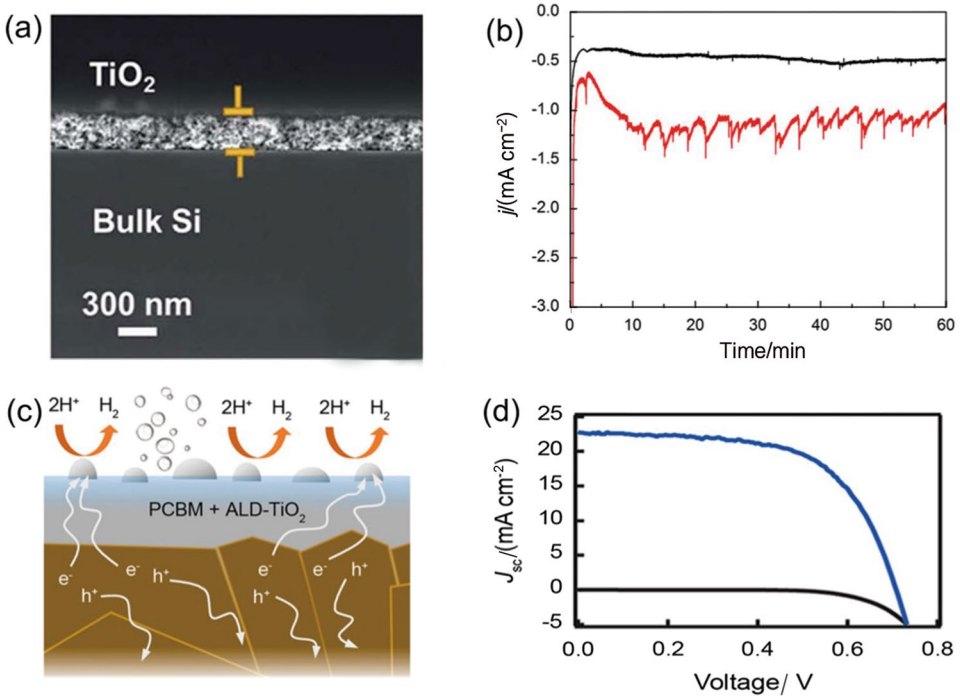

Fig. 2 **a** Cross-sectional SEM image of the ALD TiO_2-modified electrode. **b** Chronoamperometric profiles of the ALD-treated electrode (red trace) compared with the untreated electrode (black trace). (**a**) and (**b**) are reprinted with permission from Ref. [132]. Copyright 2019, The Royal Society of Chemistry. **c** Schematic of the ALD TiO_2-based protective layer for the halide perovskite absorber. **d** Catalytic performance of the ALD TiO_2-modified electrode. The current density–voltage curves for the electrodes under dark (black) and solar illumination (blue) are demonstrated. (**c**) and (**d**) are reprinted with permission from Ref. [133]. Copyright 2019, American Chemical Society

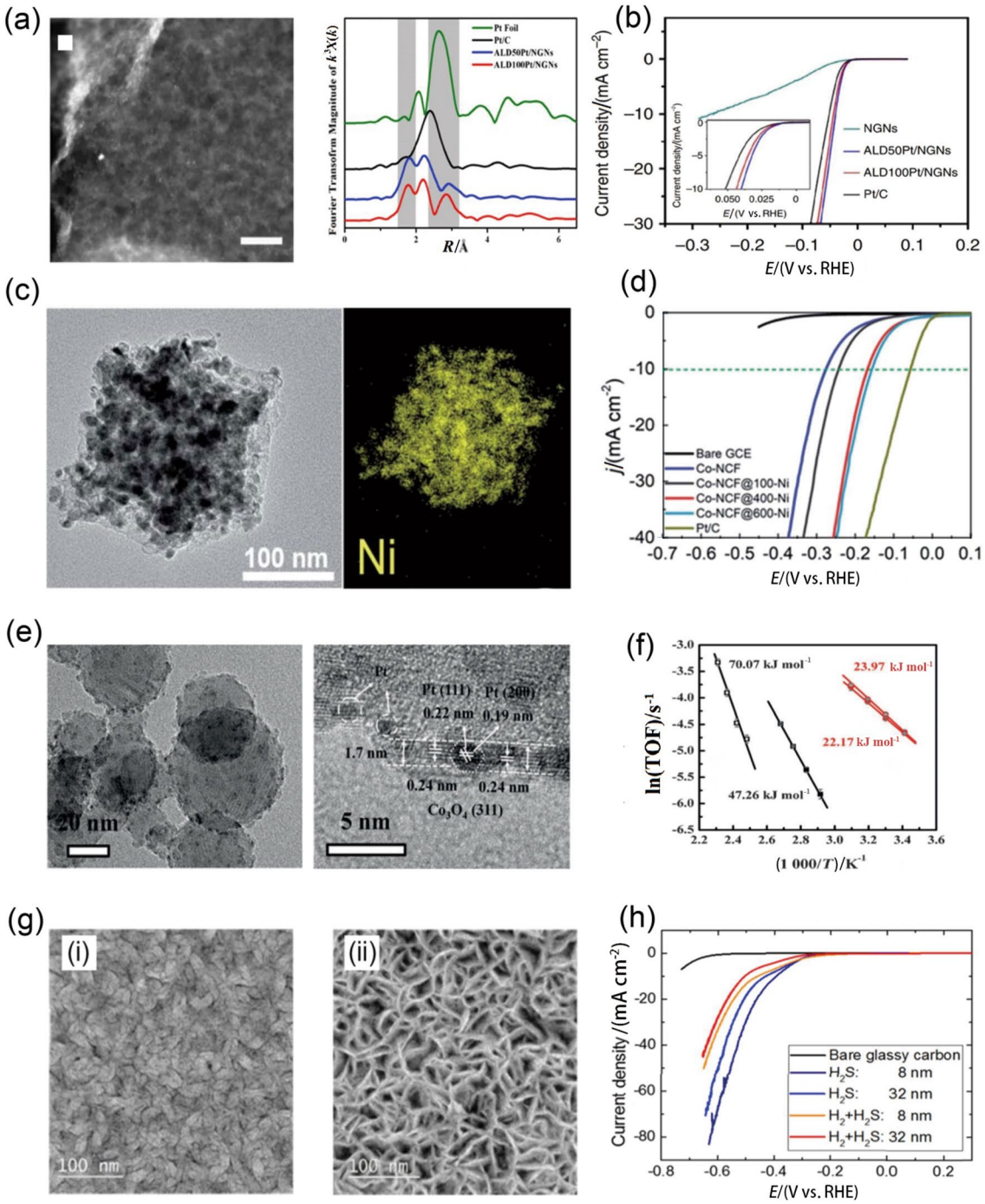

Fig. 3 **a** STEM image of ALD-prepared single-atom Pt with 50 ALD growth cycles (the scale bar: 10 nm) and the EXAFS spectrum acquired from ALD-prepared single-atom Pt compared with those from a commercial Pt/C catalyst and a Pt foil. **b** LSV curves of ALD-prepared single-atom Pt compared with the commercial Pt/C catalyst and pure graphene at a scan rate of 2 mV s^{-1} in acid. The inset image shows the enlarged curves at the potential onset region. (**a**) and (**b**) are reprinted with permission from Ref. [134]. Copyright 2016, Springer Nature Limited. **c** TEM image of ALD-prepared Ni nanograins on Co-doped carbon particles and corresponding EDS mapping of the composite showing the presence of Ni. **d** LSV curves of the composite and pure Co-doped carbon particles. (**c**) and (**d**) are adapted with permission from Ref. [135]. Copyright 2020 Royal Society of Chemistry. **e** TEM images of the selective-area ALD-deposited Pt/Co_3O_4 composite at high and low magnifications. **f** The electrocatalytic performance of the Pt/Co_3O_4 composite. (**e**) and (**f**) are adapted with permission from Ref. [141]. Copyright 2017, John Wiley & Sons, Inc. **g** SEM images of ALD WS_2 that was grown by using (i) pure H_2S plasma and (ii) H_2+H_2S plasma-enhanced processes. **h** LSV curves of the ALD WS_2 electrocatalysts with different thicknesses that was synthesized by using H_2S or H_2+H_2S plasma-enhanced processes. (**g**) and (**h**) are adapted with permission from Ref. [142]. Copyright 2019, American Chemical Society

watery environments or even humid air is still a problem [133]. To solve this problem, ALD has been used to prepare nanomembranes on the surface of active material to prohibit the dissolution of halide perovskite photocathodes. For example, Kim and co-workers provided a simple preparation method for producing a hybrid passive layer, in which a composite consisting of $PC_{61}BM$ and ALD TiO_2 nanomembrane was coated on the electrode (Fig. 2c) [133]. The ALD TiO_2 nanomembrane promoted a reduction in photo-assisted protons without further encapsulation. According to a detailed characterization, the device exhibited an average short-circuit current density of 21.4 mA cm^{-2} with a filling factor of 65.5% (Fig. 2d). In addition, an average photovoltage of 0.68 V was achieved. The authors concluded that the reason for the enhanced performance was because ALD TiO_2 can serve as a protective layer when the whole device is in contact with electrolytes, and this leads to outstanding device stability. This strategy could be directly applied to other hybrid semiconductors and organic light absorption for photoelectrochemical hydrogen production.

2.2 Direct Fabrication of Functional Materials as Catalysts

ALD can synthesize a wide range of materials with versatile morphologies as active materials. For example, considerable attention has been placed on a single-atom catalyst for hydrogen evolution due to its ultra-high catalytic efficiency. However, the process of preparing single-atom catalysts is overly complex and a hindrance in practical applications. To solve this problem, a high-efficiency and straightforward strategy was recently developed by Cheng and his co-workers, and this strategy can be applied to synthesize large-scale and stable isolated single platinum atoms utilizing the ALD technique [134]. This method generated single Pt atoms that were supported on nitrogen-doped graphene nanosheets via the ALD technique. It is worth mentioning that the Pt catalyst size and density on graphene can also be precisely controlled by simply adjusting the number of ALD growth cycles. Figure 3a shows a typical morphology of ALD Pt on a graphene substrate with 50 growth cycles, and numerous individual Pt atoms (bright spots) were uniformly dispersed on the graphene supporter. To further confirm the single atom of Pt prepared by ALD, the extended X-ray absorption fine structure (EXAFS) of the sample compared with commercial Pt/C and Pt foil is shown in Fig. 3a. The significant change in the intensity of Pt–O or Pt–C bonds and severe deviation of the Pt–Pt bond of the ALD-prepared sample compared with the Pt foil indicate the presence of single Pt atoms. The HER activity of the ALD-prepared Pt samples was evaluated in 0.5 M (1 M = 1 mol L^{-1}) H_2SO_4 by linear sweep voltammetry (LSV) scanning. Due to the high catalytic activity of the single-atom catalyst, the samples exhibited outstanding hydrogen evolution catalytic properties, e.g. a very low overpotential of 0.05 V at a current density of 12.5 mA cm^{-2} (Fig. 3b). ALD-prepared single-Pt atom catalysts can significantly reduce the cost of valuable metal consumption in catalysts for the hydrogen production industry.

Nanoparticle-like structures are commonly involved in hydrogen evolution. Zhang and his co-workers proposed a strategy of fabricating nickel nanograins coated onto Co-doped carbon particles by using ALD for hydrogen evolution catalysts in alkaline media [135]. As shown in Fig. 3c, due to the uniform deposition of Ni nanograins by ALD, a good interface phase between Ni and Co-doped carbon particles leads to an enhanced electrochemical property with a very low overpotential of 157 mV, which is much lower than that of pure Co-doped carbon (Fig. 3d). In another example, Zhang and his colleagues utilized ALD to prepare a series of Pt nanoparticle-decorated 2D $Ti_3C_2T_x$ MXene composites [136]. Due to the valuable controllability of ALD, low Pt consumption of 0.98–3.10 wt.% (wt.% means the weight percentage) was achieved. The uniformly dispersed Pt particles on MXenes showed excellent HER catalytic activity and stability with an overpotential of only 67.8 mV. It should be noted that this performance was close to that of the commercial Pt/C catalyst (64.2 mV). The excellent behaviour was attributed to the homogeneous deposition of Pt and the superior conductivity of the MXene supports.

Area-selective ALD is a promising strategy to synthesize unique nanostructures by growing particular components in a specific area. Many efforts have been devoted to this method by Chen's group [137–141]. For example, a novel structure with Pt particles anchored to metal oxide nanotraps was prepared [141]. The Pt particles were deposited on the Al_2O_3 substrates in the first step. 1-Octadecanethiol was chosen as the blocking agent to protect Pt from being covered by the subsequent Co_3O_4 deposition. After that, Co_3O_4 was selectively deposited on Al_2O_3 substrates. When the blocking agent was removed, Pt particles were re-exposed. As shown in Fig. 3e, transmission electron microscopy (TEM) images show that Pt had a uniformed dispersion and an average size of 2 nm, and a good Pt/Co_3O_4 interface can be seen. The resultant composites exhibit outstanding catalytic properties with an activation energy of 22.17 kJ mol^{-1} (Fig. 3f).

TMDs as 2D layered materials also attract widespread attention due to their excellent electrochemical properties, high catalytic activity and abundant active site exposure. They have recently been widely applied in energy devices, especially as catalysts for hydrogen evolution, and controllable growth at the atomic scale may very important. Due to its low temperature, reproducibility, self-limited process, and valuable ability to control the thickness, ALD appears to be an ideal technique to directly deposit TMDs as a one-pot method with good tenability. For instance, Song and

co-workers developed an advanced pressure-tuned stop-flow strategy by the ALD process to deposit a MoS_2 layer with a thickness of ~ 5 nm on carbon nanotube array growth on 3D graphite foam, which is applied as an electrode for Li-O_2 batteries [124]. Taking advantage of ALD-prepared MoS_2, the whole architecture can lower the energy barrier, and the unique 3D electrode exhibited high catalytic activity for both the oxygen reduction reaction and oxygen evolution reaction. Kwon and his co-workers developed a facile strategy that directly deposited the MoS_x film on porous carbon papers for high-performance hydrogen evolution reaction (HER) catalysts [125]. They chose molybdenum hexacarbonyl and dimethyldisulphide as the reactants to generate Mo and S, respectively, and the MoS_x film was deposited at 100 °C. The ALD-prepared MoS_x catalysts exhibited exponentially increased catalytic properties for the HER with a very low overpotential and Tafel slope, providing a simple method for the fabrication of high-efficiency hydrogen production catalysts. In addition, Balasubramanyam and his colleagues maximized the density of reactive edge sites of TMDs by using the plasma-enhanced ALD technique for high-performance electrochemical hydrogen evolution reactions [142]. They precisely controlled the morphology and composition as well as edge site density of the resultant WS_2 layer by adjusting the plasma atmosphere of H_2 and H_2S. As shown in Fig. 3g, WS_2 was grown by using a pure H_2S process (Fig. 3g(i)) that displayed densely packed "nanoflakes" with individual lateral flake sizes that ranged from 10 to 20 nm. When the plasma atmosphere switched to $H_2 + H_2S$, the morphology of WS_2 transferred to 2D lamellar nanosheets

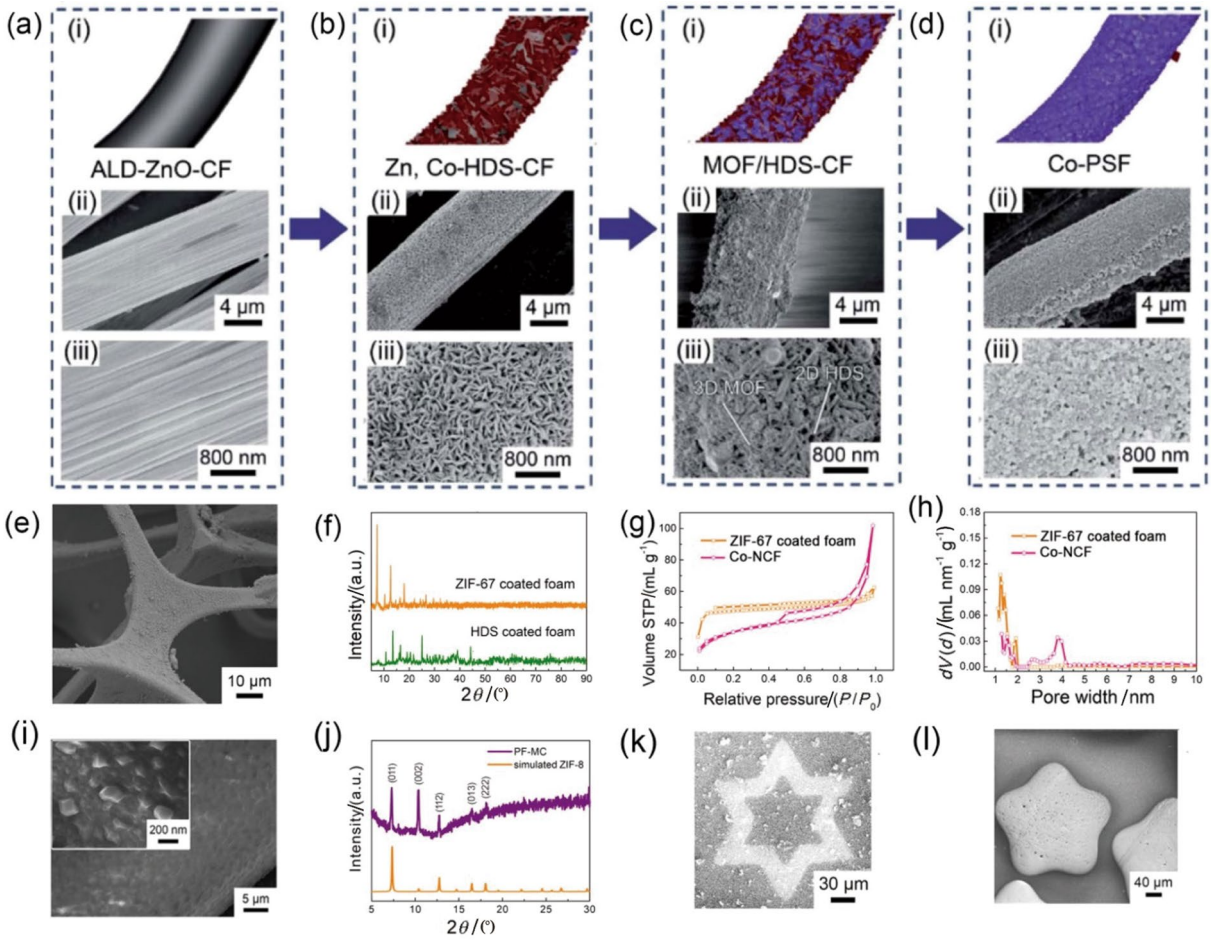

Fig. 4 **a**–**d** Schematic illustrations of the MOF layer growth using ALD oxide as a reactant. Panels (i), (ii), and (iii) are the corresponding scheme, the SEM image at low magnification, and the SEM image at high magnification, respectively. Reprinted with permission from Ref. [128]. Copyright 2020, Royal Society of Chemistry. **e** SEM image of the fabricated ZIF-67 layer on melamine foam. **f** XRD patterns of Zn and Co-HDS on melamine foam and ZIF-67 on melamine foam. **g** Nitrogen adsorption/desorption isotherms and **h** pore size distributions of the ZIF-67 layer on melamine foam and the pyrolysed ZIF-67 layer on melamine foam. Orange represents the ZIF-67 layer on melamine foam, and pink represents the pyrolysed ZIF-67 layer on melamine foam. (**e**-**h**) are adapted with permission from Ref. [127]. Copyright 2021, Elsevier B.V. **i** SEM image of the ZIF-8 film grown on a microtubular structure. The inset shows the enlarged image. **j** XRD pattern of the ZIF-8 film grown on a microtubular structure (the purple line), and the orange line is the simulated diffraction pattern. (**i**) and (**j**) are adapted with permission from Ref. [131]. Copyright 2021, American Chemical Society. **k** SEM image of the PCN-333 pattern. **l** SEM image of the ZIF-8 pattern. (**k**) and (**l**) are adapted with permission from Ref. [126]. Copyright 2022, The Author(s)

stacking with each other (Fig. 3g(ii)). This open structure exhibits a large surface area, and its electrochemical catalytic property is shown in Fig. 3h. When LSV curves of the WS_2 layer with various thicknesses are compared with that of a neat glassy carbon electrode, a low onset potential (200 mV) for HER can be observed. Moreover, the electrochemical catalytic performance for hydrogen production of the sample prepared with pure H_2S plasma is significantly better than that of the sample prepared with $H_2 + H_2S$ plasma, as reflected by the lower overpotential at a standard current density of 10 mA cm^{-2}. This work demonstrated that plasma-enhanced ALD is a reliable technique for growing TMDs for electrochemical catalysts.

2.3 ALD Layer as a Catalyst Reactant

Recently, researchers have devoted particular attention to MOFs [143–148]. MOFs are 3D long-range ordered assemblies of transition metal clusters and the corresponding organic frameworks [5, 46, 149–152]. However, MOFs commonly exist as individual particles, limiting their wide applications in energy devices [46, 153, 154]. Some researchers have developed several promising methods to build MOF films via various techniques, such as electrodeposition [155], room temperature ageing [156, 157], layer-by-layer deposition [158], suspension sprays [159], and microwave-facilitated techniques [160]. However, weak adhesion and nonuniformity are still problems that hinder its comprehensive application [161]. To handle these challenges, Zhao et al. [59, 86, 126–131] developed a novel strategy by using ALD oxide nanomembranes as reactants/seed layers to grow layers of MOFs on specific substrates. When the MOFs were applied in hydrogen evolution catalysts, outstanding uniformity and conformal deposition and close attachment were achieved, leading to excellent electrochemical properties.

For electrochemical energy applications, MOFs are typically prepared by an ALD oxide-induced growth approach on conductive substrates, e.g. carbon fibre [128]. Specifically, for the growth of ZIF-67 film, a thin ZnO nanomembrane was first deposited on the surface of the carbon fibre as a reactant. Due to the uniform and conformal deposition, the morphology of the ALD ZnO-pretreated carbon fibre is similar to that of the pristine carbon fibre (Fig. 4a). As shown in Fig. 4b, 2D layered lamellar crystals emerge after the introduction of cobaltous nitrate hexahydrate, implying that a phase transition possibly occurred, and the intermediate product is considered to be a (Zn, Co) hydroxy double salt [59]. When the organic linker was added, some (Zn, Co) hydroxy double salts reacted with the organic linker, and a new phase emerged (Fig. 4c). During this process, N^{3-} and NH^{2-} in organic linkers provide active electrons to break the crystal structure, and highly active NO^{3-} and OH^- in the hydroxy double salt tend to cause rapid anion exchanges. Therefore, with gradual exposure to organic linkers, the lamellar sheets begin to collapse, and NO^{3-} and OH^- are removed to release Co^{2+}, and this was continuously coordinated in situ with 2-MI. This process leads to the formation of target 3D particle-like crystals. After a complete ageing process, a ZIF-67 film is formed (Fig. 4d). Apart from the growth of MOF films on carbon substrates, a similar approach was also used to prepare the ZIF-67 layer on melamine foam [127]. The SEM image in Fig. 4e shows the uniformed and firm attachment of the obtained ZIF-67 film on melamine foam. The corresponding X-ray diffraction (XRD) pattern in Fig. 4f demonstrates the fabrication of Zn and Co-HDS layers during the induction process, while the final ZIF-67 layer exhibits a different XRD pattern. It should be noted that this novel strategy can produce a hierarchically porous structure, and the coexistence of micropores and mesopores in the film is different from that of normal MOF particles. The apparent mesopore peaks (Fig. 4g and h) can be attributed to the stack of particles in the film, which further enhances the electrochemical property due to more active sites being exposed and ion transportation being faster in the MOF film grown with the assistance of ALD oxide [59, 161]. Taking advantage of the precise controllability of ALD, MOF films can also be precisely deposited on micro/nanostructures. For instance, the SEM image in Fig. 5i shows a uniform ZIF-8 film adhering to the surface of a microtubular structure, and the crystal structure of ZIF-8 was confirmed by the XRD pattern demonstrated in Fig. 5j [131].

Moreover, since the growth of the MOF film is crucially dependent on ALD oxide, the MOF film patterning can be achieved by pattering oxide nanomembranes. Experimentally, a patterned ZnO nanomembrane was obtained by using photolithography and acid etching and then was applied in the MOF film growth process. The PCN-333 pattern (Fig. 5k) and ZIF-8 pattern (Fig. 5l) were successfully prepared by this strategy [126]. Patterned MOF films should be very promising for future on-chip energy devices.

To explore the applications of MOF that is prepared by inducing ALD oxide in electrochemical catalysis, we first fabricated MOF film on carbon foam and then treated the sample in N_2 at a high temperature. In this carbonization process, the obtained ZIF-67 film (Fig. 5a) was converted into a hierarchically porous carbon layer (Fig. 5b) consisting of spherical carbon particles, which preserved a large surface area and high pore volume [59], while a 3D carbon foam framework was used as a flexible substrate and provided multiple conductive pathways. In addition, the strong connection between active materials and substrates due to the ALD oxide layer prohibited the aggregation of Co-doped carbon particles during the pyrolysis process [59]. It was experimentally found that this fabrication approach using the induction effect of an ALD oxide layer can achieve a

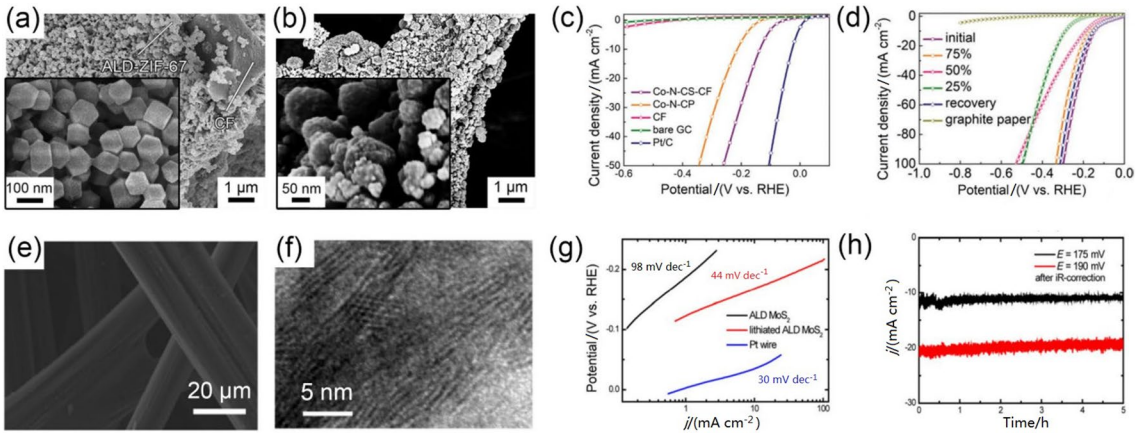

Fig. 5 **a** SEM image of the ZIF-67 layer on carbon foam. **b** SEM image of the pyrolysed ZIF-67 layer on carbon foam. The insets in (**a**) and (**b**) are corresponding SEM images at high magnification. **c** LSV curves of the pyrolysed ZIF-67 layer on carbon foam compared with pyrolysed ZIF-67 particles and carbon foam. **d** LSV curves of the pyrolysed ZIF-67 layer on carbon foam under different compression rates. (**a**-**d**) are reprinted with permission from Ref. [59]. Copyright 2019, John Wiley & Sons, Inc. **e** SEM image of the ALD-prepared MoO_3 film. **f** TEM image of the obtained MoS_2 film. **g** Tafel plots of the obtained MoS_2 film and the reference samples. **h** Electrocatalytic current of the obtained MoS_2 film as a function of time. (**e**-**h**) are reprinted with permission from Ref. [123]. Copyright 2013, National Academy of Sciences

high mass loading of active materials (the porous carbon layer derived from the MOF film) of up to 40%. Abundant carbon spherical particles with vast active sites and high Co–N contents also led to the superior electrochemical catalytic performance of the composite. As shown in Fig. 5c, in an acid electrolyte, the resultant composite exhibits a low overpotential of 142 mV to reach a current density of 10 mA cm^{-2}. More importantly, due to the support of elastic and deformation-tolerant carbon foam, the electrode shows outstanding flexibility, and they can endure repeated compressions and releases and maintain a stable electrochemical property (Fig. 5d). With the help of ALD, this pioneering work provides a new strategy to prepare next-generation flexible hydrogen production electrodes.

To date, several MOFs have been prepared by this approach. Here we list some classic works. Zhao et al. [162] fabricated UiO-66-NH_2 particle-modified polyamide-6 nanofibres by using an ALD TiO_2 nanomembrane as one reactant. A UiO-66-NH_2 particle layer with high mass loading was then grown on the surface of the nanofibres, and the resultant composite possessed a large specific surface area of 205.9 m^2 g^{-1}. The same group also grew HKUST-1 MOF crystals on ALD Al_2O_3-coated polypropylene fibres [163]. Solvent-free synthesis of MOFs has also been realized by using the ALD oxide layer as the reactant. For example, Stassen et al. [164] developed a method to prepare ZIF-8 membranes on a silicon wafer with ALD ZnO and 2-ethylimidazole powder. Krishtab and his coworkers [165] successfully synthesized ZIF-67 as a gap-filling ultralow-*k* dielectric by using ALD CoO and 2-methylimidazole powder. Apart from this, Stassen et al. [166] synthesized MAF-6 with ALD ZnO and 2-ethylimidazole. Remarkably, the thickness of the MOF layer is positively associated with the thickness of the ALD metal oxide layer [165] and can therefore be precisely tuned by the number of ALD growth cycles, making it possible to combine MOF with more micro/nanostructures for more applications. Investigations on the electrochemical energy-related application of such MOF-related structures are still scarce. Thus far, the strategies are promising, considering the broad applications of MOFs in a related field. We believe that more MOF layers will be successfully fabricated in the future, and devices with high performances are expected.

Because of its unique advantages, ALD has also been used to deposit materials for reactions, and TMD has been obtained via the following post-treatment. For instance, Wang et al. [123] fabricated a MoO_3 nanomembrane via ALD (Fig. 5e), and a MoS_2 film was formed with the subsequent rapid sulfurization process. The TEM image shown in Fig. 5f confirms that MoS_2 has a layered structure. Due to its maximally exposed active edge sites, the MoS_2 film can maintain high HER catalytic activity with reduced film thickness, and a dramatically improved Tafel slope of 98 mV per decade was experimentally observed (Fig. 5g). Additionally, outstanding cycling performance was achieved, and no decay was observed after a 5 h stability test (Fig. 5h). This work provides a new perspective for the convenient fabrication of highly effective electrochemical catalysts.

Table 2 summarizes some recent efforts that were devoted to the fabrication of functional materials as electrochemical catalysts with the assistance of ALD. It is expected that more

Table 2 Fabrication of functional materials as electrochemical catalysts by ALD

Material	Substrate	Morphology	ALD cycles (thickness)	Performance	Reference
Ni	Pyrolysis ZIF-67	Particle	600	157 mV at 10 mA cm^{-2}	[135]
MoS_x	Carbon fibre paper	Film	100	55.8 mV dec^{-1}	[125]
WS_2	Wafer	Nanosheet	100	394 mV at 10 mA cm^{-2}	[142]
Pt	Graphene	Single-atom	50	0.05 V at 16 mA cm^{-2}	[134]
Pt	MoS_2	Particle	80	31 mV at 1 mA cm^{-2}	[167]
MoN_x	Porous carbon	Film	700	236 mV at 10 mA cm^{-2}	[168]
RuO_x	CNTs	Film	30	33 mV at 10 mA cm^{-2}	[169]
Pt	MXenes	Particle	40	67.8 mV at 10 mA cm^{-2}	[136]
MoS_2	Wafer	Nanosheet	1 000	98 mV dec^{-1}	[123]
Pt	Graphene	Film	200	0.188 V at 1 mA cm^{-2}	[170]
CoS_y and FeS_y	CNTs	Film	11 nm	294 mV at 10 mA cm^{-2}	[171]
Pt	Porous Ni	Film	20	225 mV at 100 mA cm^{-2}	[172]
Pt and Ru	CNTs	Single-atom	/	28.9 mV dec^{-1}	[173]
MoS_2	Wafer	Film	9.4 nm	200 mV at 15 mA cm^{-2}	[174]
CoP	Wafer	Film	6.7 nm	254 mV at 10 mA cm^{-2}	[175]
CoS_x	Graphite foil	Particle	100	0.12 V at 1 mA cm^{-2}	[176]
ZIF-67	Carbon foam	Film	300	142 mV at 10 mA cm^{-2}	[59]
Pt	Hollow fibres	Particle	250	190 mV at 10 mA cm^{-2}	[177]
Pt	Tungsten monocarbide	Particle	10	Nearly Pt/C	[178]
MoS_2	SiO_2/Si	Film	1 000	300 mV at 20 mA cm^{-2}	[179]
Ni_3C	CNT	Film	300	132 mV at 10 mA cm^{-2}	[180]
$Fe_{0.54}Co_{0.46}S_{0.92}$	Carbon cloth	Film	11 nm	70 mV at 10 mA cm^{-2}	[171]

materials and structures will be fabricated in the future for effective catalysis.

3 ALD to Improve the Performance of Energy Storage Devices

ALD is a unique technology that enables various thin film materials to be coated from the vapour phase [181–183]. In electrochemical energy storage devices, the ALD technique is frequently used for the modification of electrode surfaces [102, 184, 185], as protective layers for solid-state electrolytes [94, 186], and for modifying separators [187, 188]. Additionally, due to its surface-controlled nature, ALD exhibits great potential for fabricating novel nanostructures by using either template-assisted growth or bottom-up controlled nucleation mechanisms [189]. Nanoparticles, nanowires, and nanosheets can be effectively grown by ALD [190–192]. Hence, the electrode architecture of the energy storage device can be designed with the assistance of ALD. In this section, the modification of the electrode, solid-state electrolyte, and separator as well as the design of the electrode architecture by ALD will be discussed.

3.1 ALD for Surface Modification of Batteries

Batteries generally consist of electrodes, electrolytes, and separators. By decorating these three components, ALD can enhance their electrochemical performances. The related research will be briefly summarized in the following sections.

3.1.1 Electrodes

For batteries, the dissolution of electrode materials, which leads to diminished capacity, has been a key scientific issue [193]. Researchers found that a passivation layer, which is named the solid electrolyte interphase (SEI), may form between electrode surfaces and electrolyte when the redox potential of the electrodes in a battery lies outside the electrochemical window of the electrolyte, and the natural SEI can prohibit the decomposition of active materials in the electrode, thereby solving the problem [194]. This concept was proposed by Peled [195] for the first time in 1979. A dense SEI can highly enhance the electrochemical stability of batteries. Nevertheless, the SEI could grow thicker during charge/discharge cycles, consuming active materials and electrolytes, increasing the internal resistance and losing capacity [194, 196]. Controlling and stabilizing the SEI layer

have become hot topics among battery-related researchers. It is now widely accepted that artificial SEIs are essential for enhancing battery performances [197]. The artificial SEI is a thin film with a complex and heterogeneous structure and is situated between the electrode and the electrolyte, providing electrical insulation and ionic conductivity [198]. Among the approaches to generate artificial SEI, preparing a layer by ALD is a good choice. The ALD technique has been widely applied in constructing a protective layer on the electrode to form an artificial SEI, thereby achieving a stable performance. Uniform and firm films deposited by ALD can be used to separate active electrodes from harsh environments. Numerous studies have been devoted to applying ALD to the formation of artificial SEIs, and this strategy has already become a standard method. Generally, Al_2O_3, TiO_2, ZnO, ZrO_2, etc., are used the most frequently. For example, Luo et al. [199] formed an artificial SEI via ALD Al_2O_3 to stabilize the Na metal anode. They discovered that a 2.8-nm ultra-thin ALD Al_2O_3 layer protects Na metal from electrolyte decomposition, prevents 3D dendrite formation, and significantly enhances its cycling performance. Similarly, Zhao and his co-workers also deposited 25 cycles of ALD Al_2O_3 as an artificial SEI to wrap the surface of the anode for Na batteries [200]. The resultant battery exhibited a remarkable cycling life that remained unchanged after 500 charge/discharge cycles. The advantages of ALD films make the ALD approach quite promising in the field of artificial SEIs.

In addition to Na batteries, the construction of artificial SEIs by ALD is widely applied in Li-ion batteries. Zhao and co-workers developed a new strategy that involved ALD to prepare a lithium zirconium oxide (LZO) film to provide sufficient Li^+ ion flux at the cathode interface and to prevent side reactions (Fig. 6a) [201]. The TEM image shown in Fig. 6b indicates that the thin ~ 5 nm LZO film is continuous and acts as the outermost shell, wrapping the surface of $LiCoO_2$ cathodes. As shown in the compositional mappings, the signal intensity of the Co element in the edge region is weaker than that in the centre, while the Zr signal indication is consistent in the whole area. This illustrates that the LZO film is conformally coated on the $LiCoO_2$ active particle. The cycling performance of the entire battery is shown in Fig. 6c. It should be noted that in the case of a low current density of 0.05 C, the charge specific capacity of a full battery reaches 117.2 mAh g^{-1}, and the capacity remains 72% after 100 cycles. However, without the LZO coating, the initial reversible capacity is 56.7 mAh g^{-1} and drops dramatically after the 50th cycle. Obviously, the Li-containing interface layer can prevent side reactions and provide essential support for the migration of Li ions between the electrode and electrolyte. Moreover, Guan and his colleagues applied the ALD technique to fabricate a protection layer to prevent electrode damage from occurring in the electrolyte [202]. The preparation of a highly conformal and uniform Al_2O_3 coating on the surface of a $LiMn_2O_4$ cathode with precise thickness control at the atomic scale was achieved by the ALD technique. As shown in the scanning electron microscopy (SEM) image in Fig. 6d, the commercial $LiMn_2O_4$ powders are composed of dispersed particles with a size of 1–8 μm, and these were mixed and pressed with carbon black to prepare a $LiMn_2O_4$ electrode for a battery. After treating the $LiMn_2O_4$ electrode with ALD Al_2O_3 film for 20 cycles, the particles preserved their original shape and morphology, indicating that conformal deposition had occurred. The charge/discharge curves of the ALD Al_2O_3-treated electrode are demonstrated in Fig. 6e, in which a high capacity with excellent cycling performance can be observed. With the protection of this ALD Al_2O_3 layer, the whole electrode alleviated the severe dissolution of active ions into the electrolyte.

As an example of ALD applied in modifying low-dimensional composite electrodes, Yu and colleagues [203] fabricated an ALD TiO_2-modified nitrogen-doped graphene composite and used it as a cathode for lithium-sulphur batteries. In this work, TiO_2 thin films were deposited by ALD, and the thickness was precisely controlled by adjusting the growth cycles. The deposition of TiO_2 thin film on the electrode was performed with the goal of avoiding the deterioration of the overall specific capacity and the energy density of the whole battery system with negligible additional weight. As shown in Fig. 6f, the TEM image and corresponding energy-dispersive spectroscopy (EDS) analysis confirm that the elements of O, N, S, and Ti are evenly distributed in the whole composite, revealing that the ALD-prepared TiO_2 layer was successfully and uniformly wrapped on the surface of the electrode. The cycling performance of the ALD TiO_2-modified electrode and the pristine electrode was also compared (Fig. 6g). The pristine electrode (the black trace) exhibits poor cycling stability, although it delivers a moderate capacity, and after 230 cycles, the electrochemical performance drops dramatically. On the other hand, the ALD-modified electrode (20 growth cycles of TiO_2, red trace in Fig. 6g) still shows excellent and stable properties even after 500 cycles. The improved electrochemical performance could be attributed to the on-site absorption of polysulfide on the TiO_2 coating layer as well as the charge transfer enhancement. These results indicate that the ALD-modified electrode has excellent potential in the electrode preparation industry for high-performance lithium-sulphur batteries.

3.1.2 Solid-State Electrolyte

In the electrochemical process, the surface/interface plays an essential role [204]. Side reactions and chemical dissolution

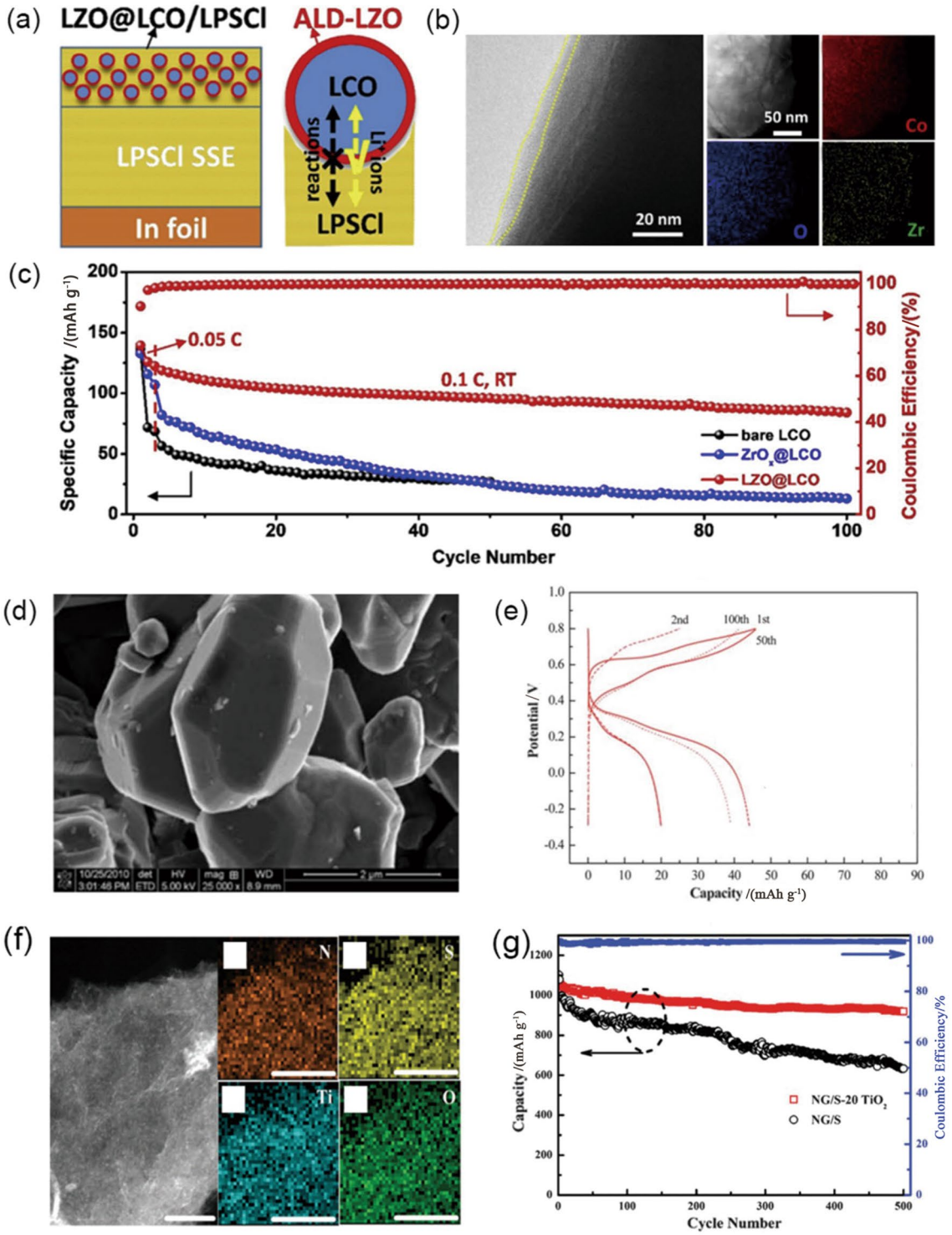

of active materials could severely diminish the capacitance and cycling performance [204–208]. Therefore, in addition to modifying the electrode surface, engineering other interfaces is of great importance for electrochemical energy devices [209–214]. The approach was intensively investigated in the case of an all-solid-state battery.

All-solid-state batteries have recently attracted wide attention as a new generation energy storage device due to the probability of delivering a higher energy density and superior safety performance than that of standard lithium-ion batteries with liquid electrolytes [215–220]. However, there are still challenges for developing all-solid-state batteries

◂**Fig. 6** **a** Schematic of the cathode of the lithium-ion battery and the solid electrolyte demonstrating that the LZO film is coated on the surface of LCO by ALD. **b** TEM image of the ALD LZO-coated LCO composites and EDS mapping of Co, O, and Zr elements on ALD LZO-coated LCO composites. **c** Long-term cycling stability tests of the batteries with pristine electrodes and ALD-modified cathodes. (**a**) and (**b**) are reprinted with permission from Ref. [201]. Copyright 2020, Elsevier B.V. **d** SEM image of the $LiMn_2O_4$ cathode coated with the ALD Al_2O_3 film and 20 ALD cycles. **e** Charge/discharge curves of the cathode that was modified with Al_2O_3 at a current density of 240 mA g^{-1}. (**d**) and (**e**) are adapted with permission from Ref. [202]. Copyright 2011, Royal Society of Chemistry. **f** TEM image of ALD TiO_2 on the graphene composite and the corresponding elemental mapping of O, N, S, and Ti. The scale bar: 100 nm. **g** Cycling performances of pure graphene (black trace) and ALD TiO_2-modified graphene composite (red trace) electrodes at 1 C. The Coulombic efficiency of the ALD-modified electrode is also shown. (**f**) and (**g**) are reprinted with permission from Ref. [203]. Copyright 2016, Royal Society of Chemistry

with a higher energy density and greater cycling performance [221–223]. Modifying the electrode and solid electrolyte interface is an effective route to solve these challenges [224–226]. One promising strategy is taking advantage of the ALD technique to fabricate a stable interface phase [94, 227, 228]. In a typical example, Han and colleagues [186] pioneered the use of ultra-thin Al_2O_3 to produce an interfacial film between a lithium metal anode and the garnet electrolyte through the ALD technique. In this work, the surface of $Li_7La_{2.75}Ca_{0.25}Zr_{1.75}Nb_{0.25}O_{12}$ (LLCZN) garnet was treated with an ALD Al_2O_3 nanomembrane with 40 growth cycles, as demonstrated in Fig. 7a and b, and an interface phase can be seen between Li and garnet. Researchers found that the Al_2O_3 interface layer caused the molten Li to conformally wrap on the surface without empty space, further enhancing the contact between the garnet electrolyte surface and Li metal. The excellent cycling performance is shown in Fig. 7c, and a stable voltage response occurred at 22 mV for nearly 90 h. Outstanding cycling with small polarization confirms that a stable interface was obtained with the ALD interface layer, and this was possibly due to the high ductility of the lithiated Al_2O_3. The performance improvement can also be attributed to the wetting of lithium metal that is in contact with the garnet electrolyte and the efficacious lithium ion transport through the interfacial layer provided by the ALD Al_2O_3 [186].

There are also applications of ALD in maintaining the stability of the interface between the electrode and sulphide electrolyte by constructing a uniform layer via ALD. Liang et al. [94] grew ALD Al_2O_3 on a solid electrolyte called NASICON-type $Li_{3-2x}(Al_{1-x}Ti_x)_2(PO_4)_3$ (LATP) for a high-performance lithium-sulphur battery. After 100 charge/discharge cycles, the neat LATP demonstrates grain pulverization and structural collapse (Fig. 7d). Furthermore, pulverization can be observed as deep as 50 μm into the LATP electrolyte, and the severe destruction of LATP was the reason for the rapid capacity decline. After 10 growth cycles of ALD Al_2O_3 growth, the LATP destruction was almost completely inhibited, and the smooth surface of the solid electrolyte was maintained. Due to the modification of the solid electrolyte, the cycling performance exhibited a stable property as follows: a high capacity retention of 823 mAh g^{-1} after 100 charge/discharge cycles can be observed (Fig. 7e), which is much better than that in the case of the unmodified electrolyte (e.g. green trace). The significant enhancement of the electrochemical property can be primarily attributed to the interface separation between the electrode and sulphide electrolyte [215]. More importantly, the side reactions between the sulphide electrolyte and electrode active materials lead to considerable resistance at the interface with the decomposition of solid-state electrolytes during the charge/discharge cycles [229], and an ALD-deposited interface layer with an appropriate thickness may be the key process to diminish the side reactions and maintain the stable electrochemical performance [230]. It is expected that thin films prepared by the ALD technique will have potential applications in more complex 3D all-solid-state batteries.

3.1.3 Separator

Porous polyolefin separators are commonly used in batteries due to their favourable electrochemical and mechanical properties. However, polymeric separators still have two challenges: high thermal shrinkage and poor wettability towards electrolytes containing Li salts [231]. It is vital to design advanced separators with high thermal stability and improved affinity to handle these challenges. Hence, the modification of the separator by ALD has become an effective method to improve the stability of the whole battery device. Lee and his co-workers deposited an ultra-thin (10 nm) Al_2O_3 film on a commercial Celgard separator to enhance the capacity retention of the lithium-ion battery [187]. As shown in Fig. 8a, the Al_2O_3 coating layer is deposited on both sides of the Celgard separator. Experimental investigation revealed that the function of ALD Al_2O_3 is suppressing the thermal shrinkage, and this enhances the wettability of the polar electrolyte, improves the tensile strength, and correspondingly enhances the rate capability and cycle life. Figure 8b shows the cycling performance of the battery with an ALD-modified separator compared to a commercial separator. The battery with the ALD-modified separator exhibits high capacitance retention of 79.5% after 100 cycles, while the commercial Celgard separator retains only 70%. Similarly, Chen et al. [188] modified porous polypropylene (PP) membranes with ALD TiO_2 to serve as a separator for lithium-ion batteries. The SEM image in Fig. 8c shows a fully conformal deposition of ALD TiO_2, and such a conformal ultra-thin layer could overcome both the thermal

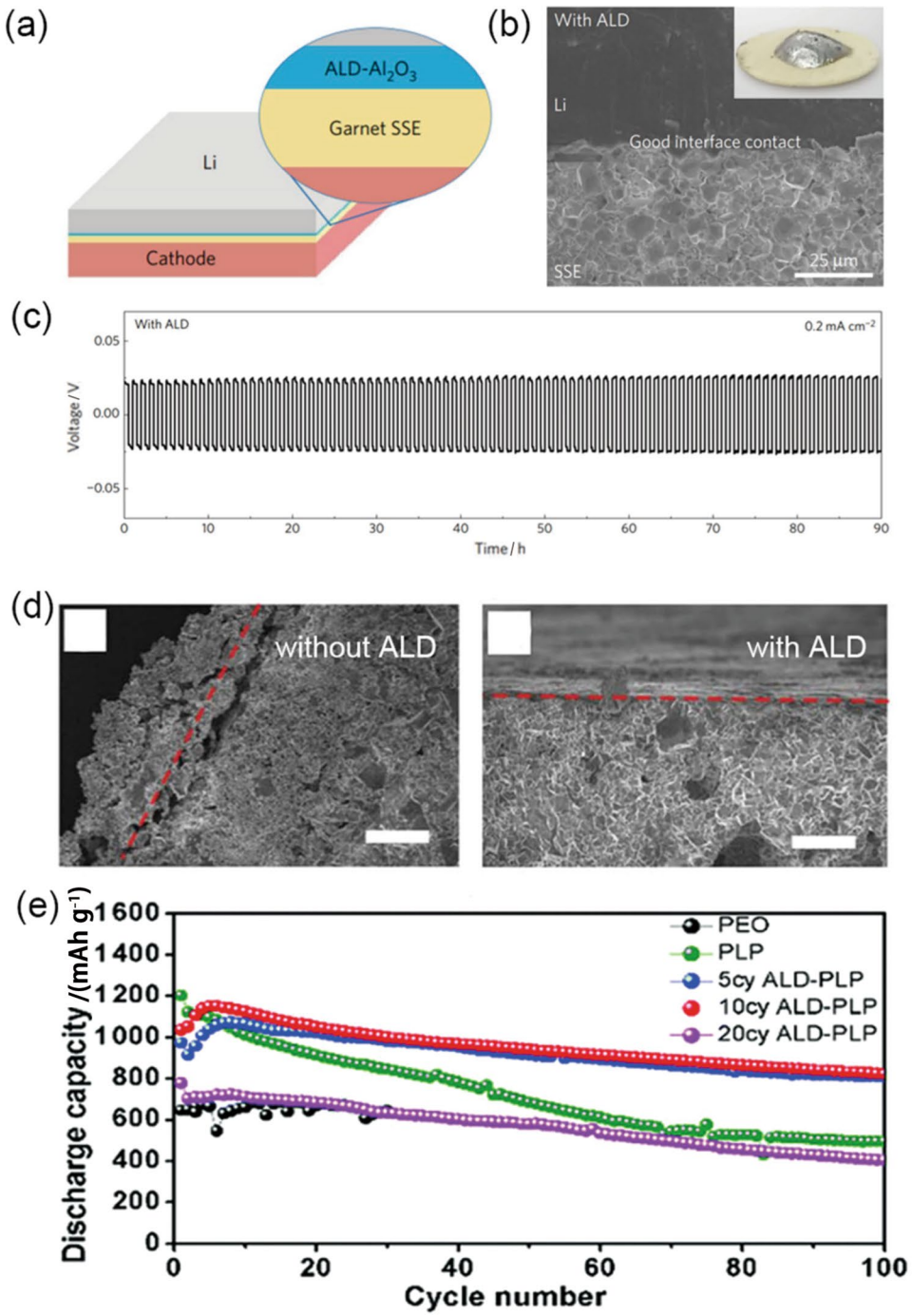

Fig. 7 **a** Schematic of the ALD Al_2O_3-modified solid-state electrolyte. **b** SEM image of the ALD Al_2O_3-coated solid-state electrolyte/Li metal interface. The inset is a photograph of melted Li on top of the garnet surface, and this demonstrates the wetting behaviour of the ALD-modified garnet surface. **c** Galvanostatic cycling performance of the battery, including the ALD Al_2O_3-coated solid-state electrolyte, at a current density of 0.2 A cm^{-2}. (**a**-**c**) are reprinted with permission from Ref. [186]. Copyright 2017, Springer Nature Limited. **d** Cross-sectional SEM images of bare LATP and ALD-modified LATP after 100 charge/discharge cycles. **e** Cycling performance of lithium-sulphur batteries with different electrolytes. Violet, red, and blue traces represent the ALD-modified electrolyte with 20, 10, and 5 ALD growth cycles, respectively, while black and green traces represent two solid-state electrolytes without ALD coating. (**d**) and (**e**) are reprinted with permission from Ref. [94]. Copyright 2018, Royal Society of Chemistry

shrinkage and poor wettability of the PP membranes. Benefitting from the improved wettability, the discharge capacities were significantly enhanced with the battery compared with the commercial PP separator (Fig. 8d).

3.2 Electrode Architecture Designed by ALD

Apart from preparing traditional nanomembranes/films for surface modification, ALD can also be used to fabricate active materials that have significant functions. Functional materials in the form of nanostructures [190–192] have been fabricated, and experimental investigations have demonstrated that they can provide the desired functions, such as high catalytic activity and outstanding capacitance [232–234]. Generally, in electrochemical energy devices, these active materials are combined with other structures to form a composite. This is because active nanostructures are typically separated and need substrates for support and

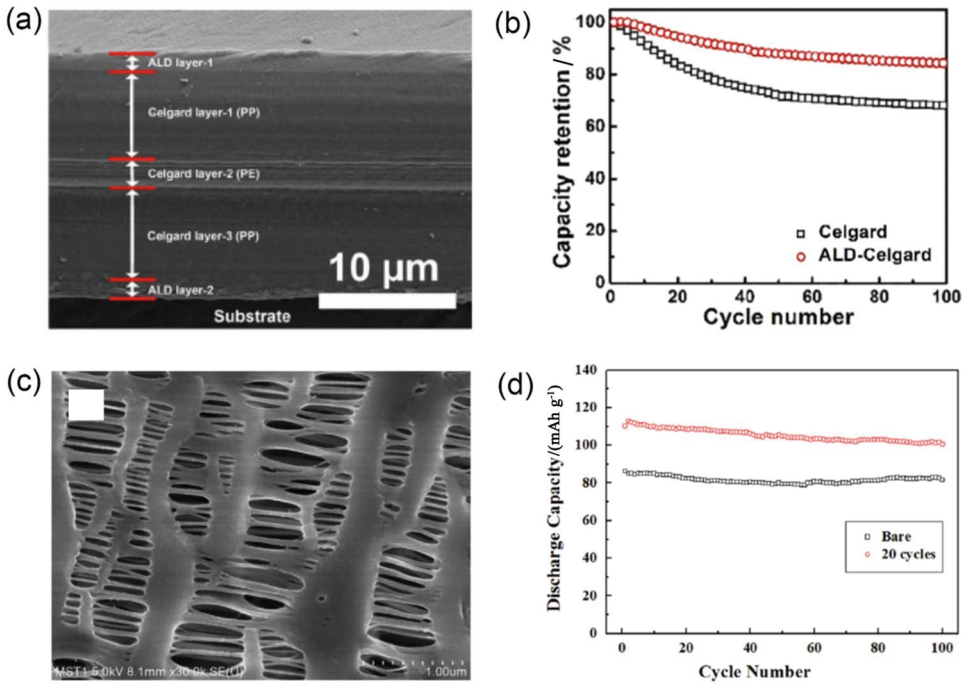

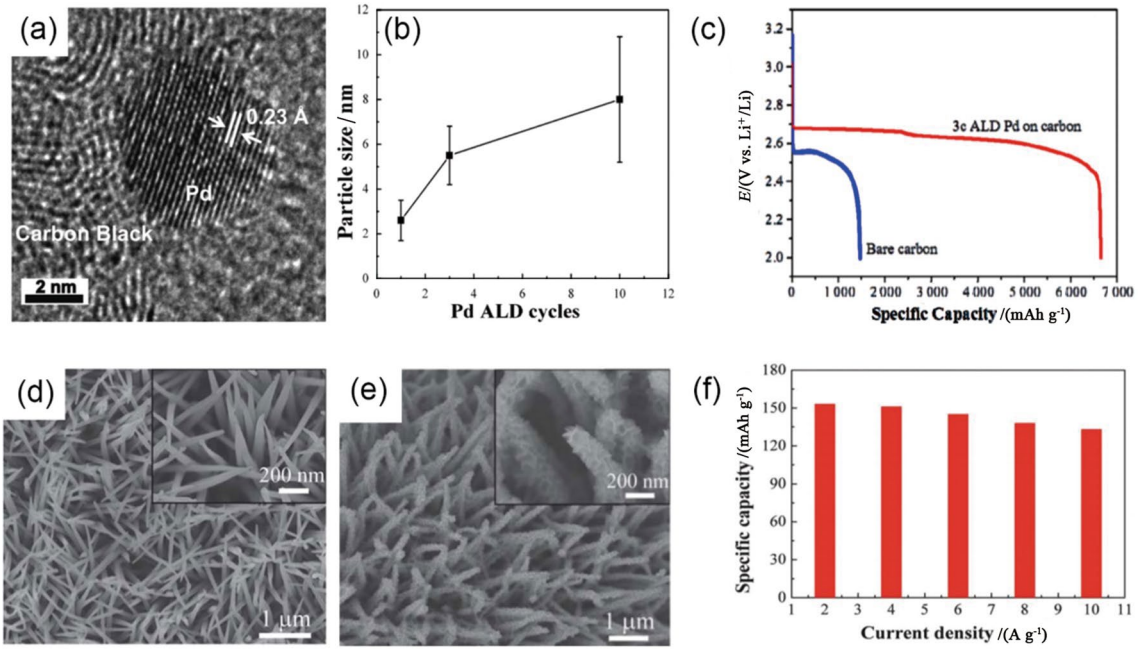

Fig. 8 **a** Cross-sectional SEM image of the ALD-modified Celgard separator. **b** Cyclic performance of the batteries based on Celgard and ALD-modified Celgard separators at 1 C for 100 cycles. (**a**) and (**b**) are reprinted with permission from Ref. [187]. Copyright 2020, John Wiley & Sons, Inc. **c** SEM image of the ALD-modified PP separator. **d** Long-term cycling performance of the batteries based on the ALD-modified PP separator and the commercial PP separator. (**c**) and (**d**) are reprinted with permission from Ref. [188]. Copyright 2014, Elsevier B.V

Fig. 9 **a** TEM image of an ALD-deposited Pd nanoparticle with a size of ~ 5.5 nm. **b** Particle size as a function of the number of ALD growth cycles. **c** Voltage profile of the first discharge for a cathode containing bare carbon (black trace) and Pd particles with 3 ALD cycles (red trace). Reprinted with permission from Ref. [190]. Copyright 2013, American Chemical Society. **d** SEM image of ALD-prepared TiO_2 hollow nanowires. **e** SEM image of NiO-coated TiO_2 hollow nanowires. The insets are the magnified image. **f** Specific capacities of the electrode made from the NiO/TiO_2 composite at different current densities. (**d**-**f**) are reprinted with permission from Ref. [247]. Copyright 2013, Royal Society of Chemistry

carrier transportation [46, 59]. The applications of composites involving ALD-prepared active materials in electrochemical energy devices have been intensively explored [235–240]. Basically, the quantity and morphology of active material in the composite are conveniently tuned by adjusting the parameters of the deposition process, and stable

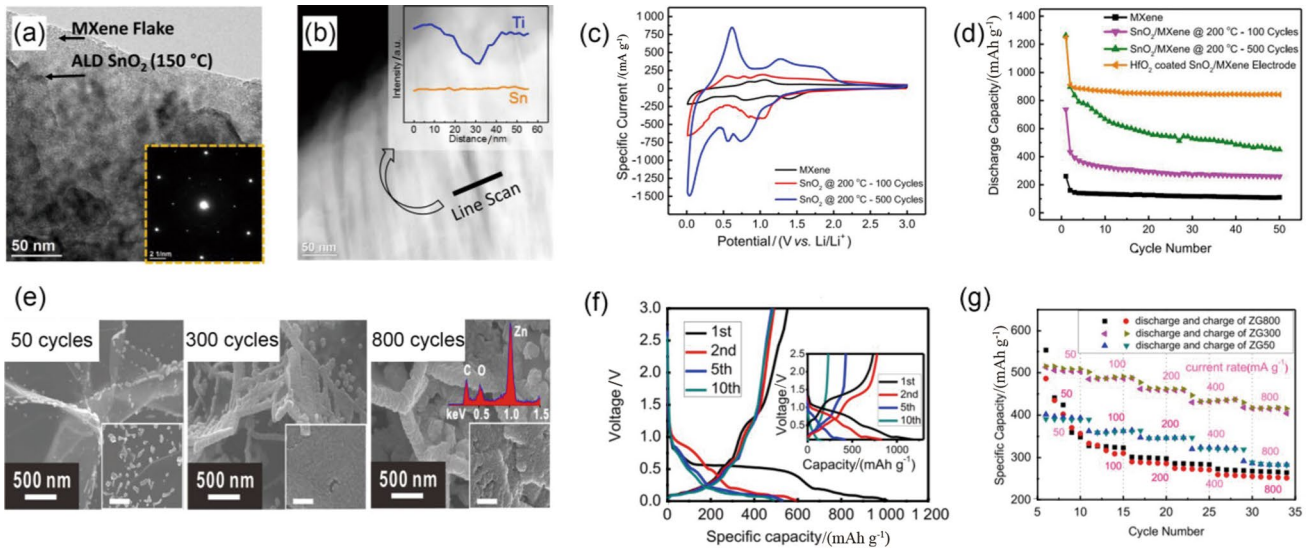

Fig. 10 **a** HRTEM of a MXene sheet coated with 50 nm ALD SnO_2 and the corresponding SAED pattern. **b** STEM image along with the EDS line scan of the composite showing the conformal SnO_2 coating. **c** The first cycle of CV at 0.2 mV s^{-1} of MXene coated with ALD SnO_2 that was generated from various ALD growth cycles. The result from pure MXene is also shown for comparison. **d** Cycling performance after 50 cycles at 500 mA g^{-1} of MXene sheets with and without the ALD SnO_2 nanomembrane. (**a**–**d**) are reprinted with permission from Ref. [248]. Copyright 2017, Elsevier B.V. **e** SEM image and enlarged image (the inset) of ALD ZnO deposited on expanded graphite with 50, 300, and 800 growth cycles. The inset is the corresponding EDS result. **f** CV curves (first three cycles) of an anode made from ALD ZnO on expanded graphite at 0.2 mV s^{-1}. The inset shows the corresponding CV results from the pure ZnO anode. **g** Rate performances of anodes made from ALD ZnO on expanded graphite with various ALD growth cycles. (**e**–**g**) are adapted with permission from Ref. [250]. Copyright 2017, American Chemical Society

composite structures with optimized performance can be obtained [241–246].

Lei et al. [190] utilized the ALD technique to deposit Pd particles on porous carbon substrates, and the composite was used as the cathode material for Li-O_2 batteries. Due to the conformal deposition of ALD, Pd particles were uniformly dispersed on the carbon support, and the substrate preserved the initial porous structure. As shown in Fig. 9a, the TEM image demonstrates a Pd particle with a size of ~ 5.5 nm, and the lattice fringes of ~ 0.23 nm are consistent with the d-spacing for the Pd [111] plane. In addition, the average size of Pd particles can be conveniently controlled by ALD cycles (Fig. 9b). As active materials, the ALD-prepared Pd particles exhibited a high capacity of 6 600 mAh g^{-1} (Fig. 9c) since the composite with nanoparticles can provide more active sites to adsorb O_2. In addition to the above particle-like structures, Xia et al. [247] proposed a novel strategy to prepare TiO_2 hollow nanowires by ALD. In the experiment, TiO_2 hollow nanowires were fabricated with the help of a self-standing $Co_2(OH)_2CO_3$ nanowire array. When the template was subsequently removed, hollow TiO_2 nanowires were obtained (Fig. 9d). A NiO coating can be further synthesized on the surface of the TiO_2 structure by a wet chemistry approach (Fig. 9e). Electrochemical characterizations demonstrate that ALD-prepared hollow TiO_2 nanowires provide considerable charge storage contributions and that the outer NiO can further enhance the capacitance of the battery. The composite exhibits a high capacity of 153 mAh g^{-1}, which is a promising result for an energy storage device (Fig. 9f).

Ahmed and his colleagues developed a method by which metal oxide nanomembranes can be deposited on two-dimensional titanium-based metal carbides and nitrides (MXenes) [248]. They employed a low temperature (150 °C) ALD technique to conformally deposit metal oxides on MXene sheets. As shown in Fig. 10a, the high-resolution TEM (HRTEM) image demonstrates that an ALD SnO_2 nanomembrane with an average thickness of 50 nm was grown on the surface of the $Ti_3C_2T_x$ MXene sheet. The layered stack of MXene flakes was well preserved under SnO_2 deposition, and the corresponding selected area electron diffraction (SAED) pattern confirms the unique hexagonal crystal structures of MXene. Since the SAED pattern of SnO_2-coated MXene exhibits no noticeable change, the SnO_2 nanomembrane prepared by ALD is amorphous. Furthermore, a scanning transmission electron microscopy (STEM) image in Fig. 10b illustrates that the layered structure of the MXene was preserved after ALD. The inset in Fig. 10b shows the EDS line scans for Sn and Ti, which clearly indicate the presence of a uniform Sn layer. In the resultant ALD SnO_2-coated MXene composite, SnO_2 had a

high theoretical capacity and provided an enhanced electrochemical property. In addition, the $Ti_3C_2T_x$ MXene substrate provided a stable structure that possesses a high electronic conductivity during the charge/discharge process. As demonstrated in Fig. 10c, the area enclosed by the CV curves of the ALD-treated MXene is much larger than that of pure MXene, indicating the advantages of the ALD technique in preparing functional composites. The cycling performance shown in Fig. 10d further illustrates the best electrochemical property of ALD SnO_2-coated MXene. The pure MXene delivered a first-cycle discharge capacity of 260 mAh g^{-1} and exhibited a stable capacity of 109 mAh g^{-1} after 50 cycles. In comparison, the SnO_2-coated MXene delivered a first-cycle discharge capacity of 736 mAh g^{-1} and exhibited a stable capacity of 258 mAh g^{-1} after 50 cycles.

More ALD oxide/carbon material composites were previously reported for high-performance batteries. Wang and his co-workers deposited ALD ZnO nanomembranes on graphene aerogels [249] and specifically controlled the composition of ZnO/graphene aerogels by changing the number of ALD cycles. Due to the high capacity of ZnO, the capacity of the composite reached 1 200 mAh g^{-1}. Similarly, Li et al. [250] developed a binder-free battery anode using expanded graphite deposited with an ALD ZnO nanomembrane as the active material (Fig. 10e). Here, the morphology of the active materials can be controlled by ALD cycles. With 50 ALD cycles, the ZnO coating shows a punctate distribution on the graphite. When the number of ALD cycles increases to 300, a uniform and smooth ZnO layer can be observed. As the number of growth cycles reaches 800, ZnO nanomembranes overlap to form a thick layer (Fig. 10e). The anode made from this ALD ZnO/expanded graphite composite exhibited high stable capacities, especially with a moderate ZnO concentration, and the highest capacity of 438 mAh g^{-1} was obtained at 200 mA g^{-1} after 500 cycles (Fig. 10f). Additionally, the capability is relatively stable, and there is almost no capacity decay (Fig. 10g). The excellent performance is attributed to the combined effect of the high capacity of the ZnO prepared by ALD and the support of the expanded graphite framework, which has a great potential in low-cost and flexible batteries.

In addition to preparing composite active materials, the ALD-prepared nanomembrane can be removed and adopted as an active material alone. For example, a sandwich-like porous carbon/ZnO/porous carbon nanosheet composite was obtained by using the ALD technique [251]. In the experiment, a ZnO nanomembrane was deposited on a sacrificial polyurethane sponge template via ALD. With the subsequent high-temperature treatment in N_2, the nanomembrane was lifted off, and evaporation and pyrolysis of the polymer material led to the formation of a porous C/ZnO/porous C composite; in this process, the ZnO layer thickness (~ 30 nm) was controlled by ALD growth cycles and was further confined between two porous carbon layers. The carbon coating layer hindered the volume change during the charge/discharge process and facilitated the transport of Li^+ into the inner ZnO layer. When serving as anodes for lithium storage, the ALD-prepared architecture enables a fast charge/discharge process, and the experimental result demonstrates a capacity of 330 mAh g^{-1} at 5 000 mA g^{-1}. Furthermore, the thickness of the ZnO functional layer can be accurately adjusted by the number of ALD cycles and can thus be used for optimization. In a similar study, Naeem et al. [192] fabricated a pristine ZnO nanomembrane-based supercapacitor electrode by utilizing free-standing ALD ZnO nanomembranes. The polymer template in the experiment was chemically removed by high-temperature annealing in O_2. The ultra-thin structure with a high surface-to-volume ratio remarkably enhanced the electrochemical properties of the supercapacitor; a large capacitance of 846 F g^{-1} and a high energy density of 42.5 Wh kg^{-1} that corresponded to the ZnO nanomembrane with 100 ALD growth cycles was observed in the experiment.

Well-designed 3D micro/nanostructures can enhance the comprehensive performance of electrochemical energy devices, and ALD was experimentally used to construct complex 3D structures and their composites [241, 252–255]. The obtained 3D micro/nanostructures can be applied widely in electrochemical energy devices. For instance, Zhao and her colleagues reported an interesting 3D architecture that was fabricated with the help of ALD for application in lithium-ion batteries [256]. In the composite structure, 3D carbon foam is used as a conductive scaffold, and a ZnO nanomembrane is wrapped on the skeleton of carbon foam as an active material to generate high capacity. More importantly, vast void volume among the architectures can accommodate large deformation, leading to great flexibility for constructing the 3D structure and corresponding electrode (Fig. 11a). During charge/discharge cycles, due to the close and uniform attachment of ZnO nanomembranes, the composite exhibits excellent structural stability. As shown in Fig. 11b, the composite exhibits an outstanding and stable electrochemical performance of 200 mA h g^{-1} at 320 mA g^{-1}, and 92% capacity was retained after 700 cycles at 2 A g^{-1} and 500 cycles at 5 A g^{-1}. This research may have significant potential applications in many fields that require high energy storage capacities. Kim et al. [257] designed and fabricated a 3D network of hollow TiO_2 nanoribbons with the assistance of ALD (Fig. 11c). The nanoribbon network was applied in the lithium-ion battery as an anode and achieved a significantly enhanced performance (Fig. 11d). These ALD-prepared nanostructures generally possess outstanding electrochemical properties, such as specific capacity, rate capability, and cyclability. It is believed that the 3D network provided effective transportation of electrons and

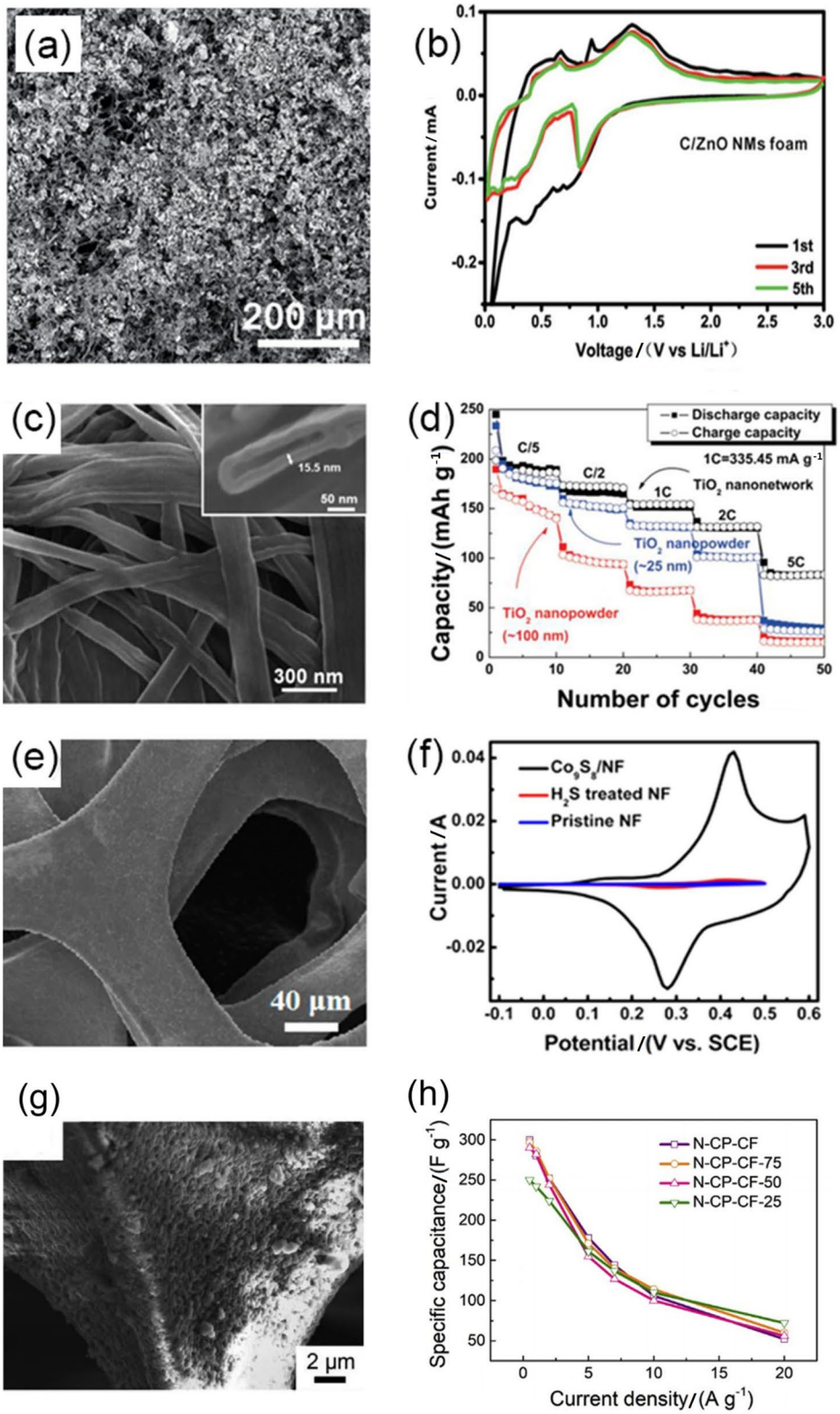

Fig. 11 **a** SEM image of the 3D ALD ZnO nanomembrane/carbon foam composite. **b** CV curves of the composite. (**a**) and (**b**) are reprinted with permission from Ref. [256]. Copyright 2018, Royal Society of Chemistry. **c** SEM image of a 3D network of the TiO_2 hollow nanoribbon network. The inset is the enlarged cross-sectional image. **d** The rate capability of the ALD TiO_2 hollow nanoribbon network (black trace) compared with the 25 nm TiO_2 nanopowders (blue trace) and 100 nm TiO_2 nanopowders (red trace). (**c**) and (**d**) are reprinted with permission from Ref. [259]. Copyright 2020, AIP Publishing LLC. **e** SEM image of the ALD Co_9S_8-coated Ni foam electrode. **f** CV curves of the ALD Co_9S_8-coated Ni foam compared with the H_2S-treated Ni foam electrode and the pure Ni foam electrode at a scan rate of 100 mV s^{-1}. (**e**) and (**f**) are reprinted with permission from Ref. [258]. Copyright 2015, American Chemical Society. **g** SEM image of the pyrolysed ZIF-8 layer on carbon foam. **h** Specific capacitances of the pyrolysed ZIF-8 layer on carbon foam under different compression rates as a function of current density. (**g**) and (**h**) are reprinted with permission from Ref. [130]. Copyright 2020, Elsevier B.V

Table 3 Studies of ALD-designed electrode architectures for energy storage devices

Materials	Substrate	Device	ALD cycles (thickness)	Capacity	Reference
Pd	Porous carbon	Li-O_2 battery	3	6 600 mAh g^{-1}	[190]
TiO_2	Ni foam	Battery	10 nm	153 mAh g^{-1}	[247]
SnO_2	MXenes	Li-ion battery	500	736 mAh g^{-1}	[248]
ZnO	Graphene aerogel	Li-ion battery	100	1 200 mAh g^{-1}	[249]
ZnO	Expanded graphite	Li-ion battery	300	438 mAh g^{-1}	[250]
ZnO	/	Li-ion battery	200	330 mAh g^{-1}	[256]
ZnO	Carbon foam	Li-ion battery	200	200 mAh g^{-1}	[256]
TiO_2	/	Li-ion battery	15 nm	154.5 mAh g^{-1}	[257]
TiO_2	$Co_2(OH)_2CO_3$	Li-ion battery	10 nm	600 mAh g^{-1}	[260]
RuO_2	CNTs	Li-ion battery	600	1 400 mAh g^{-1}	[261]
ZnO	/	Supercapacitor	100	846 F g^{-1}	[192]
TiO_2	Polymer sponge	Supercapacitor	100	2 332 F g^{-1}	[262]
Co_9S_8	Ni foam	Supercapacitor	2 000	1 645 F g^{-1}	[258]
NiO	CNTs	Supercapacitor	200	2 013 F g^{-1}	[263]
Co_3O_4	Carbon cloth	Supercapacitor	1 600	347.2 mF cm^{-2}	[232]
V_2O_5	Porous carbon	Supercapacitor	25	540 F g^{-1}	[233]
TiO_2	CNTs	Supercapacitor	200	1 364 F g^{-1}	[264]
VO_x	CNTs	Supercapacitor	100	1 550 F g^{-1}	[234]
WO_3 and TiO_2	Wafer	Supercapacitor	12 nm	625.53 F g^{-1}	[265]
ZIF-8	Carbon foam	Supercapacitor	300	300 F g^{-1}	[130]

Li ions and thus led to outstanding enhanced performance [256].

The ALD technique can also engineer supercapacitor electrodes. Li and coworkers developed a process in which ALD was used to produce a high-quality complex Co_9S_8 film with bis(N,N-diisopropylacetamidinato)cobalt(II) and H_2S as the reactants (Fig. 11e), and the film was coated on the surface of Ni foam and then engaged as a supercapacitor electrode [258]. Since Co_9S_8 is a novel and promising electrochemically active material, the ALD-prepared electrode exhibits remarkable electrochemical performance, such as high specific capacitance, outstanding rate performance, and excellent cycling performance. As shown in Fig. 11f, the performance of the ALD-prepared electrode is substantially improved compared with that of pristine Ni foam and Ni foam pretreated by H_2S. It is worth noting that such a one-pot process makes this strategy promising and available in actual industry.

MOF-based composites that are fabricated by using ALD oxide as a reactant also have advantageous applications in the field of high-performance flexible supercapacitors [130]. For example, a zeolitic imidazolate framework-8 (ZIF-8) film was successfully prepared on flexible carbon foam by using ALD ZnO as the reactant for the induction effect. With the following carbonization process, a flexible carbon framework with a hierarchically porous structure was obtained (Fig. 11g). The resultant composite exhibited a large specific surface area of 538 m^2 g^{-1} and a large specific capacitance of 300 F g^{-1}. Great flexibility was demonstrated, as a stable electrochemical performance was maintained under severe and repeated compression cycles (Fig. 11h).

As a summary of Sect. 3.2, recent studies regarding the ALD-designed electrode architecture of energy storage devices are summarized in Table 3.

4 Moving Towards Industrialization

For future practical applications of electrochemical energy-related devices, industrial manufacturing is necessary. It was reported that between 2013 and 2014, a total of 65 500 t LIBs were consumed in Europe [266]. This indicates that if ALD is being incorporated in the manufacturing of energy devices with enhanced performance for surface coating, nanostructure fabrication, or reactant/seed layer deposition, the process should meet the requirements of industrialization and commercialization, and high throughput and low cost are considered to be important prerequisites. It is worth noting that both the strong and weak points of ALD technology are apparent. A well-known feature of ALD is its self-limiting ability of precursor chemisorption that occurs on the substrate

surface and sequential reactions [267]. Thus, in most cases, ALD provides accurate control of thickness in the sub-nanometre range. The corresponding near-equal growth-per-cycle values for identical precursors in different equipment are also suitable for transferring the technology/process [267, 268]. In addition, ALD is capable of depositing materials onto complex structures with excellent conformality. This is quite meaningful for the electrochemical energy industry because electrodes with porous structures and large surface areas are common. Compared with other deposition techniques, ALD can create layers that conform extremely well to the substrate topography, in which identical thicknesses are deposited on the tops, sides, and bottoms; therefore, an enhanced and stabilized performance can be expected. Despite these advantages, ALD is still only recognized as the leading emerging technology in the industry, and other deposition techniques, such as conventional chemical vapour deposition and physical vapour deposition, are more popular. Compared with those deposition techniques, the major drawback of ALD is the low deposition rate due to layer-by-layer deposition. The uniform deposition of the materials in both the desired substrate and the chamber also leads to severe precursor waste. It is believed that more than half of the energy and concomitant labour are wasted in most ALD processes [269, 270]. The low deposition rate also has a negative effect on cost-effectiveness, which has also become a major drawback for commercial manufacturing. Scientists and engineers have developed several approaches to eliminate these constraints, and the progress will be reviewed in the following parts.

4.1 Thermal and Plasma-Enhanced ALD

The ALD process is based on the half-reaction cycles. Studies have demonstrated that chemical reactions in the ALD process can be activated by thermal energy or plasma enhancement [267]. Although both mechanisms are commonly used, the term ALD usually refers to thermal ALD. Plasma-enhanced ALD or plasma-assisted ALD involves plasma species with a high reactivity, which leads to reduced chamber temperature and shorter deposition time while maintaining the quality of the film [271, 272]. This enhances the throughput since more substrates can be deposited and may be particularly meaningful for coating electrochemical energy materials with temperature sensitivity. Plasma-enhanced ALD also broadens the spectrum of materials that are either challenging or inaccessible in the normal thermal ALD process, and the increased purity of the deposited materials therein should be of importance for practical devices. ASM and Tokyo Electron Limited have provided plasma-enhanced ALD systems with capacitively coupled plasmas for industrial applications, while Oxford Instruments, Veeco, and Picosun have supplied plasma-enhanced ALD setups with inductively coupled plasma for research. Microwave electron cyclotron resonance may also be utilized to generate plasma for plasma-enhanced ALD. In a typical system, the key of equipment design is to obtain a high flux of plasma species on the surface of the substrate. To control the flux, three typical classes, direct plasma, remote plasma, and radically enhanced plasma, are commonly adopted in deposition systems [106, 272]. In direct plasma, the substrate is placed in the central plasma zone and is involved in plasma generation. For remote plasma, the substrate is positioned outside of the central plasma zone. Altering the experimental parameters can tune the flux of species towards the substrate. In the case of radical-enhanced plasma, only the radicals generated in the plasma have a sufficient lifetime to reach the substrate, and the term remote plasma is also used in some cases. To date, some successes have been obtained for plasma-enhanced ALD with promoted throughput, and there are still noteworthy challenges for future industrialization. The nature of the plasma makes predicting what happens in the reaction during the deposition process very complex, and surface recombination is considered a challenge for conformality. In addition, although the energy of the flux is low, ions in the plasma may still damage the substrate due to the sputtering effect [273, 274]. It is not easy to understand the exact roles of radicals, ions, electrons, and photons in plasma. Moreover, due to the complexity of the plasma-enhanced ALD process, it is difficult to perform process optimization, and more future work is needed. Since the throughput of current plasma-enhanced ALD systems is still insufficient for many industrial manufacturing processes, modified designs in plasma sources and reactors may be necessary [275]. Mass production of electrochemical energy devices such as batteries will undoubtedly benefit from the corresponding enhanced throughput.

4.2 Area-Selective ALD System

ALD typically leads to uniform deposition on the entire sample surface. For practical device fabrication, the material needs to be patterned into different geometries, and specific areas of the electrode may need modification for commercial production. However, this is difficult to achieve in the traditional ALD process since the lateral arrangements of atoms often cannot be controlled [276], and patterning can only be realized with post-treatment, as mentioned in Sect. 2.3. It is well known that the ALD process strongly depends on the surface chemistry of the substrate, as growth initiation is closely related to the surface status. Therefore, it is feasible to implement area-selective deposition during the initial ALD cycles when nucleation is delayed in some areas compared with other areas [277–279]. In contrast to

the standard patterning technique that requires a physical mask, area-selective ALD can be considered a "chemical" patterning method [280]. To implement the area-selective ALD process, the definition of the growth and non-growth areas may be realized with the assistance of electron/ion beams, self-assembled monolayers, or polymer resists [281]. Although the approach is not widely involved in electrochemical energy, the capability of area-selective ALD in fabricating devices, core–shell structure/embedded structure, and interesting 3D structure suggests that the technique will have great potential once it is industrialized.

There are several challenges that areas-selective ALD is still facing, and more research and development efforts are needed. The first challenge is the lateral broadening of the growth area, which is due to the isotropic growth nature of the ALD [282]. The second challenge is the insufficient selectivity, which means that unwanted growth occurs in the non-growth area [276], and this may significantly influence the device performance. The selectivity can be evaluated by the difference in the material deposited in the growth and non-growth areas. Selectivity can be conventionally achieved by means of selective precursor adsorption [283]. However, the non-growth area may change in the reactor when it is exposed to the precursor and co-reactant or high temperature [284], which finally leads to the loss of selectivity. The introduction of correction steps, including functionalization steps and selective etching steps during the area-selective ALD process, was reported to be able to promote selectivity [276]. Nevertheless, this increases the cycle time, leading to low productivity. In addition, the use of correction steps is process-specific and lacks a general strategy. A combination of area-selective ALD and other techniques, such as plasma enhancement, can be used for optimization.

4.3 Typical Configurations Towards Industrial Manufacturing

Industrial manufacturing emphasizes the throughput and productivity of processes. As mentioned above, plasma has been employed to enhance productivity. In addition, with the aim of promoting throughput, researchers have invented various system configurations to meet the requirements of mass production.

4.3.1 Batch ALD System

A typical ALD reactor can only process one single wafer or a small number of samples at a time. Designing ALD systems with larger reactors could be an option for higher throughputs [275]. Companies such as Beneq, ASM, and Picosun all launched such products. The so-called batch ALD system that is equipped with a large hot-wall reactor can process up to 125 parallel wafers. Vertical and horizontal reactors are two major configurations of such ALD systems and are distinguished by the different precursor inlet positions. A batch ALD system has a longer overhead time because the large chamber leads to a longer pump-down step and heat-up step. However, the overhead time per wafer can be as low as 10–20 s, which leads to much higher productivity and the possibility of mass production [285]. The cost-per-wafer is also calculated to be lower even if the space and the price of the batch ALD system are taken into consideration [271]. However, it was noted that for such ALD systems, there are still challenges that need to be addressed in industrial manufacturing. A lack of understanding regarding the influence of the gas-phase profile in the case of the complex geometry of the reactor and a large number of wafers is a critical problem [286]. The corresponding thickness non-uniformity, poor conformality, and particle specs are

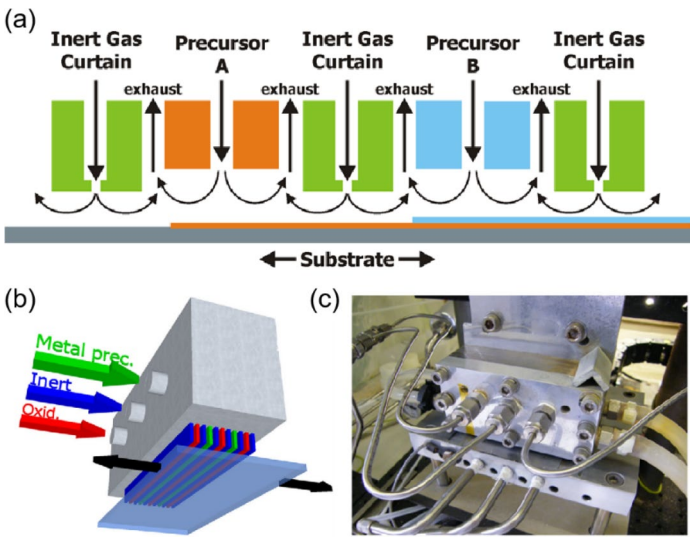

Fig. 12 **a** Concept of spatial ALD, in which the precursor half-reaction regions are physically separated by inert gas. (**a**) is reprinted with permission from Ref. [293]. Copyright 2012, AI P Publishing LLC. **b** 3D scheme of the spatial ALD setup. **c** Photo of actual equipment. (**b**) and (**c**) are reprinted with permission from Ref. [298]. Copyright 2013, John Wiley & Sons, Inc.

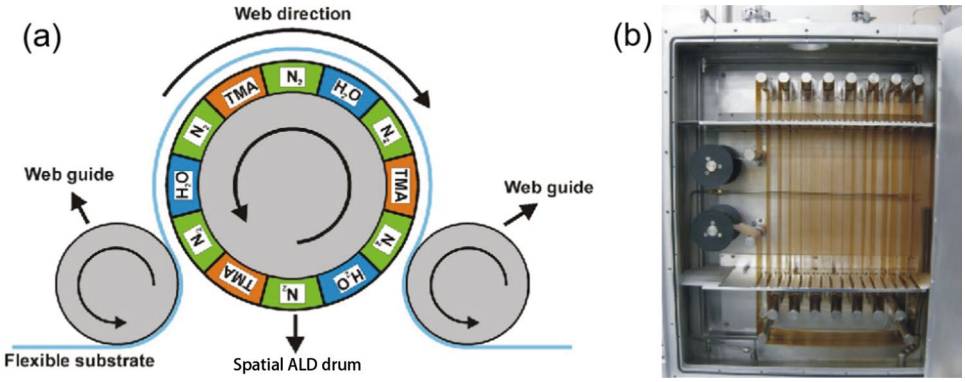

Fig. 13 **a** Schematic of a roll-to-roll spatial ALD. **b** Photograph of a roll-to-roll spatial ALD reactor, which was designed by Lotus Applied Technology. (**a**) and (**b**) are reprinted with permission from Ref. [293]. Copyright 2012, AI P Publishing LLC

noted by the researchers. For such a large system with a long processing time, tests exploring the optimal conditions also require high costs [275]. On-line controllers integrated with run-to-run control schemes are considered to reduce batch-to-batch variation and process disturbances [287]. Optimization via theoretical simulation might be another solution, and many efforts have been made in this regard [288–292]. To enhance the throughput of the ALD process and avoid the drawbacks mentioned above, multi-chamber single-wafer platforms have recently been developed [271], and these platforms provide an additional option for mass production.

4.3.2 Spatial ALD System

Batch processing is not always compatible with in-line processes [273, 293]. Even using a reactor may hinder device fabrication in the industry since flow line production is always preferred. New approaches to implement ALD for mass production have been proposed and explored to achieve a high throughput and low cost. Traditional ALD is developed on a temporal process in which the precursors are sequentially dosed into a chamber and are separated in time by a purge step to achieve the reaction and deposition. In a spatial ALD, the precursors are supplied continuously but in different regions (Fig. 12a), and the precursor regions are separated in space or by purge regions. The substrate remains in the first precursor region for a sufficiently long period, and a saturated monolayer forms in the precursor. The substrate is then moved to the second precursor region to finish one ALD cycle, and one monolayer of designed material is deposited. The process can be repeated for thicker films. In this deposition process, the half-reactions are spatially and physically separated; therefore, the process is called spatial ALD. This idea was first created in 1977 [294, 295] and then developed in recent decades. In addition to the compatibility with the flow line production, another major advantage here is that the purge steps, which are time-consuming in conventional ALD, become obsolete. The deposition rate is mainly limited by the time necessary for the movement between different half-reaction regions since the time scale of chemical reactions is generally in the range of a few milliseconds for flat substrates [293]. Therefore, it was reported that spatial ALD is much faster (up to > 10) than typical ALD [296]. In addition, the deposition of materials on the wall of the reactor leads to precursor waste, and the purge step in the normal ALD removes the surplus precursor. Thus, the low utilization efficiency of the chemicals in the process leads to increased cost. In contrast, a remarkable reduction in precursor consumption and cost can be expected in the spatial ALD since the precursors are spatially separated and no purge step is required. Because there is no deposition on the reactor wall, the precursor waste is further reduced. Several designs have been reported that implement the spatial ALD process. The following are typical examples: (1) a design involving a translating gas source head or substrate that moves horizontally back-and-forth (as schematically demonstrated in Fig. 12b and c) [293, 297, 298]; (2) a design involving a substrate spinning underneath a gas source head [299]; and (3) a rotating cylinder design [300, 301]. Although spatial ALD may be limited in preparing complex materials or coating porous structures [302], due to its high throughput and processing cost, spatial ALD has been intensively investigated and has become one of the fastest developing areas in the industrial deposition of materials. ALD has the potential to become a commercialized manufacturing technique that can be mass produced in the industrial fields of energy, electronics, etc.

Combining plasma and spatial ALD could further increase the deposition efficiency. The so-called plasma spatial ALD was first demonstrated more than 10 years ago, and thus far, several companies have provided such systems. However, for plasma spatial ALD, high pressure is considered to be suitable for isolating the precursor regions, while the optimal plasma pressure may be relatively low. In such a case, additional plasma control is necessary. To solve this contradiction, spatial ALD that utilizes atmospheric pressure plasma has been developed, in which surface dielectric barrier discharge plasmas are used [303–308]. Nevertheless,

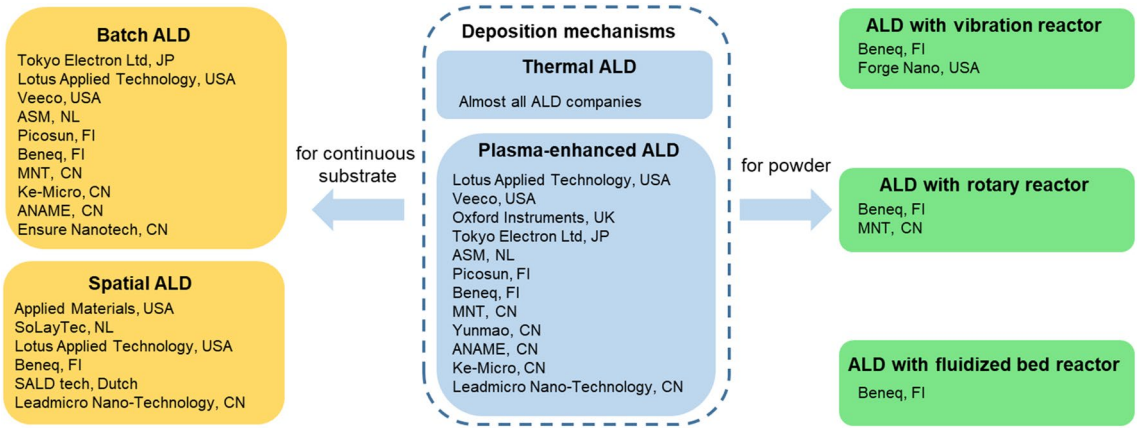

Fig. 14 Typical ALD techniques and systems with the possibility of industrialization and the related companies

for the industrial application of this idea, further optimization is necessary.

For flexible substrates, Lotus Applied Technology and Veeco designed spatial ALD setups for roll-to-roll purposes [293]. The principle of a typical roll-to-roll spatial ALD for Al_2O_3, which was developed by TNO, is demonstrated in Fig. 13a [293]. The reactor consists of a central drum that contains combinations of trimethylaluminium (TMA) and water regions, and nitrogen gas bearings separate the precursor regions. The flexible substrate is then pulled over this drum, and the gas bearing ensures that there is a fixed space (tens to hundreds of micrometres) between the substrate and the drum. When the flexible substrate is moved over the drum, spatial ALD is realized, and the thickness of deposition is determined by the number of half-reaction region pairs that the substrate passes. It is worth noting that the deposition rates can be further increased if the drum is rotated in the opposite direction. In addition to the high efficiency, the advantage of the roll-to-roll spatial ALD concept is that there is no mechanical contact between the substrate and the reactor, and this minimizes contamination. A photograph of a roll-to-roll spatial ALD system is exhibited in Fig. 13b, and such equipment can be used for the industrial coating of electrodes of electrochemical energy devices.

4.3.3 ALD System for Powder/Particles

Many electrode materials are in the form of powders or particles. Coating onto particles via ALD is another emergent field and will inevitably be applied in industrial manufacturing. However, interparticle attractive forces cause agglomeration [309], thus conformal coating is nearly impossible. In a typical reactor, most of the particles remained uncoated since there was no accessible path for the precursor to reach all the surfaces. ALD under atmospheric pressure in a fluidized bed reactor was then developed to solve this problem. Acoustic waves, mechanical vibrations, magnetic fields, and electric fields could be used to improve particle fluidization [309–312]. However, the precursor utilization rate is significantly influenced as the gas fluidization dilutes the reactants [313], making the process uneconomical. To efficiently use precursors, a rotary reactor was developed, and longer precursors residence times for conformal coating on particles were achieved [314]. The cost of such a reactor is lower than that for other reactors [314], and some companies, such as MNTs, have already patented the idea and configuration of such an ALD system. However, a detailed analysis indicated that small agglomerates are formed in rotary reactors [315]. On the other hand, the assistance of centrifugal force in a fluidized bed was found to reduce agglomerate sizes and the required dosing time [316]. Nevertheless, homogeneous ALD coating on particles, especially those with irregular and porous surfaces, is still challenging. A better understanding of the dynamics is needed for future industrialization. For productivity enhancement, combining a specifically designed reactor with the idea of spatial and physical separation of precursor regions could be a good idea, and companies such as Forge Nano have already made good progress.

4.4 Available Systems and Future Development

Figure 14 summarizes the possible industrialized ALD techniques and systems, based on public information, and the companies that provide corresponding systems/equipment or are developing related techniques are also listed. Generally, there are two ALD mechanisms, i.e. thermal ALD and plasma-enhanced ALD, for material deposition, while plasma-enhanced ALD has a higher deposition rate

and should be more acceptable for industrial manufacturing. To further enhance the throughput, researchers invented different ALD system configurations. For deposition on a wafer-like continuous substrate, spatial ALD (including the roll-to-roll configuration for the flexible substrate) and batch ALD can be employed. They can be used to deposit functional materials and to modify the electrodes of energy devices. Deposition on solid-state electrolytes and separators can also be realized in such systems. On the other hand, many raw active materials for electrochemical energy devices are in the form of powder/particles, which can hardly be used as deposition substrates in a regular ALD system, as agglomeration makes it impossible to achieve uniform deposition on all surfaces. Researchers then invented ALD systems with fluidized bed reactors, vibration reactors, and rotary reactors, which effectively disperse the particles to expose all the surfaces. After deposition, the modified particles can be handled according to the normal procedure for electrode preparation. The introduction of plasma enhancement in all these systems should further enhance productivity. However, many developments are still in progress, especially the combination of plasma with the ALD system for powder. Future industrialization of the ALD technique in electrochemical energy should involve optimizing the current techniques and/or combining the existing approaches to reduce the waste of the precursor and the consumption of energy. Together with the increased deposition rate and productivity, the cost of ALD for industrial manufacturing could be reduced significantly. Accurately controlling the thickness and morphology also provides the possibility of investigating the structure–property relationship for device optimization, and higher performances should be obtained even in mass production. In addition, the future development of new techniques can accelerate the industrialization of ALD in the electrochemical energy field. Since these developments are primarily technique-related, many researchers from companies are now working on these areas.

5 Summary and Outlook

In this review, recent progress regarding ALD application in electrochemical energy devices is summarized, and the main content is demonstrated in Fig. 15. ALD with a thermal activation or plasma enhancement mechanism is conventionally an important gas-phase thin film deposition technique that can produce conformal coatings on the surface of the substrate. With developments in recent decades, deposition processes for many materials, including oxides, nitrides, sulphides, carbides, and elementary metals, have been explored, confirming the remarkable conveniences that come with the expansion of ALD applications in the electrochemical energy field (e.g. batteries, supercapacitors, electrocatalysis, etc.), and the compositional and structural designs of ALD are delicate. First, ultra-thin deposition from the self-limiting nature of the ALD process is crucial for surface modifications. Thus, the performance of the energy devices can be enhanced by properly optimizing the unit interface. Second, in addition to film deposition, ALD is capable of fabricating functional materials with nanoscale structures. Combined with the versatility of the materials, nanostructures with large surface areas were employed as

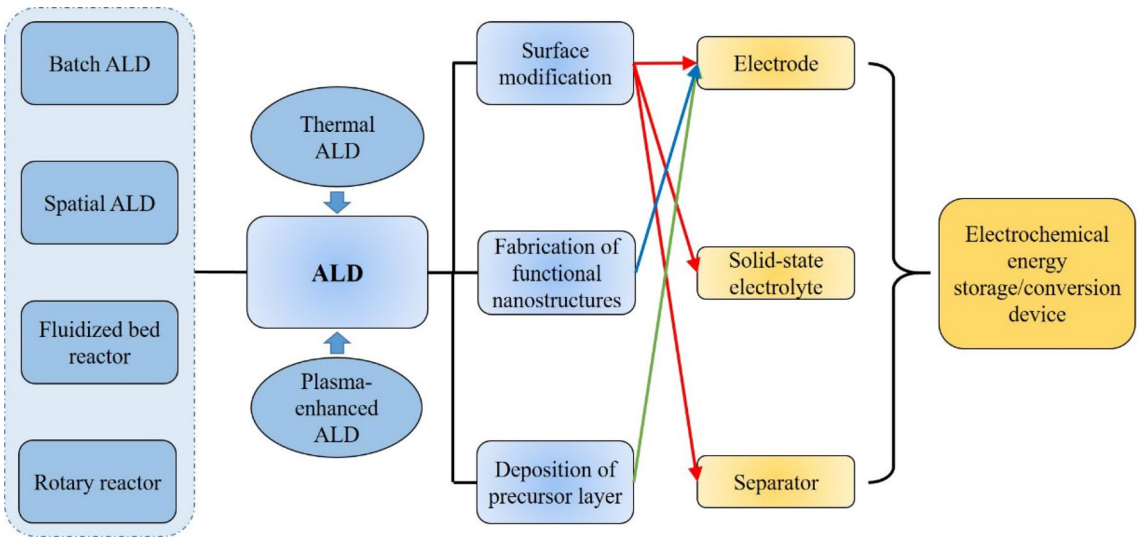

Fig. 15 Diagram showing the mechanisms and configurations of ALD and its possible applications in electrochemical energy (storage/conversion) devices

key components, such as electrodes. Third, with appropriate posttreatment, the film deposited by ALD can be used as a reactant or seed layer to guide the growth of other materials in the form of a uniform film. Typical examples are MOFs and TMDs, which are widely used in the electrochemical energy field. Moreover, although most of these studies are still in the laboratory, we also consider the future mass production of the materials and structures by ALD to have great potential, since there is a very large and increasing demand for electrochemical energy devices in human society. Aiming to meet the requirements of industrialization, researchers have explored new possibilities for enhancing the throughput and reducing the cost, and several new ALD system configurations have been developed. For instance, as shown in Fig. 15, a large reactor directly promotes throughput (i.e. batch ALD system), while spatial ALD with a completely different concept can also be suitable for mass production. A spatial ALD system integrated with a roll-to-roll configuration could deposit materials on a flexible substrate in a way that is compatible with flow line production. With the modified reactors (e.g. fluidized bed reactor and rotary reactor), ALD has been made compatible with powder coating, and this may be promising in preparing raw electrode materials.

It is worth noting that, except for the typical deposition on a flat substrate, the investigation of ALD on complex substrates for producing novel nanostructures is still insufficient. Understanding the mechanism and kinetics in these cases is mostly not comprehensive. For the future of ALD on electrochemical energy, more materials and structures should be explored. By introducing new precursors and applying multiple binary ALD processes of different materials into a supercycle or the co-dosing process, ALD gains the capability of atomic level design and can control various multicomponent materials. The performance of these newly created materials and structures should be systematically evaluated to establish a database for further optimization.

For the industrialization of ALD, the possibility of incorporating ALD with faster deposition rates, design flexibility, and easy scalability makes spatial ALD promising and attractive for energy-related applications in the coming years. The combination of spatial ALD and roll-to-roll configuration is widely accepted as the most important pathway for industrial mass production. However, ALD on particles/powders, which is not compatible with roll-to-roll processing, should also be intensively explored because many energy materials have a powder form. Above all, there is a significant amount of work to be done to scale up the manufacturing process either by combining existing techniques or by developing new ones, and active collaboration between academia and industry is necessary to drive future innovations. There is no doubt that ALD has a bright future in the electrochemical energy field.

Acknowledgements This work is supported by the Natural Science Foundation of China (No. 51961145108, 61975035, and 51850410502) and the Science and Technology Commission of Shanghai Municipality (No. 21142200200, 19XD1400600, 20501130700, and 19JC1415500).

Declarations

Conflict of interest The authors declare no conflict of interest.

References

1. Zhu, Y., Murali, S., Stoller, M.D., et al.: Carbon-based supercapacitors produced by activation of graphene. Science **332**, 1537–1541 (2011). https://doi.org/10.1126/science.1200770
2. Dunn, B., Kamath, H., Tarascon, J.: Electrical energy storage for the grid: a battery of choices. Science **334**, 928–935 (2011). https://doi.org/10.1126/science.1212741
3. Hu, C.G., Xiao, Y., Zou, Y.Q., et al.: Carbon-based metal-free electrocatalysis for energy conversion, energy storage, and environmental protection. Electrochem. Energy Rev. **1**, 84–112 (2018). https://doi.org/10.1007/s41918-018-0003-2
4. Li, Y.H., Li, Q.Y., Wang, H.Q., et al.: Recent progresses in oxygen reduction reaction electrocatalysts for electrochemical energy applications. Electrochem. Energy Rev. **2**, 518–538 (2019). https://doi.org/10.1007/s41918-019-00052-4
5. Zhang, X., Chen, A., Zhong, M., et al.: Metal–organic frameworks (MOFs) and MOF-derived materials for energy storage and conversion. Electrochem. Energy Rev. **2**, 29–104 (2019). https://doi.org/10.1007/s41918-018-0024-x
6. Fan, L.L., Li, M., Li, X.F., et al.: Interlayer material selection for lithium-sulfur batteries. Joule **3**, 361–386 (2019). https://doi.org/10.1016/j.joule.2019.01.003
7. Burschka, J., Pellet, N., Moon, S.J., et al.: Sequential deposition as a route to high-performance perovskite-sensitized solar cells. Nature **499**, 316–319 (2013). https://doi.org/10.1038/nature12340
8. Liu, S.L., Zhao, Z., Jin, L., et al.: Nitrogen-doped carbon networks with consecutive conductive pathways from a facile competitive carbonization-etching strategy for high-performance energy storage. Small **18**, 2104375 (2022). https://doi.org/10.1002/smll.202104375
9. Liu, C., Li, F., Ma, L.P., et al.: Advanced materials for energy storage. Adv. Mater. **22**, E28–E62 (2010). https://doi.org/10.1002/adma.200903328
10. Goodenough, J.B., Park, K.S.: The Li-ion rechargeable battery: a perspective. J. Am. Chem. Soc. **135**, 1167–1176 (2013). https://doi.org/10.1021/ja3091438
11. Armand, M., Tarascon, J.M.: Building better batteries batteries. Nature **451**, 652–657 (2008). https://doi.org/10.1038/451652a
12. Cortright, R.D., Davda, R.R., Dumesic, J.A.: Hydrogen from catalytic reforming of biomass-derived hydrocarbons in liquid water. Nature **418**, 964–967 (2002). https://doi.org/10.1038/nature01009
13. Dresselhaus, M.S., Thomas, I.L.: Alternative energy technologies. Nature **414**, 332–337 (2001). https://doi.org/10.1038/35104599
14. Hu, C.G., Xiao, Y., Zou, Y.Q., et al.: Carbon-based metal-free electrocatalysis for energy conversion, energy storage, and environmental protection. Electrochem. Energy Rev. **1**, 238–238 (2018). https://doi.org/10.1007/s41918-018-0005-0
15. Lai, J.P., Chao, Y.G., Zhou, P., et al.: One-pot seedless aqueous design of metal nanostructures for energy electrocatalytic

applications. Electrochem. Energy Rev. **1**, 531–547 (2018). https://doi.org/10.1007/s41918-018-0018-8
16. Wang, X.R., Tan, G.Q., Bai, Y., et al.: Multi-electron reaction materials for high-energy-density secondary batteries: current status and prospective. Electrochem. Energy Rev. **4**, 35–66 (2021). https://doi.org/10.1007/s41918-020-00073-4
17. Qian, H., Xu, S., Cao, J., et al.: Air pollution reduction and climate co-benefits in China's industries. Nat. Sustain. **4**, 188–188 (2021). https://doi.org/10.1038/s41893-021-00683-w
18. Cortés-Arriagada, D., Villegas-Escobar, N., Ortega, D.E.: Fe-doped graphene nanosheet as an adsorption platform of harmful gas molecules (CO, CO_2, SO_2 and H_2S), and the co-adsorption in O_2 environments. Appl. Surf. Sci. **427**, 227–236 (2018). https://doi.org/10.1016/j.apsusc.2017.08.216
19. Nandanwar, S.U., Coldsnow, K., Utgikar, V., et al.: Capture of harmful radioactive contaminants from off-gas stream using porous solid sorbents for clean environment: a review. Chem. Eng. J. **306**, 369–381 (2016). https://doi.org/10.1016/j.cej.2016.07.073
20. Lu, R.F., Meng, Z.S., Rao, D.W., et al.: A promising monolayer membrane for oxygen separation from harmful gases: nitrogen-substituted polyphenylene. Nanoscale **6**, 9960–9964 (2014). https://doi.org/10.1039/c4nr02315c
21. Britt, D., Tranchemontagne, D., Yaghi, O.M.: Metal-organic frameworks with high capacity and selectivity for harmful gases. Proc. Natl. Acad. Sci. U. S. A. **105**, 11623–11627 (2008). https://doi.org/10.1073/pnas.0804900105
22. Meinshausen, M., Meinshausen, N., Hare, W., et al.: Greenhouse-gas emission targets for limiting global warming to 2 °C. Nature **458**, 1158–1196 (2009)
23. Lou, S., Zhao, Y., Wang, J., et al.: Ti-based oxide anode materials for advanced electrochemical energy storage: lithium/sodium ion batteries and hybrid pseudocapacitors. Small **15**, e1904740 (2019). https://doi.org/10.1002/smll.201904740
24. Gentili, V., Brutti, S., Hardwick, L.J., et al.: Lithium insertion into anatase nanotubes. Chem. Mater. **24**, 4468–4476 (2012). https://doi.org/10.1021/cm302912f
25. Li, Y., Pizer, W.A., Wu, L.: Climate change and residential electricity consumption in the Yangtze River Delta. China. Proc. Natl. Acad. Sci. U. S. A. **116**, 472–477 (2019). https://doi.org/10.1073/pnas.1804667115
26. Dalton, R.: Good times for green energy. Nature **443**, 743–743 (2006)
27. Service, R.F.: Another biofuels drawback: the demand for irrigation. Science **326**, 516–517 (2009). https://doi.org/10.1126/science.326_516
28. Ding, Y.L., Cano, Z.P., Yu, A.P., et al.: Automotive Li-ion batteries: current status and future perspectives. Electrochem. Energy Rev. **2**, 1–28 (2019). https://doi.org/10.1007/s41918-018-0022-z
29. Lu, J., Chen, Z.W., Pan, F., et al.: High-performance anode materials for rechargeable lithium-ion batteries. Electrochem. Energy Rev. **1**, 35–53 (2018). https://doi.org/10.1007/s41918-018-0001-4
30. Reddy, M.V., Subba Rao, G.V., Chowdari, B.V.: Metal oxides and oxysalts as anode materials for Li ion batteries. Chem. Rev. **113**, 5364–5457 (2013). https://doi.org/10.1021/cr3001884
31. Simon, P., Gogotsi, Y., Dunn, B.: Where do batteries end and supercapacitors begin? Science **343**, 1210–1211 (2014). https://doi.org/10.1126/science.1249625
32. Augustyn, V., Come, J., Lowe, M.A., et al.: High-rate electrochemical energy storage through Li^+ intercalation pseudocapacitance. Nat. Mater. **12**, 518–522 (2013). https://doi.org/10.1038/nmat3601
33. Wan, K.N., Liu, S.L., Zhang, C., et al.: Supramolecular assembly of 1D pristine carbon nanotubes and 2D graphene oxides into macroscopic all-carbon hybrid sponges for high-energy-density supercapacitors. ChemNanoMat **3**, 447–453 (2017). https://doi.org/10.1002/cnma.201700037
34. Liu, M., Johnston, M.B., Snaith, H.J.: Efficient planar heterojunction perovskite solar cells by vapour deposition. Nature **501**, 395–398 (2013). https://doi.org/10.1038/nature12509
35. Lee, M.M., Teuscher, J., Miyasaka, T., et al.: Efficient hybrid solar cells based on meso-superstructured organometal halide perovskites. Science **338**, 643–647 (2012). https://doi.org/10.1126/science.1228604
36. Jacobson, M.Z., Delucchi, M.A.: Providing all global energy with wind, water, and solar power, Part I: Technologies, energy resources, quantities and areas of infrastructure, and materials. Energy Policy **39**, 1154–1169 (2011). https://doi.org/10.1016/j.enpol.2010.11.040
37. Díaz-González, F., Sumper, A., Gomis-Bellmunt, O., et al.: A review of energy storage technologies for wind power applications. Renew. Sustain. Energy Rev. **16**, 2154–2171 (2012). https://doi.org/10.1016/j.rser.2012.01.029
38. Wang, S., Xie, Y., Niu, S., et al.: Freestanding triboelectric-layer-based nanogenerators for harvesting energy from a moving object or human motion in contact and non-contact modes. Adv. Mater. **26**, 2818–2824 (2014). https://doi.org/10.1002/adma.201305303
39. Guan, X.Y., Xu, B.G., Wu, M.J., et al.: Breathable, washable and wearable woven-structured triboelectric nanogenerators utilizing electrospun nanofibers for biomechanical energy harvesting and self-powered sensing. Nano Energy **80**, 105549 (2021). https://doi.org/10.1016/j.nanoen.2020.105549
40. Halámková, L., Halámek, J., Bocharova, V., et al.: Implanted biofuel cell operating in a living snail. J. Am. Chem. Soc. **134**, 5040–5043 (2012). https://doi.org/10.1021/ja211714w
41. Zebda, A., Gondran, C., le Goff, A., et al.: Mediatorless high-power glucose biofuel cells based on compressed carbon nanotube-enzyme electrodes. Nat. Commun. **2**, 370 (2011). https://doi.org/10.1038/ncomms1365
42. De Pontieu, B., McIntosh, S.W., Carlsson, M., et al.: Chromospheric alfvenic waves strong enough to power the solar wind. Science **318**, 1574–1577 (2007). https://doi.org/10.1126/science.1151747
43. Service, R.F.: Fuel cells: shrinking fuel cells promise power in your pocket. Science **296**, 1222–1224 (2002). https://doi.org/10.1126/science.296.5571.1222
44. Su, Z., Liu, J.H., Li, M., et al.: Defect engineering in titanium-based oxides for electrochemical energy storage devices. Electrochem. Energy Rev. **3**, 286–343 (2020). https://doi.org/10.1007/s41918-020-00064-5
45. Yu, L.P., Chen, G.Z.: Supercapatteries as high-performance electrochemical energy storage devices. Electrochem. Energy Rev. **3**, 271–285 (2020). https://doi.org/10.1007/s41918-020-00063-6
46. Zhao, Z., Liu, S., Zhu, J., et al.: Hierarchical nanostructures of nitrogen-doped porous carbon polyhedrons confined in carbon nanosheets for high-performance supercapacitors. ACS Appl. Mater. Interfaces **10**, 19871–19880 (2018). https://doi.org/10.1021/acsami.8b03431
47. Lokhande, P.E., Chavan, U.S., Pandey, A.: Materials and fabrication methods for electrochemical supercapacitors: overview. Electrochem. Energy Rev. **3**, 155–186 (2020). https://doi.org/10.1007/s41918-019-00057-z
48. Zhou, J.Q., Zhang, S.L., Zhou, Y.N., et al.: Biomass-derived carbon materials for high-performance supercapacitors: current status and perspective. Electrochem. Energy Rev. **4**, 219–248 (2021). https://doi.org/10.1007/s41918-020-00090-3
49. Hao, Y., Li, X., Liu, W., et al.: Asynchronous reactions of "self-matrix" dual-crystals effectively accommodating volume expansion/shrinkage of electrode materials with enhanced sodium storage. Chem. Commun. **55**, 9076–9079 (2019). https://doi.org/10.1039/c9cc03406d

50. Wang, Y.M., Wang, X., Li, X.F., et al.: A high-performance, tailorable, wearable, and foldable solid-state supercapacitor enabled by arranging pseudocapacitive groups and MXene flakes on textile electrode surface. Adv. Funct. Mater. **31**, 2008185 (2021). https://doi.org/10.1002/adfm.202008185
51. Li, L., Zhang, X.X., Li, M., et al.: The recycling of spent lithium-ion batteries: a review of current processes and technologies. Electrochem. Energy Rev. **1**, 461–482 (2018). https://doi.org/10.1007/s41918-018-0012-1
52. Xiong, S.Z., Regula, M., Wang, D.H., et al.: Toward better lithium–sulfur batteries: functional non-aqueous liquid electrolytes. Electrochem. Energy Rev. **1**, 388–402 (2018). https://doi.org/10.1007/s41918-018-0015-y
53. Wismann, S.T., Engbæk, J.S., Vendelbo, S.B., et al.: Electrified methane reforming: a compact approach to greener industrial hydrogen production. Science **364**, 756–759 (2019). https://doi.org/10.1126/science.aaw8775
54. Liu, Z.Q., Zhang, X., Gong, Y., et al.: Synthesis of MoX_2 (X = Se or S) monolayers with high-concentration 1T' phase on 4H/fcc-Au nanorods for hydrogen evolution. Nano Res. **12**, 1301–1305 (2019). https://doi.org/10.1007/s12274-018-2212-8
55. Yang, J., Sudik, A., Wolverton, C., et al.: High capacity hydrogen storage materials: attributes for automotive applications and techniques for materials discovery. Chem. Soc. Rev. **39**, 656–675 (2010). https://doi.org/10.1039/b802882f
56. Cheng, B., Mazzola, G., Pickard, C.J., et al.: Evidence for supercritical behaviour of high-pressure liquid hydrogen. Nature **585**, 217–220 (2020). https://doi.org/10.1038/s41586-020-2677-y
57. Desgreniers, S.: A milestone in the hunt for metallic hydrogen. Nature **577**, 626–627 (2020). https://doi.org/10.1038/d41586-020-00149-7
58. Lu, J.J., Yin, S.B., Shen, P.K.: Carbon-encapsulated electrocatalysts for the hydrogen evolution reaction. Electrochem. Energy Rev. **2**, 105–127 (2019). https://doi.org/10.1007/s41918-018-0025-9
59. Zhao, Z., Zhang, Z.W., Zhao, Y.T., et al.: Atomic layer deposition inducing integration of Co, N codoped carbon sphere on 3D foam with hierarchically porous structures for flexible hydrogen producing device. Adv. Funct. Mater. **29**, 1906365 (2019). https://doi.org/10.1002/adfm.201906365
60. Chen, Z.L., Ha, Y., Jia, H.X., et al.: Water splitting: oriented transformation of Co-LDH into 2D/3D ZIF-67 to achieve Co–N–C hybrids for efficient overall water splitting. Adv. Energy Mater. **9**, 1970066 (2019). https://doi.org/10.1002/aenm.201970066
61. Chen, Z., Wu, R., Liu, Y., et al.: Ultrafine co nanoparticles encapsulated in carbon-nanotubes-grafted graphene sheets as advanced electrocatalysts for the hydrogen evolution reaction. Adv. Mater. **30**, e1802011 (2018). https://doi.org/10.1002/adma.201802011
62. Sun, J., Guo, N.K., Shao, Z.Y., et al.: Electrocatalysts: a facile strategy to construct amorphous spinel-based electrocatalysts with massive oxygen vacancies using ionic liquid dopant. Adv. Energy Mater. **8**, 1870121 (2018). https://doi.org/10.1002/aenm.201870121
63. Nature Podcast. Podcast: improving battery charging, and harnessing energy from the air. Nature. https://doi.org/10.1038/d41586-020-00482-x (2020). Accessed 17 Feb 2022
64. Attia, P.M., Grover, A., Jin, N., et al.: Closed-loop optimization of fast-charging protocols for batteries with machine learning. Nature **578**, 397–402 (2020). https://doi.org/10.1038/s41586-020-1994-5
65. Zhao, E.W., Liu, T., Jónsson, E., et al.: In situ NMR metrology reveals reaction mechanisms in redox flow batteries. Nature **579**, 224–228 (2020). https://doi.org/10.1038/s41586-020-2081-7
66. Guo, N.K., Xue, H., Bao, A., et al.: Frontispiece: achieving superior electrocatalytic performance by surface copper vacancy defects during electrochemical etching process. Angew. Chem. Int. Ed. **59**, 13778–13784 (2020). https://doi.org/10.1002/anie.202083361
67. Liu, H., Zhu, Z., Yan, Q., et al.: A disordered rock salt anode for fast-charging lithium-ion batteries. Nature **585**, 63–67 (2020). https://doi.org/10.1038/s41586-020-2637-6
68. Nong, H.N., Falling, L.J., Bergmann, A., et al.: Key role of chemistry versus bias in electrocatalytic oxygen evolution. Nature **587**, 408–413 (2020). https://doi.org/10.1038/s41586-020-2908-2
69. Zhang, Y., Chen, B., Guan, D., et al.: Thermal-expansion offset for high-performance fuel cell cathodes. Nature **591**, 246–251 (2021). https://doi.org/10.1038/s41586-021-03264-1
70. Sari, M.K., Li, H., F, X.: Batteries: controllable cathode–electrolyte interface of $Li[Ni^{0.8}Co_{0.1}Mn_{0.1}]O_2$ for lithium ion batteries: a review. Adv. Energy Mater. **9**, 19701 (2019). https://doi.org/10.1002/aenm.201970151
71. Aricò, A.S., Bruce, P., Scrosati, B., et al.: Nanostructured materials for advanced energy conversion and storage devices. Nat. Mater. **4**, 366–377 (2005). https://doi.org/10.1038/nmat1368
72. Yan, B., Li, X.F., Xiao, W., et al.: Design, synthesis, and application of metal sulfides for Li–S batteries: progress and prospects. J. Mater. Chem. A **8**, 17848–17882 (2020). https://doi.org/10.1039/d0ta06220k
73. Liu, W., Yuan, J.J., Hao, Y.C., et al.: Heterogeneous structured $MoSe_2$–MoO_3 quantum dots with enhanced sodium/potassium storage. J. Mater. Chem. A **8**, 23395–23403 (2020). https://doi.org/10.1039/d0ta08674f
74. Li, M., Lu, J., Chen, Z., et al.: 30 years of lithium-ion batteries. Adv. Mater. **30**, 1800561 (2018). https://doi.org/10.1002/adma.201800561
75. Cano, Z.P., Banham, D., Ye, S., et al.: Batteries and fuel cells for emerging electric vehicle markets. Nat. Energy **3**, 279–289 (2018). https://doi.org/10.1038/s41560-018-0108-1
76. Schmuch, R., Wagner, R., Hörpel, G., et al.: Performance and cost of materials for lithium-based rechargeable automotive batteries. Nat. Energy **3**, 267–278 (2018). https://doi.org/10.1038/s41560-018-0107-2
77. Ding, J., Hu, W., Paek, E., et al.: Review of hybrid ion capacitors: from aqueous to lithium to sodium. Chem. Rev. **118**, 6457–6498 (2018). https://doi.org/10.1021/acs.chemrev.8b00116
78. Zheng, S.S., Xue, H.G., Pang, H.: Supercapacitors based on metal coordination materials. Coord. Chem. Rev. **373**, 2–21 (2018). https://doi.org/10.1016/j.ccr.2017.07.002
79. Lan, Y., Zhao, H., Zong, Y., et al.: Phosphorization boosts the capacitance of mixed metal nanosheet arrays for high performance supercapacitor electrodes. Nanoscale **10**, 11775–11781 (2018). https://doi.org/10.1039/c8nr01229f
80. Liu, W., Li, X.F., Xiong, D.B., et al.: Significantly improving cycling performance of cathodes in lithium ion batteries: the effect of Al_2O_3 and $LiAlO_2$ coatings on $LiNi_{0.6}Co_{0.2}Mn_{0.2}O_2$. Nano Energy **44**, 111–120 (2018). https://doi.org/10.1016/j.nanoen.2017.11.010
81. Wu, J.H., Shen, L., Zhang, Z.H., et al.: All-solid-state lithium batteries with sulfide electrolytes and oxide cathodes. Electrochem. Energy Rev. **4**, 101–135 (2021). https://doi.org/10.1007/s41918-020-00081-4
82. Wang, Y., Wang, Y., Hosono, E., et al.: The design of a $LiFePO_4$/carbon nanocomposite with a core-shell structure and its synthesis by an in situ polymerization restriction method. Angew. Chem. Int. Ed. **47**, 7461–7465 (2008). https://doi.org/10.1002/anie.200802539
83. Xue, Y.H., Liu, J., Chen, H., et al.: Nitrogen-doped graphene foams as metal-free counter electrodes in high-performance dye-sensitized solar cells. Angew. Chem. Int. Ed. **51**, 12124–12127 (2012). https://doi.org/10.1002/anie.201207277

84. Manthiram, A., Yu, X., Wang, S.: Lithium battery chemistries enabled by solid-state electrolytes. Nat. Rev. Mater. **2**, 16103 (2017). https://doi.org/10.1038/natrevmats.2016.103
85. Xiao, W., Wang, J.Y., Fan, L.L., et al.: Recent advances in $Li_{1+x}Al_xTi_{2-x}(PO_4)_3$ solid-state electrolyte for safe lithium batteries. Energy Storage Mater. **19**, 379–400 (2019). https://doi.org/10.1016/j.ensm.2018.10.012
86. Zhao, Z., Kong, Y., Zhang, Z.W., et al.: Atomic layer–deposited nanostructures and their applications in energy storage and sensing. J. Mater. Res. **35**, 701–719 (2020). https://doi.org/10.1557/jmr.2019.329
87. Zhang, Z.W., Zhao, Y.T., Zhao, Z., et al.: Atomic layer deposition-derived nanomaterials: oxides, transition metal dichalcogenides, and metal-organic frameworks. Chem. Mater. **32**, 9056–9077 (2020). https://doi.org/10.1021/acs.chemmater.9b04414
88. Liu, Y., Sun, Q., Zhao, Y., et al.: Stabilizing the interface of NASICON solid electrolyte against Li metal with atomic layer deposition. ACS Appl. Mater. Interfaces **10**, 31240–31248 (2018). https://doi.org/10.1021/acsami.8b06366
89. Ma, D.T., Li, Y.L., Yang, J.B., et al.: New strategy for polysulfide protection based on atomic layer deposition of TiO_2 onto ferroelectric-encapsulated cathode: toward ultrastable free-standing room temperature sodium-sulfur batteries. Adv. Funct. Mater. **28**, 1705537 (2018). https://doi.org/10.1002/adfm.201705537
90. Cremers, V., Puurunen, R.L., Dendooven, J.: Conformality in atomic layer deposition: current status overview of analysis and modelling. Appl. Phys. Rev. **6**, 021302 (2019). https://doi.org/10.1063/1.5060967
91. Liu, C., Wang, Y., Tian, Z.A., et al.: Low-dimensional vanadium dioxide nanomaterials: fabrication, properties and applications. J. Phys. Mater. **3**, 032007 (2020). https://doi.org/10.1088/2515-7639/aba1d6
92. Faraz, T., Knoops, H.C.M., Verheijen, M.A., et al.: Tuning material properties of oxides and nitrides by substrate biasing during plasma-enhanced atomic layer deposition on planar and 3D substrate topographies. ACS Appl. Mater. Interfaces **10**, 13158–13180 (2018). https://doi.org/10.1021/acsami.8b00183
93. Shen, X., Li, C., Shi, C., et al.: Core-shell structured ceramic nonwoven separators by atomic layer deposition for safe lithium-ion batteries. Appl. Surf. Sci. **441**, 165–173 (2018). https://doi.org/10.1016/j.apsusc.2018.01.222
94. Liang, J.N., Sun, Q., Zhao, Y., et al.: Stabilization of all-solid-state Li–S batteries with a polymer–ceramic sandwich electrolyte by atomic layer deposition. J. Mater. Chem. A **6**, 23712–23719 (2018). https://doi.org/10.1039/c8ta09069f
95. Ma, D.T., Li, Y.L., Yang, J.B., et al.: Atomic layer deposition-enabled ultrastable freestanding carbon-selenium cathodes with high mass loading for sodium-selenium battery. Nano Energy **43**, 317–325 (2018). https://doi.org/10.1016/j.nanoen.2017.11.042
96. Li, M., Tu, X., Wang, Y., et al.: Highly enhanced visible-light-driven photoelectrochemical performance of ZnO-modified In_2S_3 nanosheet arrays by atomic layer deposition. Nano Micro Lett. **10**, 45 (2018). https://doi.org/10.1007/s40820-018-0199-z
97. Hou, Y.N., Li, X.F., Liu, W., et al.: ALD derived $Fe3^{+-}$ doping toward high performance P2-$Na_{0.75}Ni_{0.2}Co_{0.2}Mn_{0.6}O_2$ cathode material for sodium ion batteries. Mater. Today Energy **14**, 100353 (2019). https://doi.org/10.1016/j.mtener.2019.100353
98. O'Neill, B.J., Jackson, D.H.K., Lee, J., et al.: Catalyst design with atomic layer deposition. ACS Catal. **5**, 1804–1825 (2015). https://doi.org/10.1021/cs501862h
99. Johnson, R.W., Hultqvist, A., Bent, S.F.: A brief review of atomic layer deposition: from fundamentals to applications. Mater. Today **17**, 236–246 (2014). https://doi.org/10.1016/j.mattod.2014.04.026
100. Meng, X.B., Yang, X.Q., Sun, X.L.: Emerging applications of atomic layer deposition for lithium-ion battery studies. Adv. Mater. **24**, 3589–3615 (2012). https://doi.org/10.1002/adma.201200397
101. Mackus, A.J.M., Bol, A.A., Kessels, W.M.M.: The use of atomic layer deposition in advanced nanopatterning. Nanoscale **6**, 10941–10960 (2014). https://doi.org/10.1039/c4nr01954g
102. Knez, M., Nielsch, K., Niinistö, L.: Synthesis and surface engineering of complex nanostructures by atomic layer deposition. Adv. Mater. **19**, 3425–3438 (2007). https://doi.org/10.1002/adma.200700079
103. George, S.M.: Atomic layer deposition: an overview. Chem. Rev. **110**, 111–131 (2010). https://doi.org/10.1021/cr900056b
104. Groner, M.D., Fabreguette, F.H., Elam, J.W., et al.: Low-temperature Al_2O_3 atomic layer deposition. Chem. Mater. **16**, 639–645 (2004). https://doi.org/10.1021/cm0304546
105. Mondloch, J.E., Bury, W., Fairen-Jimenez, D., et al.: Vapor-phase metalation by atomic layer deposition in a metal-organic framework. J. Am. Chem. Soc. **135**, 10294–10297 (2013). https://doi.org/10.1021/ja4050828
106. Profijt, H.B., Potts, S.E., van de Sanden, M.C.M., et al.: Plasma-assisted atomic layer deposition: basics, opportunities, and challenges. J. Vac. Sci. Technol. A Vac. Surf. Films **29**, 050801 (2011) https://doi.org/10.1116/1.3609974
107. Lim, B.S., Rahtu, A., Gordon, R.G.: Atomic layer deposition of transition metals. Nat. Mater. **2**, 749–754 (2003). https://doi.org/10.1038/nmat1000
108. Lu, J., Fu, B., Kung, M.C., et al.: Coking- and sintering-resistant palladium catalysts achieved through atomic layer deposition. Science **335**, 1205–1208 (2012). https://doi.org/10.1126/science.1212906
109. Ma, F., Yang, B., Zhao, Z., et al.: Sonication-triggered rolling of Janus porous nanomembranes for electrochemical sensing of dopamine and ascorbic acid. ACS Appl. Nano Mater. **3**, 10032–10039 (2020). https://doi.org/10.1021/acsanm.0c02019
110. Ma, F., Yang, B., Zhang, Z.W., et al.: Self-rolled TiO_2 microscroll/graphene composite for electrochemical dopamine sensing. Prog. Nat. Sci. Mater. Int. **30**, 337–342 (2020). https://doi.org/10.1016/j.pnsc.2020.02.008
111. Mackus, A.J.M., Schneider, J.R., MacIsaac, C., et al.: Synthesis of doped, ternary, and quaternary materials by atomic layer deposition: a review. Chem. Mater. **31**, 1142–1183 (2019). https://doi.org/10.1021/acs.chemmater.8b02878
112. Detavernier, C., Dendooven, J., Pulinthanathu Sree, S., et al.: Tailoring nanoporous materials by atomic layer deposition. Chem. Soc. Rev. **40**, 5242 (2011). https://doi.org/10.1039/c1cs15091j
113. Wang, T., Luo, Z., Li, C., et al.: Controllable fabrication of nanostructured materials for photoelectrochemical water splitting via atomic layer deposition. Chem. Soc. Rev. **43**, 7469–7484 (2014). https://doi.org/10.1039/c3cs60370a
114. Asundi, A.S., Raiford, J.A., Bent, S.F.: Opportunities for atomic layer deposition in emerging energy technologies. ACS Energy Lett. **4**, 908–925 (2019). https://doi.org/10.1021/acsenergylett.9b00249
115. Schwartzberg, A.M., Olynick, D.: Complex materials by atomic layer deposition. Adv. Mater. **27**, 5778–5784 (2015). https://doi.org/10.1002/adma.201500699
116. Lu, J., Low, K.B., Lei, Y., et al.: Toward atomically-precise synthesis of supported bimetallic nanoparticles using atomic layer deposition. Nat. Commun. **5**, 3264 (2014). https://doi.org/10.1038/ncomms4264
117. Zhu, M., Yu, L.B., He, S.S., et al.: Highly efficient and stable cellulose-based ion gel polymer electrolyte for solid-state supercapacitors. ACS Appl. Energy Mater. **2**, 5992–6001 (2019). https://doi.org/10.1021/acsaem.9b01109
118. Lu, J.L., Elam, J.W., Stair, P.C.: Atomic layer deposition—sequential self-limiting surface reactions for advanced catalyst

"bottom-up" synthesis. Surf. Sci. Rep. **71**, 410–472 (2016). https://doi.org/10.1016/j.surfrep.2016.03.003
119. Peng, Q., Lewis, J.S., Hoertz, P.G., et al.: Atomic layer deposition for electrochemical energy generation and storage systems. J. Vac. Sci. Technol. A **30**, 010803 (2012). https://doi.org/10.1116/1.3672027
120. Meng, X.B.: Atomic-scale surface modifications and novel electrode designs for high-performance sodium-ion batteries via atomic layer deposition. J. Mater. Chem. A **5**, 10127–10149 (2017). https://doi.org/10.1039/c7ta02742g
121. Lu, J.L., Elam, J.W., Stair, P.C.: Synthesis and stabilization of supported metal catalysts by atomic layer deposition. Acc. Chem. Res. **46**, 1806–1815 (2013). https://doi.org/10.1021/ar300229c
122. Pickrahn, K.L., Park, S.W., Gorlin, Y., et al.: Active MnO_x electrocatalysts prepared by atomic layer deposition for oxygen evolution and oxygen reduction reactions. Adv. Energy Mater. **2**, 1269–1277 (2012). https://doi.org/10.1002/aenm.201200230
123. Wang, H., Lu, Z., Xu, S., et al.: Electrochemical tuning of vertically aligned MoS_2 nanofilms and its application in improving hydrogen evolution reaction. Proc. Natl. Acad. Sci. U. S. A. **110**, 19701–19706 (2013). https://doi.org/10.1073/pnas.1316792110
124. Song, M., Tan, H., Li, X.L., et al.: Atomic-layer-deposited amorphous MoS_2 for durable and flexible Li–O_2 batteries. Small Methods **4**, 1900274 (2020). https://doi.org/10.1002/smtd.201900274
125. Kwon, D.H., Jin, Z.Y., Shin, S., et al.: A comprehensive study on atomic layer deposition of molybdenum sulfide for electrochemical hydrogen evolution. Nanoscale **8**, 7180–7188 (2016). https://doi.org/10.1039/c5nr09065b
126. Zhao, Z., Kong, Y., Huang, G.S., et al.: Area-selective and precise assembly of metal organic framework particles by atomic layer deposition induction and its application for ultra-sensitive dopamine sensor. Nano Today **42**, 101347 (2022). https://doi.org/10.1016/j.nantod.2021.101347
127. Zhao, Z., Kong, Y., Liu, C., et al.: Atomic layer deposition-assisted fabrication of 3D Co-doped carbon framework for sensitive enzyme-free lactic acid sensor. Chem. Eng. J. **417**, 129285 (2021). https://doi.org/10.1016/j.cej.2021.129285
128. Zhao, Z., Kong, Y., Lin, X.Y., et al.: Oxide nanomembrane induced assembly of a functional smart fiber composite with nanoporosity for an ultra-sensitive flexible glucose sensor. J. Mater. Chem. A **8**, 26119–26129 (2020). https://doi.org/10.1039/d0ta09211h
129. Zhao, Z., Kong, Y., Huang, G.S., et al.: Nickel-based metal-organic frameworks-modified flexible fiber: preparation and its dopamine sensing application. Chin. Sci. Bull. **66**, 4187–4196 (2021). https://doi.org/10.1360/tb-2021-0093
130. Zhao, Z., Kong, Y., Liu, C., et al.: Atomic layer deposition-induced integration of N-doped carbon particles on carbon foam for flexible supercapacitor. J. Materiomics **6**, 209–215 (2020). https://doi.org/10.1016/j.jmat.2020.01.011
131. Kong, Y., Zhao, Z., Wang, Y.Q., et al.: Integration of a metal-organic framework film with a tubular whispering-gallery-mode microcavity for effective CO_2 sensing. ACS Appl. Mater. Interfaces **13**, 58104–58113 (2021). https://doi.org/10.1021/acsami.1c16322
132. Chandrasekaran, S., Kaeffer, N., Cagnon, L., et al.: A robust ALD-protected silicon-based hybrid photoelectrode for hydrogen evolution under aqueous conditions. Chem. Sci. **10**, 4469–4475 (2019). https://doi.org/10.1039/c8sc05006f
133. Kim, I.S., Pellin, M.J., Martinson, A.B.F.: Acid-compatible halide perovskite photocathodes utilizing atomic layer deposited TiO_2 for solar-driven hydrogen evolution. ACS Energy Lett. **4**, 293–298 (2019). https://doi.org/10.1021/acsenergylett.8b01661
134. Cheng, N., Stambula, S., Wang, D., et al.: Platinum single-atom and cluster catalysis of the hydrogen evolution reaction. Nat. Commun. **7**, 13638 (2016). https://doi.org/10.1038/ncomms13638
135. Zhang, Z.W., Deng, L.J., Zhao, Z., et al.: Nickel nanograins anchored on a carbon framework for an efficient hydrogen evolution electrocatalyst and a flexible electrode. J. Mater. Chem. A **8**, 3499–3508 (2020). https://doi.org/10.1039/c9ta13632k
136. Zhang, X.B., Shao, B.Y., Sun, Z.M., et al.: Platinum nanoparticle-deposited $Ti_3C_2T_x$ MXene for hydrogen evolution reaction. Ind. Eng. Chem. Res. **59**, 1822–1828 (2020). https://doi.org/10.1021/acs.iecr.9b05046
137. Cao, K., Shi, L., Gong, M., et al.: Nanofence stabilized platinum nanoparticles catalyst via facet-selective atomic layer deposition. Small **13**, 1700648 (2017). https://doi.org/10.1002/smll.201700648
138. Cai, J., Zhang, J., Cao, K., et al.: Selective passivation of Pt nanoparticles with enhanced sintering resistance and activity toward CO oxidation via atomic layer deposition. ACS Appl. Nano Mater. **1**, 522–530 (2018). https://doi.org/10.1021/acsanm.7b00026
139. Cao, K., Zhu, Q., Shan, B., et al.: Controlled synthesis of Pd/Pt core shell nanoparticles using area-selective atomic layer deposition. Sci. Rep. **5**, 8470 (2015). https://doi.org/10.1038/srep08470
140. Chen, R., Kim, H., McIntyre, P.C., et al.: Achieving area-selective atomic layer deposition on patterned substrates by selective surface modification. Appl. Phys. Lett. **86**, 191910 (2005). https://doi.org/10.1063/1.1922076
141. Liu, X., Zhu, Q., Lang, Y., et al.: Oxide-nanotrap-anchored platinum nanoparticles with high activity and sintering resistance by area-selective atomic layer deposition. Angew. Chem. Int. Edit. **56**, 1648–1652 (2017). https://doi.org/10.1002/anie.201611559
142. Balasubramanyam, S., Shirazi, M., Bloodgood, M.A., et al.: Edge-site nanoengineering of WS_2 by low-temperature plasma-enhanced atomic layer deposition for electrocatalytic hydrogen evolution. Chem. Mater. **31**, 5104–5115 (2019). https://doi.org/10.1021/acs.chemmater.9b01008
143. Wu, M.X., Yang, Y.W.: Metal-organic framework (MOF)-based drug/cargo delivery and cancer therapy. Adv. Mater. **29**, 1606134 (2017). https://doi.org/10.1002/adma.201606134
144. Stock, N., Biswas, S.: Synthesis of metal-organic frameworks (MOFs): routes to various MOF topologies, morphologies, and composites. Chem. Rev. **112**, 933–969 (2012). https://doi.org/10.1021/cr200304e
145. Shekhah, O., Liu, J., Fischer, R.A., et al.: MOF thin films: existing and future applications. Chem. Soc. Rev. **40**, 1081 (2011). https://doi.org/10.1039/c0cs00147c
146. Stavila, V., Talin, A.A., Allendorf, M.D.: MOF-based electronic and opto-electronic devices. Chem. Soc. Rev. **43**, 5994–6010 (2014). https://doi.org/10.1039/c4cs00096j
147. Chaikittisilp, W., Ariga, K., Yamauchi, Y.: A new family of carbon materials: synthesis of MOF-derived nanoporous carbons and their promising applications. J. Mater. Chem. A **1**, 14–19 (2013). https://doi.org/10.1039/c2ta00278g
148. Sheberla, D., Bachman, J.C., Elias, J.S., et al.: Conductive MOF electrodes for stable supercapacitors with high areal capacitance. Nat. Mater. **16**, 220–224 (2017). https://doi.org/10.1038/nmat4766
149. Zou, F., Hu, X.L., Li, Z., et al.: MOF-derived porous ZnO/$ZnFe_2O_4$/C octahedra with hollow interiors for high-rate lithium-ion batteries. Adv. Mater. **26**, 6622–6628 (2014). https://doi.org/10.1002/adma.201402322
150. Liu, Y.L., Eubank, J., Cairns, A., et al.: Assembly of metal–organic frameworks (MOFs) based on indium-trimer building blocks: a porous MOF with soc topology and high hydrogen

storage. Angew. Chem. Int. Ed. **46**, 3278–3283 (2007). https://doi.org/10.1002/anie.200604306
151. Yang, S.J., Kim, T., Im, J.H., et al.: MOF-derived hierarchically porous carbon with exceptional porosity and hydrogen storage capacity. Chem. Mater. **24**, 464–470 (2012). https://doi.org/10.1021/cm202554j
152. Sun, D.F., Ma, S.Q., Ke, Y.X., et al.: An interweaving MOF with high hydrogen uptake. J. Am. Chem. Soc. **128**, 3896–3897 (2006). https://doi.org/10.1021/ja058777l
153. Jiang, H.L., Tatsu, Y., Lu, Z.H., et al.: Non-, micro-, and mesoporous metal–organic framework isomers: reversible transformation, fluorescence sensing, and large molecule separation. J. Am. Chem. Soc. **132**, 5586–5587 (2010). https://doi.org/10.1021/ja101541s
154. Ge, X.L., Li, Z.Q., Yin, L.W.: Metal-organic frameworks derived porous core/shell CoP@C polyhedrons anchored on 3D reduced graphene oxide networks as anode for sodium-ion battery. Nano Energy **32**, 117–124 (2017). https://doi.org/10.1016/j.nanoen.2016.11.055
155. Liu, H.P., Wang, H.M., Chu, T.S., et al.: An electrodeposited lanthanide MOF thin film as a luminescent sensor for carbonate detection in aqueous solution. J. Mater. Chem. C **2**, 8683–8690 (2014). https://doi.org/10.1039/c4tc01551g
156. Zhang, W., Yao, X., Zhou, S., et al.: ZIF-8/ZIF-67-derived Co-N_x-embedded 1D porous carbon nanofibers with graphitic carbon-encased Co nanoparticles as an efficient bifunctional electrocatalyst. Small Weinheim Der Bergstrasse Ger. **14**, e1800423 (2018). https://doi.org/10.1002/smll.201800423
157. Jia, G., Zhang, W., Fan, G.Z., et al.: Three-dimensional hierarchical architectures derived from surface-mounted metal-organic framework membranes for enhanced electrocatalysis. Angew. Chem. Int. Ed. **56**, 13781–13785 (2017). https://doi.org/10.1002/anie.201708385
158. So, M.C., Jin, S., Son, H.J., et al.: Layer-by-layer fabrication of oriented porous thin films based on porphyrin-containing metal-organic frameworks. J. Am. Chem. Soc. **135**, 15698–15701 (2013). https://doi.org/10.1021/ja4078705
159. Zhang, A.J., Li, X.Y., Zhang, S.Y., et al.: Spray-drying-assisted reassembly of uniform and large micro-sized MIL-101 microparticles with controllable morphologies for benzene adsorption. J. Colloid Interface Sci. **506**, 1–9 (2017). https://doi.org/10.1016/j.jcis.2017.07.022
160. Yoo, Y., Jeong, H.K.: Rapid fabrication of metal organic framework thin films using microwave-induced thermal deposition. Chem. Commun. (2008). https://doi.org/10.1039/b800061a
161. Ruan, J.F., Mo, F.J., Chen, Z.L., et al.: Rational construction of nitrogen-doped hierarchical dual-carbon for advanced potassium-ion hybrid capacitors. Adv. Energy Mater. **10**, 1904045 (2020). https://doi.org/10.1002/aenm.201904045
162. Zhao, J.J., Lee, D.T., Yaga, R.W., et al.: Ultra-fast degradation of chemical warfare agents using MOF-nanofiber kebabs. Angew. Chem. Int. Ed. **55**, 13224–13228 (2016). https://doi.org/10.1002/anie.201606656
163. Zhao, J.J., Losego, M.D., Lemaire, P.C., et al. (2014) Metal-organic frameworks: highly adsorptive, MOF-functionalized nonwoven fiber mats for hazardous gas capture enabled by atomic layer deposition. Adv. Mater. Interfaces (Adv. Mater. Interfaces 4/2014) **1**, inside front cover. https://doi.org/10.1002/admi.201470023
164. Stassen, I., Styles, M., Grenci, G., et al.: Chemical vapour deposition of zeolitic imidazolate framework thin films. Nat. Mater. **15**, 304–310 (2016). https://doi.org/10.1038/nmat4509
165. Krishtab, M., Stassen, I., Stassin, T., et al.: Vapor-deposited zeolitic imidazolate frameworks as gap-filling ultra-low-*k* dielectrics. Nat. Commun. **10**, 3729 (2019). https://doi.org/10.1038/s41467-019-11703-x
166. Stassin, T., Stassen, I., Marreiros, J., et al.: Solvent-free powder synthesis and MOF-CVD thin films of the large-pore metal-organic framework MAF-6. Chem. Mater. **32**, 1784–1793 (2020). https://doi.org/10.1021/acs.chemmater.9b03807
167. Ren, W.N., Zhang, H.F., Cheng, C.W.: Ultrafine Pt nanoparticles decorated MoS_2 nanosheets with significantly improved hydrogen evolution activity. Electrochim. Acta **241**, 316–322 (2017). https://doi.org/10.1016/j.electacta.2017.04.145
168. Ramesh, R., Sawant, S.Y., Nandi, D.K., et al.: Hydrogen evolution reaction by atomic layer-deposited MoN_x on porous carbon substrates: the effects of porosity and annealing on catalyst activity and stability. Chemsuschem **13**, 4159–4168 (2020). https://doi.org/10.1002/cssc.202000350
169. Zhang, L., Zhao, Z.-J., Banis, M.N., et al.: Selective atomic layer deposition of RuO_x catalysts on shape- controlled Pd nanocrystals with significantly enhanced hydrogen evolution activity. J. Mater. Chem. A **6**, 24397–24406 (2018). https://doi.org/10.1039/c8ta08931k
170. Nayak, P., Jiang, Q., Kurra, N., et al.: Monolithic laser scribed graphene scaffolds with atomic layer deposited platinum for the hydrogen evolution reaction. J. Mater. Chem. A **5**, 20422–20427 (2017). https://doi.org/10.1039/c7ta06236b
171. Xiong, W., Guo, Z., Li, H., et al.: Rational bottom-up engineering of electrocatalysts by atomic layer deposition: a case study of $Fe_xCo_{1-x}Sy$-based catalysts for electrochemical hydrogen evolution. ACS Energy Lett. **2**, 2778–2785 (2017). https://doi.org/10.1021/acsenergylett.7b01056
172. Chen, H., Chen, J.T., Shao, L., et al.: Minimum and well-dispersed platinum nanoparticles on 3D porous nickel for highly efficient electrocatalytic hydrogen evolution reaction enabled by atomic layer deposition. Appl. Surf. Sci. **494**, 1091–1099 (2019). https://doi.org/10.1016/j.apsusc.2019.07.251
173. Zhang, L., Si, R., Liu, H., et al.: Atomic layer deposited Pt-Ru dual-metal dimers and identifying their active sites for hydrogen evolution reaction. Nat. Commun. **10**, 4936 (2019). https://doi.org/10.1038/s41467-019-12887-y
174. Shin, S., Jin, Z., Kwon, D.H., et al.: High turnover frequency of hydrogen evolution reaction on amorphous MoS_2 thin film directly grown by atomic layer deposition. Langmuir **31**, 1196–1202 (2015). https://doi.org/10.1021/la504162u
175. Zhang, H.J., Hagen, D.J., Li, X.P., et al.: Atomic layer deposition of cobalt phosphide for efficient water splitting. Angew. Chem. Int. Ed. **59**, 17172–17176 (2020). https://doi.org/10.1002/anie.202002280
176. Kim, D., Song, J.G., Yang, H., et al.: Textile-based high-performance hydrogen evolution of low-temperature atomic layer deposition of cobalt sulfide. Nanoscale **11**, 7002–7002 (2019). https://doi.org/10.1039/c9nr90074h
177. Katuri, K.P., Bettahalli, N.M.S., Wang, X.B., et al.: A microfiltration polymer-based hollow-fiber cathode as a promising advanced material for simultaneous recovery of energy and water. Adv. Mater. **28**, 9504–9511 (2016). https://doi.org/10.1002/adma.201603074
178. Hsu, I.J., Kimmel, Y.C., Jiang, X., et al.: Atomic layer deposition synthesis of platinum-tungsten carbide core-shell catalysts for the hydrogen evolution reaction. Chem. Commun. **48**, 1063–1065 (2012). https://doi.org/10.1039/c1cc15812k
179. Ho, T.A., Bae, C., Lee, S., et al.: Edge-on MoS_2 thin films by atomic layer deposition for understanding the interplay between the active area and hydrogen evolution reaction. Chem. Mater. **29**, 7604–7614 (2017). https://doi.org/10.1021/acs.chemmater.7b03212

180. Xiong, W., Guo, Q., Guo, Z., et al.: Atomic layer deposition of nickel carbide for supercapacitors and electrocatalytic hydrogen evolution. J. Mater. Chem. A **6**, 4297–4304 (2018). https://doi.org/10.1039/c7ta10202j
181. Edy, R., Zhao, Y.T., Huang, G.S., et al.: TiO_2 nanosheets synthesized by atomic layer deposition for photocatalysis. Prog. Nat. Sci. Mater. Int. **26**, 493–497 (2016). https://doi.org/10.1016/j.pnsc.2016.08.010
182. Edy, R., Huang, G.S., Zhao, Y.T., et al.: Influence of reactive surface groups on the deposition of oxides thin film by atomic layer deposition. Surf. Coat. Technol. **329**, 149–154 (2017). https://doi.org/10.1016/j.surfcoat.2017.09.047
183. Mei, Y.F., Huang, G.S., Solovev, A.A., et al.: Versatile approach for integrative and functionalized tubes by strain engineering of nanomembranes on polymers. Adv. Mater. **20**, 4085–4090 (2008). https://doi.org/10.1002/adma.200801589
184. Jung, Y.S., Cavanagh, A.S., Riley, L.A., et al.: Ultrathin direct atomic layer deposition on composite electrodes for highly durable and safe Li-ion batteries. Adv. Mater. **22**, 2172–2176 (2010). https://doi.org/10.1002/adma.200903951
185. Marichy, C., Bechelany, M., Pinna, N.: Atomic layer deposition of nanostructured materials for energy and environmental applications. Adv. Mater. **24**, 1017–1032 (2012). https://doi.org/10.1002/adma.201104129
186. Han, X., Gong, Y., Fu, K., et al.: Negating interfacial impedance in garnet-based solid-state Li metal batteries. Nat. Mater. **16**, 572–579 (2017). https://doi.org/10.1038/nmat4821
187. Lee, J.W., Soomro, A.M., Waqas, M., et al.: A highly efficient surface modified separator fabricated with atmospheric atomic layer deposition for high temperature lithium ion batteries. Int. J. Energy Res. **44**, 7035–7046 (2020). https://doi.org/10.1002/er.5371
188. Chen, H., Lin, Q., Xu, Q., et al.: Plasma activation and atomic layer deposition of TiO_2 on polypropylene membranes for improved performances of lithium-ion batteries. J. Membr. Sci. **458**, 217–224 (2014). https://doi.org/10.1016/j.memsci.2014.02.004
189. Biyikli, N., Haider, A.: Atomic layer deposition: an enabling technology for the growth of functional nanoscale semiconductors. Semicond. Sci. Technol. **32**, 093002 (2017). https://doi.org/10.1088/1361-6641/aa7ade
190. Lei, Y., Lu, J., Luo, X., et al.: Synthesis of porous carbon supported palladium nanoparticle catalysts by atomic layer deposition: application for rechargeable lithium-O_2 battery. Nano Lett. **13**, 4182–4189 (2013). https://doi.org/10.1021/nl401833p
191. Solanki, R., Huo, J., Freeouf, J.L., et al.: Atomic layer deposition of ZnSe/CdSe superlattice nanowires. Appl. Phys. Lett. **81**, 3864–3866 (2002). https://doi.org/10.1063/1.1521570
192. Naeem, F., Naeem, S., Zhao, Z., et al.: Atomic layer deposition synthesized ZnO nanomembranes: a facile route towards stable supercapacitor electrode for high capacitance. J. Power Sources **451**, 227740 (2020). https://doi.org/10.1016/j.jpowsour.2020.227740
193. Fan, L.L., Li, X.F.: Recent advances in effective protection of sodium metal anode. Nano Energy **53**, 630–642 (2018). https://doi.org/10.1016/j.nanoen.2018.09.017
194. Wang, A., Kadam, S., Li, H., et al.: Review on modeling of the anode solid electrolyte interphase (SEI) for lithium-ion batteries. Npj Comput. Mater. **4**, 15 (2018). https://doi.org/10.1038/s41524-018-0064-0
195. Peled, E.: The electrochemical behavior of alkali and alkaline earth metals in nonaqueous battery systems: the solid electrolyte interphase model. J. Electrochem. Soc. **126**, 2047–2051 (1979). https://doi.org/10.1149/1.2128859
196. Bommier, C., Leonard, D., Jian, Z.L., et al.: New paradigms on the nature of solid electrolyte interphase formation and capacity fading of hard carbon anodes in Na-ion batteries. Adv. Mater. Interfaces **3**, 1600449 (2016). https://doi.org/10.1002/admi.201600449
197. Peled, E., Menkin, S.: Review: SEI: past, present and future. J. Electrochem. Soc. **164**, A1703–A1719 (2017). https://doi.org/10.1149/2.1441707jes
198. Liu, W., Liu, P.C., Mitlin, D.: Solid electrolyte interphases: review of emerging concepts in SEI analysis and artificial SEI membranes for lithium, sodium, and potassium metal battery anodes. Adv. Energy Mater. **10**, 2070177 (2020). https://doi.org/10.1002/aenm.202070177
199. Luo, W., Lin, C.F., Zhao, O., et al.: Ultrathin surface coating enables the stable sodium metal anode. Adv. Energy Mater. **7**, 1601526 (2017). https://doi.org/10.1002/aenm.201601526
200. Zhao, Y., Goncharova, L.V., Lushington, A., et al.: Superior stable and long life sodium metal anodes achieved by atomic layer deposition. Adv. Mater. **29**, 1606663 (2017). https://doi.org/10.1002/adma.201606663
201. Zhao, F.P., Zhao, Y., Wang, J., et al.: Tuning bifunctional interface for advanced sulfide-based all-solid-state batteries. Energy Storage Mater. **33**, 139–146 (2020). https://doi.org/10.1016/j.ensm.2020.06.013
202. Guan, D., Jeevarajan, J.A., Wang, Y.: Enhanced cycleability of $LiMn_2O_4$ cathodes by atomic layer deposition of nanosized-thin Al_2O_3 coatings. Nanoscale **3**, 1465–1469 (2011). https://doi.org/10.1039/c0nr00939c
203. Yu, M.P., Ma, J.S., Song, H.Q., et al.: Atomic layer deposited TiO_2 on a nitrogen-doped graphene/sulfur electrode for high performance lithium–sulfur batteries. Energy Environ. Sci. **9**, 1495–1503 (2016). https://doi.org/10.1039/c5ee03902a
204. Zheng, H.H., Sun, Q.N., Liu, G., et al.: Correlation between dissolution behavior and electrochemical cycling performance for $LiNi_{1/3}Co_{1/3}Mn_{1/3}O_2$-based cells. J. Power Sources **207**, 134–140 (2012). https://doi.org/10.1016/j.jpowsour.2012.01.122
205. Ren, X., Lau, K.C., Yu, M., et al.: Understanding side reactions in K-O_2 batteries for improved cycle life. ACS Appl. Mater. Interfaces **6**, 19299–19307 (2014). https://doi.org/10.1021/am505351s
206. Tang, A., Bao, J., Skyllas-Kazacos, M.: Dynamic modelling of the effects of ion diffusion and side reactions on the capacity loss for vanadium redox flow battery. J. Power Sources **196**, 10737–10747 (2011). https://doi.org/10.1016/j.jpowsour.2011.09.003
207. Arora, P., White, R.E., Doyle, M.: Capacity fade mechanisms and side reactions in lithium-ion batteries. J. Electrochem. Soc. **145**, 3647–3667 (1998). https://doi.org/10.1149/1.1838857
208. Jang, D.H., Shin, Y.J., Oh, S.M.: Dissolution of spinel oxides and capacity losses in 4 V Li/$Li_xMn_2O_4$ cells. J. Electrochem. Soc. **143**, 2204–2211 (1996). https://doi.org/10.1149/1.1836981
209. Xu, C., Sun, B., Gustafsson, T., et al.: Interface layer formation in solid polymer electrolyte lithium batteries: an XPS study. J. Mater. Chem. A **2**, 7256–7264 (2014). https://doi.org/10.1039/c4ta00214h
210. Guo, S., Li, Q., Liu, P., et al.: Environmentally stable interface of layered oxide cathodes for sodium-ion batteries. Nat Commun. **8**, 135 (2017). https://doi.org/10.1038/s41467-017-00157-8
211. Xie, J., Liao, L., Gong, Y., et al.: Stitching h-BN by atomic layer deposition of LiF as a stable interface for lithium metal anode. Adv Sci (2017). https://doi.org/10.1126/sciadv.aao3170
212. Pinkert, K., Oschatz, M., Borchardt, L., et al.: Role of surface functional groups in ordered mesoporous carbide-derived carbon/ionic liquid electrolyte double-layer capacitor interfaces. ACS Appl. Mater. Interfaces **6**, 2922–2928 (2014). https://doi.org/10.1021/am4055029

213. Qin, P.P., Wang, M., Li, N., et al.: Dual-ion batteries: bubble-sheet-like interface design with an ultrastable solid electrolyte layer for high-performance dual-ion batteries. Adv. Mater. **29**, 1606805 (2017). https://doi.org/10.1002/adma.201606805
214. Wang, J., Tang, J., Xu, Y.L., et al.: Interface miscibility induced double-capillary carbon nanofibers for flexible electric double layer capacitors. Nano Energy **28**, 232–240 (2016). https://doi.org/10.1016/j.nanoen.2016.08.043
215. Agrawal, R.C., Pandey, G.P.: Solid polymer electrolytes: materials designing and all-solid-state battery applications: an overview. J. Phys. D: Appl. Phys. **41**, 223001 (2008). https://doi.org/10.1088/0022-3727/41/22/223001
216. Sun, C.W., Liu, J., Gong, Y.D., et al.: Recent advances in all-solid-state rechargeable lithium batteries. Nano Energy **33**, 363–386 (2017). https://doi.org/10.1016/j.nanoen.2017.01.028
217. Kato, Y., Hori, S., Saito, T., et al.: High-power all-solid-state batteries using sulfide superionic conductors. Nat. Energy **1**, 16030 (2016). https://doi.org/10.1038/nenergy.2016.30
218. Didwal, P.N., Singhbabu, Y.N., Verma, R., et al.: An advanced solid polymer electrolyte composed of poly(propylene carbonate) and mesoporous silica nanoparticles for use in all-solid-state lithium-ion batteries. Energy Storage Mater. **37**, 476–490 (2021). https://doi.org/10.1016/j.ensm.2021.02.034
219. Cano-Banda, F., Singh, R., Hernandez-Guerrero, A., et al.: Enhanced performance of MgH_2 composite electrode using glass-ceramic electrolytes for all-solid-state Li-ion batteries. J. Alloys Compd. **863**, 158729 (2021). https://doi.org/10.1016/j.jallcom.2021.158729
220. Shchelkanova, M.S., Shekhtman, G.S., Pershina, S.V., et al.: The study of sodium-vanadium oxide NaV_3O_8 as an electrode material for all-solid-state sodium-ion batteries. J. Alloys Compd. **864**, 158516 (2021). https://doi.org/10.1016/j.jallcom.2020.158516
221. Wang, J.L., Zhang, Z., Ying, H.J., et al.: In-situ formation of LiF-rich composite interlayer for dendrite-free all-solid-state lithium batteries. Chem. Eng. J. **411**, 128534 (2021). https://doi.org/10.1016/j.cej.2021.128534
222. Zhuang, H., Ma, W.C., Xie, J.W., et al.: Solvent-free synthesis of PEO/garnet composite electrolyte for high-safety all-solid-state lithium batteries. J. Alloys Compd. **860**, 157915 (2021). https://doi.org/10.1016/j.jallcom.2020.157915
223. Wu, L.P., Liu, G.Z., Wan, H.L., et al.: Superior lithium-stable $Li_7P_2S_8I$ solid electrolyte for all-solid-state lithium batteries. J. Power Sources **491**, 229565 (2021). https://doi.org/10.1016/j.jpowsour.2021.229565
224. Chen, C.G., Jiang, M., Zhou, T., et al.: Interface aspects in all-solid-state Li-based batteries reviewed. Adv. Energy Mater. **11**, 2003939 (2021). https://doi.org/10.1002/aenm.202003939
225. Liu, T.F., Zheng, J.L., Hu, H.L., et al.: In-situ construction of a Mg-modified interface to guide uniform lithium deposition for stable all-solid-state batteries. J. Energy Chem. **55**, 272–278 (2021). https://doi.org/10.1016/j.jechem.2020.07.009
226. TanBanerjeeChen, D.H.S.A.Z., et al.: From nanoscale interface characterization to sustainable energy storage using all-solid-state batteries. Nat. Nanotechnol. **15**, 170–180 (2021). https://doi.org/10.1038/s41565-021-00877-5
227. Donders, M.E., Arnoldbik, W.M., Knoops, H.C.M., et al.: Atomic layer deposition of $LiCoO_2$ thin-film electrodes for all-solid-state Li-ion micro-batteries. J. Electrochem. Soc. **160**, A3066–A3071 (2013). https://doi.org/10.1149/2.011305jes
228. Fan, Z.J., Ding, B., Zhang, T.F., et al.: Solid/solid interfacial architecturing of solid polymer electrolyte–based all-solid-state lithium–sulfur batteries by atomic layer deposition. Small **15**, 1903952 (2019). https://doi.org/10.1002/smll.201903952
229. Chen, Y., Wen, K.H., Chen, T.H., et al.: Recent progress in all-solid-state lithium batteries: the emerging strategies for advanced electrolytes and their interfaces. Energy Storage Mater. **31**, 401–433 (2020). https://doi.org/10.1016/j.ensm.2020.05.019
230. Zheng, F., Kotobuki, M., Song, S.F., et al.: Review on solid electrolytes for all-solid-state lithium-ion batteries. J. Power Sources **389**, 198–213 (2018). https://doi.org/10.1016/j.jpowsour.2018.04.022
231. Xie, Y., Zou, H.L., Xiang, H.F., et al.: Enhancement on the wettability of lithium battery separator toward nonaqueous electrolytes. J. Membr. Sci. **503**, 25–30 (2016). https://doi.org/10.1016/j.memsci.2015.12.025
232. Guan, C., Qian, X., Wang, X., et al.: Atomic layer deposition of Co_3O_4 on carbon nanotubes/carbon cloth for high-capacitance and ultrastable supercapacitor electrode. Nanotechnology **26**, 094001 (2015). https://doi.org/10.1088/0957-4484/26/9/094001
233. Daubert, J.S., Lewis, N.P., Gotsch, H.N., et al.: Effect of meso- and micro-porosity in carbon electrodes on atomic layer deposition of pseudocapacitive V_2O_5 for high performance supercapacitors. Chem. Mater. **27**, 6524–6534 (2015). https://doi.org/10.1021/acs.chemmater.5b01602
234. Boukhalfa, S., Evanoff, K., Yushin, G.: Atomic layer deposition of vanadium oxide on carbon nanotubes for high-power supercapacitor electrodes. Energy Environ. Sci. **5**, 6872 (2012). https://doi.org/10.1039/c2ee21110f
235. Li, N., Lan, X.W., Wang, L.B., et al.: Precisely tunable T-Nb_2O_5 nanotubes via atomic layer deposition for fast-charging lithium-ion batteries. ACS Appl. Mater. Interfaces **13**, 16445–16453 (2021). https://doi.org/10.1021/acsami.1c02207
236. Zhang, X.B., Shao, B.Y., Guo, A.P., et al.: Improved electrochemical performance of CoO_x-NiO/$Ti_3C_2T_x$ MXene nanocomposites by atomic layer deposition towards high capacitance supercapacitors. J. Alloys Compd. **862**, 158546 (2021). https://doi.org/10.1016/j.jallcom.2020.158546
237. Qi, F., Liu, K., Ma, D.K., et al.: Dual active sites fabricated through atomic layer deposition of TiO_2 on MoS_2 nanosheet arrays for highly efficient electroreduction of CO_2 to ethanol. J. Mater. Chem. A **9**, 6790–6796 (2021). https://doi.org/10.1039/d0ta11457j
238. Cao, Y.Q., Wang, S.S., Liu, C., et al.: Core–shell MWCNTs@ZnS composite prepared by atomic layer deposition for high-performance lithium-ion batteries anode. J. Mater. Res. **36**, 1262–1271 (2021). https://doi.org/10.1557/s43578-021-00142-4
239. Dufond, M.E., Chazalviel, J.N., Santinacci, L.: Electrochemical stability of n-Si photoanodes protected by TiO_2 thin layers grown by atomic layer deposition. J. Electrochem. Soc. **168**, 031509 (2021). https://doi.org/10.1149/1945-7111/abeaf3
240. Xu, H.Y., Akbari, M.K., Kumar, S., et al.: Atomic layer deposition - state-of-the-art approach to nanoscale hetero-interfacial engineering of chemical sensors electrodes: a review. Sens. Actuat. B Chem. **331**, 129403 (2021). https://doi.org/10.1016/j.snb.2020.129403
241. Ng, S., Iffelsberger, C., Michalička, J., et al.: Atomic layer deposition of electrocatalytic insulator Al_2O_3 on three-dimensional printed nanocarbons. ACS Nano **15**, 686–697 (2021). https://doi.org/10.1021/acsnano.0c06961
242. Li, Z.S., Li, J.W., Liu, X., et al.: Progress in enhanced fluidization process for particle coating via atomic layer deposition. Chem. Eng. Process. Process. Intensif. **159**, 108234 (2021). https://doi.org/10.1016/j.cep.2020.108234
243. Gandla, D., Song, G.H., Wu, C.R., et al.: Atomic layer deposition (ALD) of alumina over activated carbon electrodes enabling a stable 4 V supercapacitor operation. ChemistryOpen **10**, 402–407 (2021). https://doi.org/10.1002/open.202000352
244. Oh, J., Seo, G., Kim, J., et al.: Plasma-enhanced atomic layer deposition of zirconium oxide thin films and its application to solid oxide fuel cells. Coatings **11**, 362 (2021). https://doi.org/10.3390/coatings11030362

245. Spajić, I., Rodič, P., Šekularac, G., et al.: The effect of surface preparation on the protective properties of Al_2O_3 and HfO_2 thin films deposited on cp-titanium by atomic layer deposition. Electrochim. Acta **366**, 137431 (2021). https://doi.org/10.1016/j.electacta.2020.137431
246. Baker, J.G., Schneider, J.R., de Paula, C., et al.: Identification of highly active surface iron sites on Ni(OOH) for the oxygen evolution reaction by atomic layer deposition. J. Catal. **394**, 476–485 (2021). https://doi.org/10.1016/j.jcat.2020.09.035
247. Xia, X., Zeng, Z., Li, X., et al.: Fabrication of metal oxide nanobranches on atomic-layer-deposited TiO_2 nanotube arrays and their application in energy storage. Nanoscale **5**, 6040–6047 (2013). https://doi.org/10.1039/c3nr01606d
248. Ahmed, B., Anjum, D.H., Gogotsi, Y., et al.: Atomic layer deposition of SnO_2 on MXene for Li-ion battery anodes. Nano Energy **34**, 249–256 (2017). https://doi.org/10.1016/j.nanoen.2017.02.043
249. Wang, D.R., Li, Y.L., Zhao, Y.T., et al.: Cycling-induced capacity increase of graphene aerogel/ZnO nanomembrane composite anode fabricated by atomic layer deposition. Nanoscale Res. Lett. **14**, 69 (2019). https://doi.org/10.1186/s11671-019-2900-7
250. Li, Y.L., Zhao, Y.T., Huang, G.S., et al.: ZnO nanomembrane/expanded graphite composite synthesized by atomic layer deposition as binder-free anode for lithium ion batteries. ACS Appl. Mater. Interfaces **9**, 38522–38529 (2017). https://doi.org/10.1021/acsami.7b11735
251. Zhao, Y.T., Huang, G.S., Wang, D.R., et al.: Sandwiched porous C/ZnO/porous C nanosheet battery anodes with a stable solid-electrolyte interphase for fast and long cycling. J. Mater. Chem. A **6**, 22870–22878 (2018). https://doi.org/10.1039/c8ta07848c
252. Blendinger, F., Seitz, D., Ottenschläger, A., et al.: Atomic layer deposition of bioactive TiO_2 thin films on polyetheretherketone for orthopedic implants. ACS Appl. Mater. Interfaces **13**, 3536–3546 (2021). https://doi.org/10.1021/acsami.0c17990
253. Chang, H.K., Ko, D.S., Cho, D.H., et al.: Enhanced response of the photoactive gas sensor on formaldehyde using porous SnO_2@TiO_2 heterostructure driven by gas-flow thermal evaporation and atomic layer deposition. Ceram. Int. **47**, 5985–5992 (2021). https://doi.org/10.1016/j.ceramint.2020.10.172
254. Zhang, R.H., Li, Y., Qiao, L., et al.: Atomic layer deposition assisted superassembly of ultrathin ZnO layer decorated hierarchical Cu foam for stable lithium metal anode. Energy Storage Mater. **37**, 123–134 (2021). https://doi.org/10.1016/j.ensm.2021.01.028
255. Gehensel, R.J., Zierold, R., Schaan, G., et al.: Improved thermal stability of zirconia macroporous structures via homogeneous aluminum oxide doping and nanostructuring using atomic layer deposition. J. Eur. Ceram. Soc. **41**, 4302–4312 (2021). https://doi.org/10.1016/j.jeurceramsoc.2021.02.007
256. Zhao, Y.T., Huang, G.S., Li, Y.L., et al.: Three-dimensional carbon/ZnO nanomembrane foam as an anode for lithium-ion battery with long-life and high areal capacity. J. Mater. Chem. A **6**, 7227–7235 (2018). https://doi.org/10.1039/c8ta00940f
257. Kim, S.W., Han, T.H., Kim, J., et al.: Fabrication and electrochemical characterization of TiO_2 three-dimensional nanonetwork based on peptide assembly. ACS Nano **3**, 1085–1090 (2009). https://doi.org/10.1021/nn900062q
258. Li, H., Gao, Y.H., Shao, Y.D., et al.: Vapor-phase atomic layer deposition of Co_9S_8 and its application for supercapacitors. Nano Lett. **15**, 6689–6695 (2015). https://doi.org/10.1021/acs.nanolett.5b02508
259. Nam, T., Seo, S., Kim, H.: Atomic layer deposition of a uniform thin film on two-dimensional transition metal dichalcogenides. J. Vac. Sci. Technol. A **38**, 030803 (2020). https://doi.org/10.1116/6.0000068
260. Luo, J.S., Xia, X.H., Luo, Y.S., et al.: Rationally designed hierarchical TiO_2@Fe_2O_3 hollow nanostructures for improved lithium ion storage. Adv. Energy Mater. **3**, 737–743 (2013). https://doi.org/10.1002/aenm.201200953
261. Gregorczyk, K.E., Kozen, A.C., Chen, X., et al.: Fabrication of 3D core-shell multiwalled carbon nanotube@RuO_2 lithium-ion battery electrodes through a RuO_2 atomic layer deposition process. ACS Nano **9**, 464–473 (2015). https://doi.org/10.1021/nn505644q
262. Naeem, F., Naeem, S., Zhao, Y., et al.: TiO_2 nanomembranes fabricated by atomic layer deposition for supercapacitor electrode with enhanced capacitance. Nanoscale Res. Lett. **14**, 92 (2019). https://doi.org/10.1186/s11671-019-2912-3
263. Yu, L., Wang, G., Wan, G., et al.: Highly effective synthesis of NiO/CNT nanohybrids by atomic layer deposition for high-rate and long-life supercapacitors. Dalton Trans. **45**, 13779–13786 (2016). https://doi.org/10.1039/c6dt01927g
264. Fisher, R.A., Watt, M.R., Konjeti, R., et al.: Atomic layer deposition of titanium oxide for pseudocapacitive functionalization of vertically-aligned carbon nanotube supercapacitor electrodes. ECS J. Solid State Sci. Technol. **4**, M1–M5 (2014). https://doi.org/10.1149/2.0141502jss
265. Hai, Z.Y., Karbalaei Akbari, M., Xue, C.Y., et al.: Atomically-thin WO_3/TiO_2 heterojunction for supercapacitor electrodes developed by atomic layer deposition. Compos. Commun. **5**, 31–35 (2017). https://doi.org/10.1016/j.coco.2017.06.001
266. Velázquez-Martínez, V., Santasalo-Aarnio et al.: A critical review of lithium-ion battery recycling processes from a circular economy perspective. Batteries **5**, 68 (2019). https://doi.org/10.3390/batteries5040068
267. Oviroh, P.O., Akbarzadeh, R., Pan, D.Q., et al.: New development of atomic layer deposition: processes, methods and applications. Sci. Technol. Adv. Mater. **20**, 465–496 (2019). https://doi.org/10.1080/14686996.2019.1599694
268. Choi, H., Lee, N., Park, H., et al.: Development of a SnS film process for energy device applications. Appl. Sci. **9**, 4606 (2019). https://doi.org/10.3390/app9214606
269. Nguyen, M.T., Yonezawa, T.: Sputtering onto a liquid: interesting physical preparation method for multi-metallic nanoparticles. Sci. Technol. Adv. Mater. **19**, 883–898 (2018). https://doi.org/10.1080/14686996.2018.1542926
270. Yabu, H.: Fabrication of honeycomb films by the breath figure technique and their applications. Sci. Technol. Adv. Mater. **19**, 802–822 (2018). https://doi.org/10.1080/14686996.2018.1528478
271. Dingemans, G., Jongbloed, B., Knaepen, W., et al.: Merits of batch ALD. ECS Trans. **64**, 35–49 (2014). https://doi.org/10.1149/06409.0035ecst
272. Knoops, H.C.M., Faraz, T., Arts, K., et al.: Status and prospects of plasma-assisted atomic layer deposition. J. Vac. Sci. Technol. A **37**, 030902 (2019). https://doi.org/10.1116/1.5088582
273. Boris, D.R., Anderson, V.R., Nepal, N., et al.: Effect of varying plasma properties on III-nitride film growth by plasma enhanced atomic layer epitaxy. J. Vac. Sci. Technol. A **36**, 051503 (2018). https://doi.org/10.1116/1.5034247
274. Faraz, T., Arts, K., Karwal, S., et al.: Energetic ions during plasma-enhanced atomic layer deposition and their role in tailoring material properties. Plasma Sources Sci. Technol. **28**, 024002 (2019). https://doi.org/10.1088/1361-6595/aaf2c7
275. Zhang, Y.C., Ding, Y.Y., Christofides, P.D.: Integrating feedback control and run-to-run control in multi-wafer thermal atomic layer deposition of thin films. Processes **8**, 18 (2019). https://doi.org/10.3390/pr8010018
276. Mackus, A.J.M., Merkx, M.J.M., Kessels, W.M.M.: From the bottom-up: toward area-selective atomic layer deposition with

high selectivity. Chem. Mater. **31**, 2–12 (2019). https://doi.org/10.1021/acs.chemmater.8b03454
277. Jiang, X.R., Bent, S.F.: Area-selective ALD with soft lithographic methods: using self-assembled monolayers to direct film deposition. J. Phys. Chem. C **113**, 17613–17625 (2009). https://doi.org/10.1021/jp905317n
278. Vos, M.F.J., Chopra, S.N., Ekerdt, J.G., et al.: Atomic layer deposition and selective etching of ruthenium for area-selective deposition: temperature dependence and supercycle design. J. Vac. Sci. Technol. A **39**, 032412 (2021). https://doi.org/10.1116/6.0000912
279. Klement, P., Anders, D., Gümbel, L., et al.: Surface diffusion control enables tailored-aspect-ratio nanostructures in area-selective atomic layer deposition. ACS Appl. Mater. Interfaces **13**, 19398–19405 (2021). https://doi.org/10.1021/acsami.0c22121
280. Parsons, G.N., Clark, R.D.: Area-selective deposition: fundamentals, applications, and future outlook. Chem. Mater. **32**, 4920–4953 (2020). https://doi.org/10.1021/acs.chemmater.0c00722
281. Cao, K., Cai, J.M., Liu, X., et al.: Review article: catalysts design and synthesis via selective atomic layer deposition. J. Vac. Sci. Technol. A Vac. Surf. Films **36**, 010801 (2018) https://doi.org/10.1116/1.5000587
282. Ras, R.H.A., Sahramo, E., Malm, J., et al.: Blocking the lateral film growth at the nanoscale in area-selective atomic layer deposition. J. Am. Chem. Soc. **130**, 11252–11253 (2008). https://doi.org/10.1021/ja803471g
283. Mackus, A.J.M., Verheijen, M.A., Leick, N., et al.: Influence of oxygen exposure on the nucleation of platinum atomic layer deposition: consequences for film growth, nanopatterning, and nanoparticle synthesis. Chem. Mater. **25**, 1905–1911 (2013). https://doi.org/10.1021/cm400562u
284. Avila, J.R., DeMarco, E.J., Emery, J.D., et al.: Real-time observation of atomic layer deposition inhibition: metal oxide growth on self-assembled alkanethiols. ACS Appl. Mater. Interfaces **6**, 11891–11898 (2014). https://doi.org/10.1021/am503008j
285. Cook, R.C., Stevens, R., Schwartz, P., et al.: Substrate carrier for parallel wafer processing reactor, US20050188923A1
286. Lankhorst, A.M., Paarhuis, B.D., Terhorst, H.J.C.M., et al.: Transient ALD simulations for a multi-wafer reactor with trenched wafers. Surf. Coat. Technol. **201**, 8842–8848 (2007). https://doi.org/10.1016/j.surfcoat.2007.04.079
287. Granneman, E., Fischer, P., Pierreux, D., et al.: Batch ALD: characteristics, comparison with single wafer ALD, and examples. Surf. Coat. Technol. **201**, 8899–8907 (2007). https://doi.org/10.1016/j.surfcoat.2007.05.009
288. Shirazi, M., Elliott, S.D.: Atomistic kinetic Monte Carlo study of atomic layer deposition derived from density functional theory. J. Comput. Chem. **35**, 244–259 (2014). https://doi.org/10.1002/jcc.23491
289. Ding, Y.Y., Zhang, Y.C., Orkoulas, G., et al.: Microscopic modeling and optimal operation of plasma enhanced atomic layer deposition. Chem. Eng. Res. Des. **159**, 439–454 (2020). https://doi.org/10.1016/j.cherd.2020.05.014
290. Deng, Z., He, W.J., Duan, C.L., et al.: Atomic layer deposition process optimization by computational fluid dynamics. Vacuum **123**, 103–110 (2016). https://doi.org/10.1016/j.vacuum.2015.10.023
291. Zhang, Y.C., Ding, Y.Y., Christofides, P.D.: Multiscale computational fluid dynamics modeling of thermal atomic layer deposition with application to chamber design. Chem. Eng. Res. Des. **147**, 529–544 (2019). https://doi.org/10.1016/j.cherd.2019.05.049
292. Ding, Y.Y., Zhang, Y.C., Ren, Y.M., et al.: Machine learning-based modeling and operation for ALD of SiO_2 thin-films using data from a multiscale CFD simulation. Chem. Eng. Res. Des. **151**, 131–145 (2019). https://doi.org/10.1016/j.cherd.2019.09.005
293. Poodt, P., Cameron, D.C., Dickey, E., et al.: Spatial atomic layer deposition: a route towards further industrialization of atomic layer deposition. J. Vac. Sci. Technol. A **30**, 010802 (2012). https://doi.org/10.1116/1.3670745
294. Suntola, T., Antson, J.: Growth of thin films of compounds on base materials-by alternate deposition of mono-atomic layers of the individual elements, CS7508087-A
295. Suntola, T.S., Lindfors, S.G., Antson, J.O., et al.: Multicolour electroluminescent display device-comprising two electroluminescent layers with a light filter interposed therebetween, GB2074786-B
296. Yersak, A.S., Sharma, K., Wallas, J.M., et al.: Spatial atomic layer deposition for coating flexible porous Li-ion battery electrodes. J. Vac. Sci. Technol. A **36**, 01A123 (2018). https://doi.org/10.1116/1.5006670
297. Levy, D.H., Freeman, D., Nelson, S.F., et al.: Stable ZnO thin film transistors by fast open air atomic layer deposition. Appl. Phys. Lett. **92**, 192101 (2008). https://doi.org/10.1063/1.2924768
298. Munoz-Rojas, D., Sun, H., Iza, D.C., et al.: High-speed atmospheric atomic layer deposition of ultra thin amorphous TiO_2 blocking layers at 100 °C for inverted bulk heterojunction solar cells. Prog. Photovoltaics **21**, 393–400 (2013). https://doi.org/10.1002/pip.2380
299. Poodt, P., Lankhorst, A., Roozeboom, F., et al.: High-speed spatial atomic-layer deposition of aluminum oxide layers for solar cell passivation. Adv. Mater. **22**, 3564–3567 (2010). https://doi.org/10.1002/adma.201000766
300. Maydannik, P.S., Kääriäinen, T.O., Cameron, D.C.: An atomic layer deposition process for moving flexible substrates. Chem. Eng. J. **171**, 345–349 (2011). https://doi.org/10.1016/j.cej.2011.03.097
301. Zhao, Y., Zhang, L., Liu, J., et al.: Atomic/molecular layer deposition for energy storage and conversion. Chem. Soc. Rev. **50**, 3889–3956 (2021). https://doi.org/10.1039/d0cs00156b
302. Musselman, K.P., Muñoz-Rojas, D., Hoye, R.L.Z., et al.: Rapid open-air deposition of uniform, nanoscale, functional coatings on nanorod arrays. Nanoscale Horiz. **2**, 110–117 (2017). https://doi.org/10.1039/c6nh00197a
303. van den Bruele, F.J., Smets, M., Illiberi, A., et al.: Atmospheric pressure plasma enhanced spatial ALD of silver. J. Vac. Sci. Technol. A **33**, 01A131 (2015). https://doi.org/10.1116/1.4902561
304. Creyghton, Y., Illiberi, A., Mione, A., et al.: Plasma-enhanced atmospheric-pressure spatial ALD of Al_2O_3 and ZrO_2. ECS Trans. **75**, 11–19 (2016). https://doi.org/10.1149/07506.0011ecst
305. Mione, M.A., Katsouras, I., Creyghton, Y., et al.: Atmospheric pressure plasma enhanced spatial ALD of ZrO_2 for low-temperature, large-area applications. ECS J. Solid State Sci. Technol. **6**, N243–N249 (2017). https://doi.org/10.1149/2.0381712jss
306. Hoffmann, L., Brinkmann, K.O., Malerczyk, J., et al.: Spatial atmospheric pressure atomic layer deposition of tin oxide as an impermeable electron extraction layer for perovskite solar cells with enhanced thermal stability. ACS Appl. Mater. Interfaces **10**, 6006–6013 (2018). https://doi.org/10.1021/acsami.7b17701
307. Hoffmann, L., Theirich, D., Pack, S., et al.: Gas diffusion barriers prepared by spatial atmospheric pressure plasma enhanced ALD. ACS Appl. Mater. Interfaces **9**, 4171–4176 (2017). https://doi.org/10.1021/acsami.6b13380
308. Hoffmann, L., Theirich, D., Schlamm, D., et al.: Atmospheric pressure plasma enhanced spatial atomic layer deposition of SnO_x as conductive gas diffusion barrier. J. Vac. Sci. Technol. A Vac. Surf. Films **36**, 01A112 (2018) https://doi.org/10.1116/1.5006781

309. Seville, J.P.K., Willett, C.D., Knight, P.C.: Interparticle forces in fluidisation: a review. Powder Technol. **113**, 261–268 (2000). https://doi.org/10.1016/S0032-5910(00)00309-0
310. Valverde, J.M., Castellanos, A.: Magnetic field assisted fluidization: a modified Richardson-Zaki equation. China Particuol. **5**, 61–70 (2007). https://doi.org/10.1016/j.cpart.2007.01.001
311. Espin, M.J., Valverde, J.M., Quintanilla, M.A., et al.: Electromechanics of fluidized beds of nanoparticles. Phys. Rev. E **79**, 011304 (2009). https://doi.org/10.1103/physreve.79.011304
312. van Ommen, J.R., Yurteri, C.U., Ellis, N., et al.: Scalable gas-phase processes to create nanostructured particles. Particuology **8**, 572–577 (2010). https://doi.org/10.1016/j.partic.2010.07.010
313. Ferguson, J.D., Buechler, K.J., Weimer, A.W., et al.: SnO_2 atomic layer deposition on ZrO_2 and Al nanoparticles: pathway to enhanced thermite materials. Powder Technol. **156**, 154–163 (2005). https://doi.org/10.1016/j.powtec.2005.04.009
314. McCormick, J.A., Cloutier, B.L., Weimer, A.W., et al.: Rotary reactor for atomic layer deposition on large quantities of nanoparticles. J. Vac. Sci. Technol. A **25**, 67–74 (2007). https://doi.org/10.1116/1.2393299
315. Adhikari, S., Selvaraj, S., Kim, D.H.: Progress in powder coating technology using atomic layer deposition. Adv. Mater. Interfaces **5**, 1801853 (2018). https://doi.org/10.1002/admi.201801853
316. Nakamura, H., Watano, S.: Fundamental particle fluidization behavior and handling of nano-particles in a rotating fluidized bed. Powder Technol. **183**, 324–332 (2008). https://doi.org/10.1016/j.powtec.2008.01.007

Zhe Zhao obtained his PhD degree at Fudan University in 2022. Now, He is a postdoc researcher in the Department of Materials Science at Fudan University. His research interest includes the design and synthesis of nanomaterials, new structural electrode materials for electrocatalysts, energy storage devices, and sensors.

Gaoshan Huang received his PhD degree in condensed matter physics at Nanjing University, China in 2007. After graduation, he worked in IFW Dresden, Germany as a guest scientist. Then he moved to IMRE, Singapore as a research engineer. In 2010, he joined the Department of Materials Science, Fudan University, China. Currently, he is a professor of materials science at Fudan University. His research interest is fabrications and characterizations of low dimensional structures.

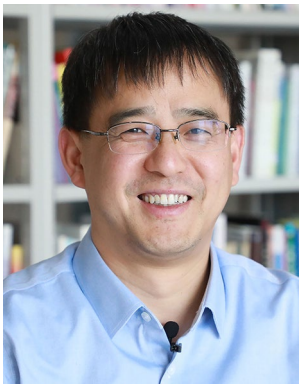

Yongfeng Mei received his BS and MS degrees in physics from Nanjing University and PhD degree in materials physics from the City University of Hong Kong. He is a professor in materials physics and chemistry and associated department head in the Department of Materials Science at Fudan University (China). Before that, he worked as a post doctoral researcher in the Max Planck Institute for Solid State Research (Germany) and then led a research group in the Leibniz Institute for Solid State and Materials Research Dresden (Germany) as a staff scientist. His research interest focuses on the materials development in micro/nanorobotics, flexible electronics/optoelectronics and nanophotonics.